THE ROLE OF VINCULIN IN THE CELL ADHESION STRENGTHENING PROCESS

A Dissertation
Presented to
The Academic Faculty

by

David W. Dumbauld

In Partial Fulfillment
of the Requirements for the Degree
Doctor of Philosophy in the
Bioengineering

Georgia Institute of Technology
May 2011

THE ROLE OF VINCULIN IN THE CELL ADHESION STRENGTHENING PROCESS

Approved by:

Dr. Andrés J. García, Advisor
School of Mechanical Engineering
Georgia Institute of Technology

Dr. Susan W. Craig
School of Medicine
The Johns Hopkins School of Medicine

Dr. Andrew P. Kowalczyk
Departments of Cell Biology and Dermatology
Emory University

Dr. Hang Lu
Department of Chemical Engineering
Georgia Institute of Technology

Dr. Evan Zamir
Department of Mechanical Engineering
Georgia Institute of Technology

Dr. Cheng Zhu
Department of Biomedical Engineering
Georgia Institute of Technology

Date Approved: March 22, 2011

To my family, whose love and support made this possible.

ACKNOWLEDGEMENTS

"Dave, what you need to understand is that graduate school is a transitory phase," my advisor, Andrés García, would often explain to me. As my time at Georgia Tech draws to a close, I am realizing the full truth of this statement. And as life-phases go, this has been an amazing one that would not have been possible without the help, guidance, and support of a number of people.

First I would like to thank Andrés, whose contagious passion for science and unwavering belief in my abilities inspired me throughout my tenure as a graduate student in his lab. I will miss his impromptu visits to my lab bench, his passion for all things spinning disk, and his willingness to engage in scientific discussions, day or night. Andrés provided me with direction and at the same time gave me the freedom to explore my own scientific curiosities. I am especially grateful to Andres for putting up with my mood swings and (often unfounded) pessimism. I'm sure there were plenty of times when he thought twice about picking up his phone when he saw I was calling ☺. In the end, he was right when he told me the hard work would pay off. But hey, that's why "he's the PI!"

I would like to thank my committee members who contributed significantly to this work. Dr. Susan Craig simultaneously inspired me to pay close attention to the details of my experiments while also challenging me to synthesize my findings to understand the broader impacts of the work. Dr. Cheng Zhu has instilled in me the importance of precision when communicating my scientific findings. Dr. Evan Zamir was always willing to engage in scientific discussions and troubleshooting and I thank him for his

candid opinions of this work. Dr. Andrew Kowalczyk reinforced the need to be hypothesis-driven, especially when working with biological systems. Dr. Hang Lu provided insightful critique of this work and taught me the importance of clarity when communicating scientific data.

Members of the Garcia lab, past and present, have been a tremendous source of support, laughter, and all around good times. I thank Sean Coyer who introduced me to the lab and taught me the ways of the spinning disk. It was a wild, hilarious, humbling, maddening, often-times ridiculous ride. I can't think of a better person to have shared it with. Thank you Sean, for never making me feel like I complained too much and for always having a great pep-talk ready whenever I needed it. I thank Dr. Charlie Gersbach for turning a hard-core mechanical engineer into a true cloning master. I'm convinced that Charlie, through hard work and creativity, will become a world famous scientist. A huge shout-out goes to Dr. Fantastic, aka Dr. Tim Petrie, who befriended me early on, despite his intense dislike for all things Midwest (read – not California). Tim taught me, among other things, the importance of reading and following the directions on frozen pizza boxes, that we can never watch a sports game involving our favorite teams and expect victory, and that a career as a scientist is way better than any alternative. Kellie Burns has been there every step of the way on this project. She taught me how to pipette (I had never seen one when I started in the lab), transform bacteria, and prep plasmid DNA. Although we both would like to forget it, Kellie and I are forever bound together by FAK, talin siRNA, and countless Western blots and flow cytometry experiments. She truly keeps the Garcia lab running and I can't thank her enough for all of her hard work and dedication. Ed Phelps has been a great friend and shining example of what happens

when you combine raw talent, scientific curiosity, and hard work. Thanks for not getting too mad at me when we fed that entire pizza to The General. Ted T. Lee showed up late in my grad school career, yet made an immediate and lasting impact. Ted taught me not to take myself too seriously and to enjoy the finer things in life. Oh, I should also mention that, in addition to our extracurricular activities, Ted was integral in helping me complete the last phase of the project. I also thank Dr. Nate Gallant for always answering the phone when I called, even though it meant digging into the details of the research project he completed many moons ago. Asha Shekaran is my favorite Singaporean with whom I have shared many laughs over the years. A word to the wise, never underestimate her considerable, almost superhuman skillz in research, billiards, shotgun shooting, fencing, and knowledge of American slang. Her only known weakness is Yahoo! Pool. My other desk mate, Dr. Jenn Phillips, deserves special credit for putting up with the Boy's Only Club consisting of Sean and me. Jenn was always ready and willing to provide advice (scientific and otherwise) or share in a joke, despite the fact that I reeked of carbs. Dr. Joe Charest is quite possibly the most talented, level-headed engineer I have ever encountered. I walked away from every conversation I had with Joe a smarter and more humble person. Abbey Wojtowicz and Amanda Walls Bridges are quite possibly the nicest and second nicest people I have ever met (no particular order). When I joined the lab, they quickly made me feel welcome, despite my inability to remember their names for the first year or so. I'd also like to thank the only adopted Garcia lab member in the history of the lab, Julia Henkels. Julia taught me that life as a grad student isn't all that bad and that being busy with lab work is no excuse for neglecting my lab notebook. In the 4+ years that I have known Nduka Enemchukwu, I

have never heard him complain about anything. And whether he knows it or not, Nduka has set an example of hard work to which I strive. Thanks go to Rachel Whitmire who fought the good fight against the Lab's most powerful force – entropy. She soothed the pain of early morning lab cleanups with amazing breakfast casseroles that would make Ron Swanson proud. Speaking of great, free, lab food, Stacie Gutowski cannot be thanked enough for the many wonderful baked treats that provided much needed sugar during long days in the lab. I thank Dr. Ankur Singh for his unsolicited support of my work and belief that I did, indeed, have more than enough data to graduate. Dr. Ram Selvam provided a fine example of how to handle the stresses of academic life with ease. I'm still not clear on the details, but I think his secret has something to do with his lunch of Spicy Cheetos, curry, and rice. Thanks to Amy Chen, Apoorva Kalasuramath, Dr. Imen Hannachi, Dr. Susan Lehman, I leave knowing that the lab is in very capable hands.

Many people provided indispensible technical guidance and tools that directly contributed to the success of this thesis work. Dr. Brock Wester is a clean room master. He gave of his time and expertise and fabricated several molds that myself and others in the Garcia Lab use on a daily basis. Thanks Brock! Special thanks go to Dr. Jan Scrimgeour who was an essential contributor to the FRAP work presented in this thesis. Jan tamed the beast that is the Nikon EZ-C1 FRAP module – an amazing feat of scientific prowess and Zen-like patience. Steve Woodard, and before him Johnafel Crowe, were instrumental in the development of the stable vinculin-eGFP expressing cell lines. In addition to running the cell sorter, Steve was always available and willing to help with the project in any way that I needed. Thank you, Steve, for never making me feel like I was bothering you, despite your crazy schedule.

My grad school experience was made whole by the strong friendships I developed with those who shared the journey. Rich Carpenedo helped me push myself harder than I ever that was possible by way of ridiculous burrito eating challenges. Crossfit was hard, too. Brent Urhig deserves thanks for showing me what a real Halloween costume looks like and for providing a daily reminder of the importance of looking people in the eye when I talk to them. Vince Fiore and I have become good friends, despite (or perhaps because of) our hometown allegiances. Yes, Vince, the Bengals are garbage, but are they'll really any worse than the Pirates? Chris Dosier is still dangerous, but he can be my wingman anytime. I also want to thank those members of wing 2D, past and present, for making the Lair of Inefficiency the funniest, busiest, most entertaining places that I will ever work.

My time at Tech wouldn't have been the same without the IBB BBUGS intramural sports teams. Tim Petrie, Bryan Bell, Brent Urhig, Andres Bratt-Leal, Rich Carpenedo, Sean Coyer, Ed Phelps, Jeremy Lim, Eric Ping, Jay Sy, Ken Dupont, Chris Edens and many others experienced many glorious victories against the likes of inferior grad departments including ChBE, ASDL, SSDL, and most importantly, the MBAs. May we never forget that we almost won the school championship in flag football.

Special thanks go to my BBUGS Industry Co-Chairs, Yash Kolambkar and Chris Lee. Yash was instrumental in helping me see the importance of activities apart from my thesis work. After Yash moved on, Chris Lee stepped in and immediately began making his own mark on the LIFE seminar series.

I thank the members of the staff of IBB whose work often goes unnoticed but makes possible the scientific achievements of the Institute. Specifically, Chris Ruffin,

Meg McDevitt, Katherine Montgomery, Floyd Wood, Alyceson Andrews, James Godard, and Vivian Johnson deserve special thanks for helping me successfully complete this thesis.

The completion of dissertation was due in no small part to the love and support I received from my wife, best friend, and fiercest supporter, ~~Dr.~~ Professor Kelly Erby. Her hard work and dedication to….well….everything she does, inspired me throughout the course of this work. Thank you.

TABLE OF CONTENTS

LIST OF TABLES

LIST OF FIGURES

LIST OF SYMBOLS AND ABBREVIATIONS

RNAi	RNA interference
FAK	focal adhesion kinase
FN	fibronectin
BSA	bovine serum albumin
PBS	phosphate buffered saline
ECM	extracellular matrix
FBS	fetal bovine serum
IF	immunoflourescence
PDMS	Polydimethlysiloxane
SAM	self-assembled monolayer
eGFP	enhanced green fluorescent protein
mPAD	microfabricated Post-Array-Detectors
FRAP	fluorescence recovery after photobleaching

SUMMARY

Cell adhesion to extracellular matrices (ECM) is essential to numerous physiological and pathological processes. Cell adhesion is initiated by binding of the transmembrane integrin family of receptors to an ECM ligand such as fibronectin (FN). Once bound, integrins cluster together and form focal adhesions (FA). FAs serve as structural links and signal transduction elements between the cell and its extracellular environment. While a great deal of progress has been made in identifying the biochemical components that comprise focal adhesions and the roles they play in migration, cell spreading, and signaling, the contributions of these proteins to mechanical interactions between the cell and its environment remain poorly understood.

A FA adhesion protein of particular importance is vinculin. When localized to focal adhesions, vinculin forms a ternary complex with talin and β1-integrin. This β1-integrin-talin-vinculin complex plays a central role in the regulation of FA assembly and cell spreading and migration. Nevertheless, the specific contribution to adhesive force generation of the β1-integrin-talin-vinculin complex remains poorly understood.

The objective of this project was to analyze the role of vinculin in the cell adhesion strengthening process. Our central hypothesis is that vinculin modulates adhesion strength via regulating the size and/or composition of the integrin-talin-vinculin complex. We used a novel combination of biochemical reagents and engineering techniques along with quantitative and sensitive adhesion strength measurements to provide new insights into how the structure of vinculin contributes to cell adhesion strength.

CHAPTER 1

INTRODUCTION

SPECIFIC AIMS

Cell adhesion to extracellular matrices (ECM) is essential to numerous physiological processes including cell migration, embryonic development, and proper inflammatory responses. Abnormalities in adhesion can lead to pathological conditions such as cancer metastasis and impaired wound-healing. Cell adhesion is initiated by binding of the transmembrane integrin family of receptors to an ECM ligand such as fibronectin (FN). Once bound, integrins cluster together and nascent focal complexes develop consisting of a coordinated mixture of signaling and scaffolding proteins. These structures, under application of force generated by the internal contractile machinery, further develop into larger, more sophisticated structures termed focal adhesions (FA). FAs serve as structural links and signal transduction elements between the cell and its extracellular environment. While a great deal of progress has been made in identifying the biochemical components that comprise focal adhesions and the roles they play in migration, cell spreading, and signaling, the contributions of these proteins to mechanical interactions between the cell and its environment remain poorly understood.

A FA adhesion protein of particular importance is vinculin, a ubiquitously expressed actin-binding protein that is found both at sites of cell-cell and cell-matrix junctions. First identified in 1979, research during the past thirty years has vastly increased our understanding of the functional and biochemical roles of vinculin. When

localized to focal adhesions, vinculin forms a ternary complex with talin and β1-integrin. This integrin-talin-vinculin complex plays a central role in the regulation of FA assembly and cell spreading and migration. Nevertheless, the specific contribution to adhesive force generation of the integrin-talin-vinculin complex remains poorly understood.

The objective of this project is to analyze the role of vinculin in the cell adhesion strengthening process. Our central hypothesis is that vinculin modulates adhesion strength via regulating the size and/or composition of the integrin-talin-vinculin complex. We base this hypothesis on previous work in our lab demonstrating that levels of bound integrin and focal adhesion assembly strongly modulate adhesion strength and recent evidence that suggests vinculin, talin, and integrin form a ternary complex that regulates the dynamics of focal adhesions. The rationale for this project is that use of a novel combination of biochemical reagents and engineering techniques along with quantitative and sensitive adhesion strength measurements will provide new insights into how the structure of vinculin contributes to cell adhesion strength. Using these methods, we will address the objective of this project with the following specific aims:

1: Examine role of vinculin in FAK-mediated steady-state adhesion strength

FAK, an essential non-receptor tyrosine kinase, plays pivotal roles in migratory responses, adhesive signaling, and mechanotransduction. Previous work in our lab indicated that FAK regulates both short and long-term adhesive force generation in fibroblasts. We demonstrated that FAK influences short-term adhesion strength by modulating integrin activation, however, it remained unclear how FAK modulated steady-state adhesion strength.

We hypothesized that FAK modulates long-term adhesion strength by controlling vinculin localization to sites of focal adhesions. Using a combination of RNAi knockdown of vinculin, RNAi knockdown of FAK, various biochemical assays, and a spinning disk for measuring adhesive strength, we analyzed the contributions of vinculin in modulating force transmission across focal adhesions during FAK-mediated steady-state adhesion strength.

2: Examine the contributions of vinculin in actin-myosin contractility induced adhesion strength

Actin-myosin contractility modulates focal adhesion assembly and stress fiber formation. These processes regulate cell behaviors including migration, neurite extension, cytokinesis, muscle cell contraction, cell cycle progression, angiogenesis, and differentiation. To date, the contributions of actin-myosin contractility to adhesive interactions have been characterized by migration and spreading assays, leaving in a gap in knowledge regarding how cell-generated contractile forces and focal adhesion assembly regulate adhesion strength.

Our working hypothesis was that actin-myosin contractility would modulate adhesion strengthening by changing levels of matrix-bound integrins and assembly of focal adhesions. Using a hydrodynamic adhesion assay in combination with chemical contractility inhibitors and various biochemical assays we analyzed the contributions of contractility to fibroblast adhesion strengthening.

3: Examine the specific contributions of the head and tail domains of vinculin to cell adhesion strength

Steady-state adhesion strength measurements in the presence or absence of FAK demonstrated the FAK modulates adhesion strength by regulating vinculin localization to focal adhesions. In addition, actin-myosin contractility modulates adhesion strength through assembly of vinculin-containing focal adhesions. These results demonstrate the importance of vinculin in generating adhesive forces, however, the relative contribution of specific domains of the vinculin molecule, remain unclear.

Our working hypothesis was that vinculin modulates adhesion strength by modulating the size, composition, and cytoskeleton connectivity of the integrin-talin-vinculin complex. We engineered cells to express wild-type and various mutants of vinculin and used them in combination with a hydrodynamic adhesion assay and various biochemical techniques to understand the relative contributions of the head and tail domains of vinculin.

4: Characterize the force-dependent dynamics of vinculin in focal adhesion

Focal adhesions (FAs) sense and respond to mechanical forces. The molecular mechanism(s) involved in this process, however, have yet to be determined. At sites of focal adhesions, vinculin adopts an open, active conformation and binds to talin and F-actin. The interaction between talin and vinculin has recently been proposed as a potential force-sensing unit. In addition, it is now known that vinculin transfers force in focal adhesions and that the dynamic behavior of the protein is dependent on the spatial location in the cell. To date, however, there exists no direct evidence that vinculin dynamics are modulated by the force applied to the focal adhesions.

Our working hypothesis was that force transferred through focal adhesion increases the dynamic stability of the vinculin molecule in focal adhesions. The rationale for this hypothesis is that as the force applied to a focal adhesion increases, so too does the force transferred across the vinculin molecule, making it less able to dissociate from its binding partners (talin and F-actin). We developed a novel technique combining fluorescent recovery after photobleaching (FRAP) with traction force measuring devices to characterize how vinculin dynamics are modulated by force across focal adhesions.

Project Significance

Cell adhesion to the extracellular matrix is required for embryogenesis and the proper organization, maintenance, and repair of tissues as it allows for the development of mechanical forces and intracellular cues that regulate cell survival and migration (Danen and Sonnenberg, 2003; De Arcangelis and Georges-Labouesse, 2000). The absolute embryonic lethality of the deletion of a wide variety of adhesion related genes, including integrin receptors, extracellular matrix and focal adhesion components, indicates the necessity of cell adhesion in development (George, 1993; Stephens et al., 1995; Xu et al., 1998a). Abnormalities in adhesion are responsible for a wide-variety of pathological states including deficient immune response, blood clotting, and tumor metastasis (Wehrle-Haller and Imhof, 2003). Integrin-mediated anchorage of cells to the ECM is a complex process that comprises integrin-ligand binding, clustering of bound receptors, and linkage to the contractile cytoskeleton of the cell (Critchley, 2000; Geiger et al., 2001). Specifically, the linkage between integrins and the actin-cytoskeleton is mediated by FAs. These supramolecular structures are composed of both structural

(talin, vinculin, α-actinin) and signaling (FAK, paxillin) molecules and are critical regulators of both adhesion force generation and cell migration (Bershadsky et al., 2006). A FA component of particular importance is vinculin, a 116-kDa cytoskeleton-associated protein found in the majority of cell and tissue types. Vinculin plays an essential role in both development and proper cardiac function in mice studies (Xu et al., 1998a; Zemljic-Harpf et al., 2007). Cell culture experiments suggest that vinculin plays important roles in migration, adhesion, survival, and proper focal adhesion dynamics. Importantly, vinculin has no known enzymatic activity and therefore must exert influence on adhesion processes by directly interacting with partner proteins. While significant progress has been made in identifying how vinculin modulates its interactions with its numerous binding partners, little is known about how the protein contributes to the generation of adhesion forces. As an outcome of the proposed investigations, we analyzed the specific contribution of vinculin to the generation of cell adhesive forces. Furthermore, using our unique combination of reagents and measurement tools, we identified the importance of specific structural domains of the vinculin molecule to the generation of cell adhesion force.

The proposed work is significant because it provides novel insights as to the relative influence of the head and tail domains of vinculin to the modulation of force transfer between the external matrix and the internal cytoskeleton. These studies add an important dimension to our existing knowledge of the dynamics, regulation, and function of adhesion complexes. In addition, the results of these experiments will provide a new context for understanding the role of vinculin in many physiologic and pathologic processes.

CHAPTER 2

LITERATURE REVIEW

Adhesion Force Generation

Adhesion to ECM components such as FN and collagen, is primarily mediated by the integrin family of heterodimeric ($\alpha\beta$) receptors (Hynes, 2002). Integrin-mediated adhesion is a highly coordinated process that is first initiated by activation and binding of the integrin to its ECM ligand (Choquet et al., 1997; Faull et al., 1993; Friedland et al., 2009). Once bound, integrins rapidly cluster together and generate linkages to the actin cytoskeleton mediated by the supramolecular structures termed focal adhesions (FA) (Geiger et al., 2001). Morphologically, FAs are elongated, streak-like structures typically 3-10μm in length located near the periphery of the cell. There, they mediate strong adhesion to the ECM by modulating force transfer between integrins and the actin cytoskeleton. In addition to their structural role, FAs serve as signaling platforms that control various functions including differentiation, proliferation, and apoptosis (Sastry and Burridge, 2000). Importantly, FAs are not static, rigid structures. Rather, they are highly dynamic units that assemble and disassemble in response to a wide variety of mechanical and chemical stimuli. Initial formation of FA is stimulated by the small GTPase Rho-A, while full maturation of focal adhesions is driven by actin-myosin contractility by an unknown mechanism (Amano et al., 1997; Chrzanowska-Wodnicka and Burridge, 1996).

The generally accepted model for adhesive force generation, proposed by McClay and Erickson, proposes a two-step process; namely initial ligand binding followed by rapid strengthening (Lotz et al., 1989). The strengthening arises from (i) increases in cell-substrate contact area (spreading) (ii) receptor recruitment to anchoring sites (recruitment and clustering), and (iii) interactions with cytoskeletal elements that lead to enhanced force distribution among bound receptors (focal adhesion assembly). This model has been validated in several independent experimental systems (Balaban et al., 2001; Choquet et al., 1997; Hato et al., 1998; Maheshwari et al., 2000).

Vinculin

Vinculin, a 116-kDa protein, was first identified in 1979 in cultured chicken gizzard smooth muscle cells as a protein that localized to sites of close contact to the substrate at the termini of microfilaments (Geiger et al., 1980). It has since been the focus of various areas of scientific research with the overall goal to understand both its physiologic relevance and how its unique structure regulates its function (Bakolitsa et al., 2004; Borgon et al., 2004; Cohen et al., 2006; Gingras et al., 2006; Izard et al., 2004; Izard and Vonrhein, 2004).

Molecular structure

Vinculin consists of five domains, each of which is built from four-helix bundles. The first three four-helix bundles, domains 1-3 (D1-D3), interact and form the globular head of the protein. The fourth and fifth domains of the protein are similar in structure to

D1 and D2, except that D5 is connected to D4 by a long, proline-rich strap. D5 is designated as the tail of vinculin (Vt).

Importantly, Vt binds strongly (Kd $<10^{-9}$) to the pincer-like pocket formed by Vh (Bakolitsa et al., 2004). This high affinity interaction is the result of two specific interactions between Vt and D1 and Vt and D4 (Cohen et al., 2005). When Vt is bound to Vh, the protein is in an inactive state, meaning that sites for many of its binding partners (talin, actin, etc.) are masked (Figure 1A). Vinculin activation involves dissociation of the Vt and Vh domains, revealing its full spectrum of binding sites (Figure 1B). There are two competing models that describe the activation process of vinculin. The first postulates that vinculin is activated through a combinatorial pathway in which the coincidence of talin and F-actin are required for vinculin activation (Chen et al., 2006; Cohen et al., 2006). This model is attractive because recent evidence suggests that in the closed-conformation, there is an exposed binding site in Vt for F-actin, which may be involved in activation (Ziegler et al., 2006). Alternatively, several studies using isolated fragments of vinculin and talin have suggested that a single ligand, such as talin, is capable of activating the vinculin molecule (Bois et al., 2006; Izard et al., 2004; Izard and Vonrhein, 2004). Interpretation of the latter model is limited by the use of protein fragments as opposed to the former, which makes use of full-length vinculin and talin.

Functional roles

Vinculin is found in numerous cells and tissues, but has the most interesting organization in skeletal and cardiac muscle costameres (Pardo et al., 1983a, b) and cardiac intercalated disks (Koteliansky et al., 1984). Here, vinculin forms a

subsarcolemmal lattice of transmembrane connections termed costameres. These functional units physically connect myofibrils to the muscle cell membrane and extracellular matrix (Craig and Pardo, 1983; Sparrow and Schöck, 2009). Importantly, focal adhesions that form when cells are cultured on stiff, 2-D substrates, are structurally and compositionally analogous to costameres (Samarel, 2005), thus making the study of FA on 2-D surfaces an appropriate model system for our analysis.

Several model systems indicate that vinculin plays an important physiologic role in force transmission, most notably in cardiomyocytes. Mice heterozygous for vinculin are predisposed to stress-induced cardiomyopathy (Zemljic-Harpf et al., 2004), while deletion of the vinculin gene in mice is embryonically lethal (Xu et al., 1998a). Cardiac specific knockout of vinculin and the vinculin homolog meta-vinculin disrupts cellular junctions and causes sudden death or dilated cardiomyopathy (Zemljic-Harpf et al., 2007) while ischemic events in mice models lead to disorganization of vinculin (Steenbergen et al., 1987). In humans, diseases that lead to cardiac stress have shown to involve irregularities in vinculin levels and localizations (Vasile et al., 2006). These effects are consistent with the paralysis and disrupted muscle organization in nematodes following deletion of the vinculin gene (Barstead and Waterston, 1991). Taking together, these studies indicate that vinculin plays an important role in force transfer.

Interestingly, cultured cells do not require vinculin for survival, proliferation, or even FA formation (Xu et al., 1998b). Cells lacking vinculin are more motile presumably as a result of their documented faster FA turnover (Xu et al., 1998b). Furthermore, vinculin-null cells exhibit altered stiffness (Alenghat et al., 2000; Mierke et al., 2008) and disruptions in Rac-mediated lamellipodia protrusion (Goldmann and Ingber, 2002), cell

shape, spreading (Coll et al., 1995; DeMali et al., 2002; Xu et al., 1998b), and apoptosis (Subauste et al., 2004). Further evidence of the functional role of vinculin in cells comes from FRET experiments demonstrating that vinculin exists in an inactive state in the cytoplasmic pool, but becomes activated at sites of FAs (Chen et al., 2005).

Importantly, extensive research has identified the numerous potential binding partners of vinculin including talin (Burridge and Mangeat, 1984), α-actinin (Belkin and Koteliansky, 1987; Kroemker et al., 1994), paxillin (Turner et al., 1990), VASP (Brindle et al., 1996), vinexin/ponsin (Kioka et al., 1999; Mandai et al., 1999), and F-actin (Jockusch and Isenberg, 1981; Johnson and Craig, 1995). However, it remains largely unclear how in vitro binding corresponds to in vivo interactions. For example, it was recently shown that vinculin head domain recruits paxillin to FA independent of vinculin tail, despite the known binding site for paxillin being located on vinculin tail (Humphries et al., 2007). Recent evidence suggests that the head domain of vinculin regulates integrin dynamics through a yet to be determined pathway while the tail domain is responsible for linking FAs to the actin cytoskeleton (Humphries et al., 2007). It remains to be determined how the different domains of vinculin contribute to cell adhesion strength.

Spinning Disk Assay for Adhesion Strength Measurements

The spinning disk device, developed by García et al (Garcia et al., 1997) has been successfully integrated into studies in our lab over the last decade to measure the adhesion strength of a population of cells (Gallant et al., 2005; Garcia et al., 1998; García et al., 1998; Michael et al., 2009). The device applies a well-defined range of shear

forces to adherent cells and provides a robust and sensitive measure of their adhesion strength. Briefly, substrates containing cells seeded on islands of controlled size and spacing are mounted on the device and spun at constant speed in spinning buffer. Fluid flow over the cells on the disk produces a detachment force that is proportional to the radius from the center of the disk and is given by the following equation:

$$\tau = 0.8r\sqrt{\rho\mu\omega^3}$$ where $\tau =$ shear stress; $r =$ radial position from center
$\rho =$ fluid density; $\mu =$ fluid viscocity; $\omega =$ rotational speed

In this system, cells at the center of the disk are exposed to negligible detachment force, while cell detachment increases towards the outside of the disk as higher shear force is applied. Thus, in a single sample, a linear range of detachment forces is applied to a population of cells (approximately 75,000 cells per 25mm disk). Following spinning, cells are fixed, stained, and counted at sixty-one radial positions. On average, approximately ~6000 cells are counted per sample. The fraction of adherent cells (f) is then calculated by dividing the number of cells at each radial position by the number of cells at the center of the disc, where negligible detachment force was applied. The detachment profile (f vs. τ) is then fit to the sigmoid:

$$f = \frac{f_0}{1+e^{b(\tau-\tau_{50})}}$$ where $f_0 =$ normalized asymtote;
$b =$ slope at inflection point;
$\tau_{50} = 50\%$ cell detachment

We define τ_{50} as the mean shear stress. Mean shear stresses are determined in response to various testing conditions including various ECM substrates, cell type, adhesive area, and adhesive time points.

Generation of Cell Adhesive Force: Contributions of Adhesive Area, Integrin Binding, and Focal Adhesion Assembly

Previous work in our lab has examined the contributions of adhesive area, integrin binding, and FA assembly to the generation of cell adhesive forces. Gallant and coworkers engineered micropatterned substrates to control cell-substrate adhesive area and eliminate the contributions of cell shape and spreading to adhesion strengthening. Microcontact printing of self-assembled monolayers of alkanethiols on gold was used to create FN-coated, cell adhesive domains within a non-fouling/non-adhesive background. Fibroblasts were cultured on substrates with adhesive areas varying from 2-20μm in diameter and for different lengths of time. Adhesion strength analysis was performed using the spinning disc and the data was analyzed in the context of integrin binding and FA assembly (Gallant et al., 2005).

These studies allowed for the development of quantitative relationships between functional (adhesive strength generation) and biochemical (integrin binding, FA assembly) events. The results revealed a strong correspondence between the biochemical and functional outputs, demonstrating that these processes are tightly coupled.

Role of Focal Adhesion Kinase in Adhesion

Focal adhesion kinase (FAK) is a widely expressed non-receptor protein tyrosine kinase that plays essential roles in adhesive interactions by functioning as a scaffold for focal adhesion components, including Src, Cas, talin, and paxillin (Hanks et al., 1992; Polte and Hanks, 1995; Schaller et al., 1992; Schaller et al., 1999) and by providing signals that promote survival by blocking apoptotic pathways (Xu et al., 2000). FAK is essential for many physiologic processes including development and organogenesis (Furuta et al., 1995). Tissue specific knock-outs have revealed important roles for FAK in angiogenesis, branching tubulogenesis, innervations and mylenation, cardiac development, and blood-testis barrier function (Braren et al., 2006; Forrest et al., 2009; Peng et al., 2008; Shen et al., 2005; Siu et al., 2009; Watanabe et al., 2008; Wei et al., 2009).

FAK modulates cell migration via focal adhesion turnover dynamics (Owen et al., 1999; Wang et al., 2001; Webb et al., 2004). FAK also plays a role in lamellipodia protrusion and actin cytoskeleton polymerization (Siesser et al., 2007). Combined, it is clear that the contributions of FAK to cell motility and FA dynamics are well defined. However, there lacks a general understanding of how FAK contributes to the generation of adhesive forces. We recently reported that FAK modulates short-term adhesion strength by promoting integrin activation (Michael et al., 2009). This work also demonstrated that FAK modulates long-term adhesion strength and implicated vinculin as a key component of force modulation.

Role of Actin-Myosin Contractility in Adhesion

Contractile forces generated inside the cell regulate migration, neurite extension, cytokinesis, muscle cell contraction, cell cycle progression, angiogenesis and differentiation (Griffin et al., 2004; Mammoto et al., 2009; Mammoto et al., 2004; McBeath et al., 2004; Parizi et al., 2000; Polte et al., 2004; Tanaka and Sabry, 1995; Wozniak et al., 2003). Contractility results from dynamic interactions between actin filaments and myosin, which are regulated via phosphorylation of myosin light chain (MLC) (Kaibuchi et al., 1999; Worthylake and Burridge, 2003). Rho GTPases control the formation of stress fibers and focal adhesion assembly by modulating MLC phosphorylation and generating actin-myosin contractility (Amano et al., 1997; Chrzanowska-Wodnicka and Burridge, 1996; Totsukawa et al., 2000). When activated by serum factors, such as lysophosphatidic acid (LPA), Rho acts through its effector Rho-kinase (also termed ROCK), to enhance the contraction of smooth muscle cells as well as nonmuscle cells by either inactivation of myosin phosphatase (Kimura et al., 1996) or direct phosphorylation of MLC (Totsukawa et al., 2000). Contractile forces can also be modulated by MLC kinase (MLCK), which promotes assembly of actin-myosin filaments and MLC phosphorylation (Gallagher et al., 1997).

The equilibrium of forces within a cell represents a balance of internal contractile forces and anchoring forces to the underlying substrate (Ingber, 2003; Zhu et al., 2000). This complex and dynamic balance is governed by the size and distribution of cell-substrate adhesive structures, cytoskeletal architecture, and spatiotemporally-regulated internal contractile forces. The contributions of actin-myosin contractility to adhesive interactions have been characterized primarily in spreading and migration assays. While these functional measurements have identified key roles for actin-myosin contractility in

focal adhesion assembly, stress fiber formation, and migratory forces (Amano et al., 1997; Chrzanowska-Wodnicka and Burridge, 1996; Worthylake and Burridge, 2003), relatively little is known about how actin-myosin contractility and focal adhesion assembly regulate cell adhesive forces.

CHAPTER 3

FOCAL ADHESION KINASE-DEPENDENT REGULATION OF ADHESIVE FORCES INVOLVES VINCULIN RECRUITMENT TO FOCAL ADHESIONS*

Abstract

Focal adhesion kinase (FAK), an essential non-receptor tyrosine kinase, plays pivotal roles in migratory responses, adhesive signaling and mechanotransduction. FAK-dependent regulation of cell migration involves turnover dynamics as well as actin cytoskeleton polymerization and lamellipodia protrusion. Whereas roles for FAK in migratory and mechanosensing responses have been established, the contribution of FAK to the generation of adhesive forces is not well understood. Using FAK-null cells expressing wild-type and mutant FAK under an inducible tetracycline promoter, we analyzed the role of FAK in the generation of steady-state adhesive forces using micropatterned substrates and a hydrodynamic adhesion assay. FAK expression reduced steady-state strength by 30% compared with FAK-null cells. FAK expression reduced

*Modified from
(1) Dumbauld DW[1], Michael KE[1], Hanks SK, García AJ. *Focal adhesion kinase-dependent regulation of adhesive forces involves vinculin recruitment to focal adhesions*. Biol. Cell. 2010.
(2) Michael KE, Dumbauld DW, Burns KL, Hanks SK, García AJ. *Focal adhesion-kinase modulates cel adhesion strengthening via integrin activation.* Mol Biol Cell. 2009.
[1]-authors contributed equally to this work.

vinculin localization to focal adhesions by 35% independently of changes in integrin binding and localization of talin and paxillin. RNAi knock-down of vinculin abrogated the FAK-dependent differences in adhesive force. FAK-dependent changes in vinculin localization and adhesive forces were confirmed in human primary fibroblasts with FAK knocked down by RNAi. We demonstrate that FAK reduces steady-state adhesion strength by modulating vinculin recruitment to focal adhesions. These findings provide new insight into the role FAK plays in regulating the mechanical interactions between a cell and the extracellular matrix.

Introduction

Mechanical interactions between a cell and its environment regulate morphogenesis, tissue homeostasis and remodeling and pathogenesis (Benlimame et al., 2005; Hynes, 2002; Kumar and Weaver, 2009; Wozniak and Chen, 2009). Cell adhesion to ECMs provides adhesive forces mediating migratory processes, tissue structure and organization, and mechanotransduction responses (Danen and Sonnenberg, 2003; Hynes, 2002; Ingber, 2003). Adhesion to ECM components such as fibronectin and laminin, is primarily mediated by the integrin family of heterodimeric αβ receptors (Hynes, 2002). After activation and ligand binding, integrins rapidly associate with the actin cytoskeleton and cluster together to form the transmembrane portion of focal adhesions, discrete supramolecular complexes that contain structural proteins, such as vinculin, talin, and α-actinin, and signaling molecules, including FAK, Src, and paxillin (Geiger et al., 2001). Focal adhesions function as structural links, providing strong adhesive forces, and signal transduction platforms between the cell and its extracellular environment. These adhesive complexes are highly dynamic structures that are actively remodeled during cell

migration (Gupton and Waterman-Storer, 2006; Ridley et al., 2003). Assembly/disassembly of focal adhesions is regulated by numerous pathways in response to external stimuli, including growth factors and mechanical force (Greenwood et al., 1998; Ridley and Hall, 1992; Riveline et al., 2001). Whereas the biochemical connections in adhesive interactions have been extensively characterized (Zaidel-Bar et al., 2007), the interplay between molecular composition and adhesive forces remains poorly understood.

FAK, a widely expressed non-receptor protein tyrosine kinase, plays central roles in adhesive interactions by functioning as a scaffold for focal adhesion components, including Src, Cas, talin, and paxillin (Hanks et al., 1992; Polte and Hanks, 1995; Schaller et al., 1992; Schaller et al., 1999; Xing et al., 1994). FAK functions as an integrator of integrin-mediated signaling to regulate cell migration, survival, cell cycle progression and differentiation (Ilic et al., 1995; Owen et al., 1999; Zhao et al., 1998) (Quach et al., 2009; Renshaw et al., 1999; Sieg et al., 2000; Tomar et al., 2009; Webb et al., 2004). FAK expression is essential to development and organogenesis. Deletion of the FAK gene results in early embryonic lethality due to defects in cell migration (Furuta et al., 1995). Tissue-specific knockout of FAK produces functional defects in angiogenesis/vasculogenesis, branching tubulogenesis, innervation and myelination, cardiac development, and blood/testis barrier function (Braren et al., 2006; Forrest et al., 2009; Peng et al., 2008; Shen et al., 2005; Siu et al., 2009; Watanabe et al., 2008; Wei et al., 2009). FAK has also been implicated in tumor invasion and metastasis (Chan et al., 2009; Shibue and Weinberg, 2009). Finally, FAK has emerged as an important

mechanotransducer (Clemente et al., 2007; Leucht et al., 2007; Pirone et al., 2006; Schober et al., 2007; Wang et al., 2001; Young et al., 2009).

FAK-dependent regulation of cell migration involves focal adhesion turnover dynamics (Owen et al., 1999; Wang et al., 2001; Webb et al., 2004). In addition, FAK modulates actin cytoskeleton polymerization and lamellipodia protrusion (Serrels et al., 2007). Whereas roles for FAK in migratory and mechanosensing responses have been established, the contribution of FAK to the generation of adhesive forces is not well understood. We recently demonstrated that FAK promotes integrin activation to enhance the generation of cell-ECM adhesive forces (Michael et al., 2009). These FAK-dependent enhancements in integrin activation and adhesive strengthening only occurred during the early stages of the adhesive process. In the present study, we analyzed the steady-state adhesive interactions and demonstrate that FAK reduces steady-state adhesion strength by modulating vinculin recruitment to focal adhesions. These findings establish a multifaceted role for FAK in the generation of cell-ECM forces.

Materials and Methods

Cells and reagents

Tet-FAK cells were maintained as described previously (Owen et al., 1999). Primary human dermal fibroblasts were kindly provided by A.P. Kowalcyzk (Emory University). The FAK siRNA construct has been described (Benlimame et al., 2005). Retrovirus packaging and transductions were performed as described previously (Byers et al., 2002). Monoclonal antibodies against vinculin (clone V284; Millipore), talin (clone 8d4; Sigma), paxillin (clone Z035; Zymed) and tensin (clone 5; BD Biosciences) were

used for immunostaining. Antibodies against vinculin (clone V284; Millipore) and FAK (06-543 polyclonal; Millipore) were used for Western
blotting.

Micropatterned substrates

Micropatterned substrates were generated by microcontact printing of self-assembled monolayers of alkanethiols on gold (Gallant et al., 2005). Arrays of CH3-terminated alkanethiol [HS-(CH2)11-CH3; Sigma] circles were stamped on to Au-coated glass coverslips using a PDMS stamp (Slygard 184/186 Elastomer-kit). The remaining exposed areas were functionalized with a tri(ethylene glycol)-terminated alkanethiol [HS-(CH2)11-(CH2CH2O)3-OH; ProChimia Surfaces]. Patterned substrates were coated with human plasma fibronectin (20ug/mL), blocked with 1% heat-denatured BSA. This process results in an array of fibronectin-coated circular islands 5μm in diameter spaced 75μm apart to promote single cell attachment to each island.

Adhesion strength assay

Adhesion strength was measured using our spinning disc system (Gallant et al., 2005; Garcia et al., 1998). Micropatterned substrates with adherent cells were spun in PBS+2mM dextrose for 5 minutes at constant speed. The applied shear stress (τ) is given by the formula

$$\boldsymbol{\tau = 0.8r\sqrt{\rho\mu\omega^3}}$$

where *r* is the radial position from the center and ρ, μ, ω are the fluid density, viscocity, and rotational speed, respectively. In some experiments, the spinning buffer was

supplemented with 5% dextran to increase the fluid viscosity. After spinning, cells were fixed in 3.7% formaldehyde, permeabilized in 1% Triton X-100, stained with ethidium homodimer-1 (Invitrogen) and counted at specific radial positions using a 10X objective lens in a Nikon TE300 microscope equipped with a Ludl motorized stage, Spot-RT camera and Image-Pro 6.3 analysis system. A total of 61 fields (80-100) cells per field before spinning were analyzed and cell counts were normalized to the number of cells in the center of the disk. The fraction of adherent cells (*f*) was then fitted to a sigmoid curve

$$f = \frac{1}{(1 + e^{[b(\tau - \tau_{50})]})}$$

where τ_{50} is the shear stress for 50% detachement and *b* is the inflection slope. τ_{50} characterizes the mean adhesion strength for a population of cells.

Focal adhesion assembly

For staining of focal adhesion components, cells were permeabilized in cytoskeleton-stabilizing buffer (0.5% Triton X-100 + 50 mM NaCl + 150 mM sucrose + 3 mM MgCl2 + 20 µg/ml aprotinin + 1 µg/ml leupeptin + 1 mM PMSF + 50 mM Tris, pH 6) for 10 min, fixed in 3.7% formaldehyde for 5 min, blocked in 5% fetal bovine serum, and incubated with primary antibodies against focal adhesion components followed by AlexaFluor-labeled secondary antibodies (Invitrogen). Images were captured using a Nikon 100X objective (1.3 NA) and Spot RT Camera/Software. Focal adhesion area fractions and intensities were quantified using calibrated image analysis software (ImagePro 6.3, Media Cybernetics).

RNA knock-down of vinculin

siRNA pooled sequences encoding for mouse vinculin (M-060130-00-0010) and a non-targeting (D-0 01210-01) negative control were purchased from Dharmacon. FAK-inducible cells were transfected using a Nucleofector II (Amaxa). For each sample, 2 million cells were resuspended in 100 µl of nucleofector solution MEF 2 with 1000 nM siRNA and 2.5 µg of pMAX GFP plasmid and co-transfected using program T-20 (60% transfection efficiency). Twenty-four hours after transfection, cells were FACS-sorted for GFP expression and cultured in appropriate tetracycline condition for 48 h. The spinning disk assay, Western blot, and immunostaining were performed 72 h after initial transfection.

Statistical analysis

Non-linear regression analysis was performed using SigmaPlot 2001 software (SPSS). Analysis of variance (ANOVA) statistical analyses were performed using SYSTAT 11 software.

Results

FAK reduces steady-state adhesion strength

To examine the role of FAK in adhesive force responses, we used FAK-null cells engineered for tetracycline-regulated expression of wild-type and mutant FAK (Tet-FAK cells)(Owen et al., 1999). In these cells, FAK is expressed to high levels in the absence of tetracycline, whereas FAK expression is repressed in the presence of tetracycline in the culture media. In the present study, Tet-FAK cells were maintained in the off-condition (FAK-) and FAK expression was induced at 48 hours prior to any experiment to ensure steady-state FAK levels (FAK+). We analyzed two independent clones with equivalent

results and present results for one clone (clone 46 for wild-type FAK).

Western blot analyses demonstrated that FAK is expressed at high levels in the absence of tetracycline, while FAK expression is repressed in the presence of tetracycline (Fig. 3.1C). This inducible behavior in response to tetracycline is specific for FAK as no differences in expression levels were detected between these two culture conditions for other proteins, including vinculin (Fig. 3.1C). In addition, we further examined levels of the FAK family member Pyk2 for potential compensatory effects in the absence of FAK. It has been reported that loss of FAK expression results in upregulation of Pyk2 levels (Lim et al., 2008). However, we did not observe differences in Pyk2 protein levels in response to inducible FAK expression in Tet-FAK cells (Fig. 3.1C). Thus while Pyk2 upregulation was associated with the establishment of FAK-/- cells and is maintained in Tet-FAK cells (Owen et al., 1999), any differences in the cell behavior resulting from induced FAK expression in the Tet-FAK cells cannot be attributed to further changes in Pyk2 expression.

To analyze cell adhesive responses, Tet-FAK cells were cultured overnight on fibronectin-coated micropatterned substrates (5 μm diameter circles, 75 μm center-to-center spacing) to ensure equivalent adhesive area and cell shape between FAK+ and FAK- conditions. Tet-FAK cells readily adhere and remain constrained to the micropatterned area as single cells, consistent with previous analyses with other cell types (Gallant et al., 2005).

We measured the steady-state levels of adhesion strength for FAK+ and FAK- cells at 24 hours using a hydrodynamic adhesion assay that provides direct and sensitive population-based measurements of adhesive force (Gallant et al., 2005). We previously

demonstrated that steady-state adhesion is reached by 4 hours in this cellular system (Michael et al., 2009). For this adhesion assay, coverslips containing micropattered cells are placed and spun on a rotating disk submerged in buffer at prescribed speeds. The disk rotation generates a well-defined 3-D fluid flow that applies a controlled hydrodynamic force to adherent cells. The hydrodynamic force increases linearly with radial position along the surface of the coverslip, such that cells at the center of the substrate experience negligible forces whereas the applied detachment force increases toward the outer edge of the disk, resulting in decreasing cell numbers. In this manner, a linear range of forces is applied to a large cell population and adhesive strength measurements are obtained for > 6,000 cells in a single experiment. After spinning, adherent cells are fixed and stained, and cell numbers at different radial positions are quantified using a motorized microscope stage and image analysis system. The fraction of adherent cells (f) is calculated by dividing the number of cells in each field by the number of cells at the center of the coverslip, where negligible forces are applied. The detachment profile is then fit to a sigmoid curve to obtain the shear stress for 50% detachment. The shear stress for 50% detachment (τ_{50}) represents the mean adhesive force. Figure 3.1A shows typical detachment profiles (gray circles (FAK+) and squares (FAK-) represent cell densities at a specific radial position and fitted points (filled circles (FAK+), empty circles (FAK-)) and sigmoid fit. The right-ward shift in the detachment profile for the FAK- cells compared to the FAK+ condition indicates a higher adhesive force. The τ_{50} values over several independent experiments were averaged (Fig. 3.1B). FAK- cells exhibited a 33% increase in adhesion strength compared to FAK+ cells ($p < 0.00005$). This finding indicates that FAK reduces steady-state adhesive forces.

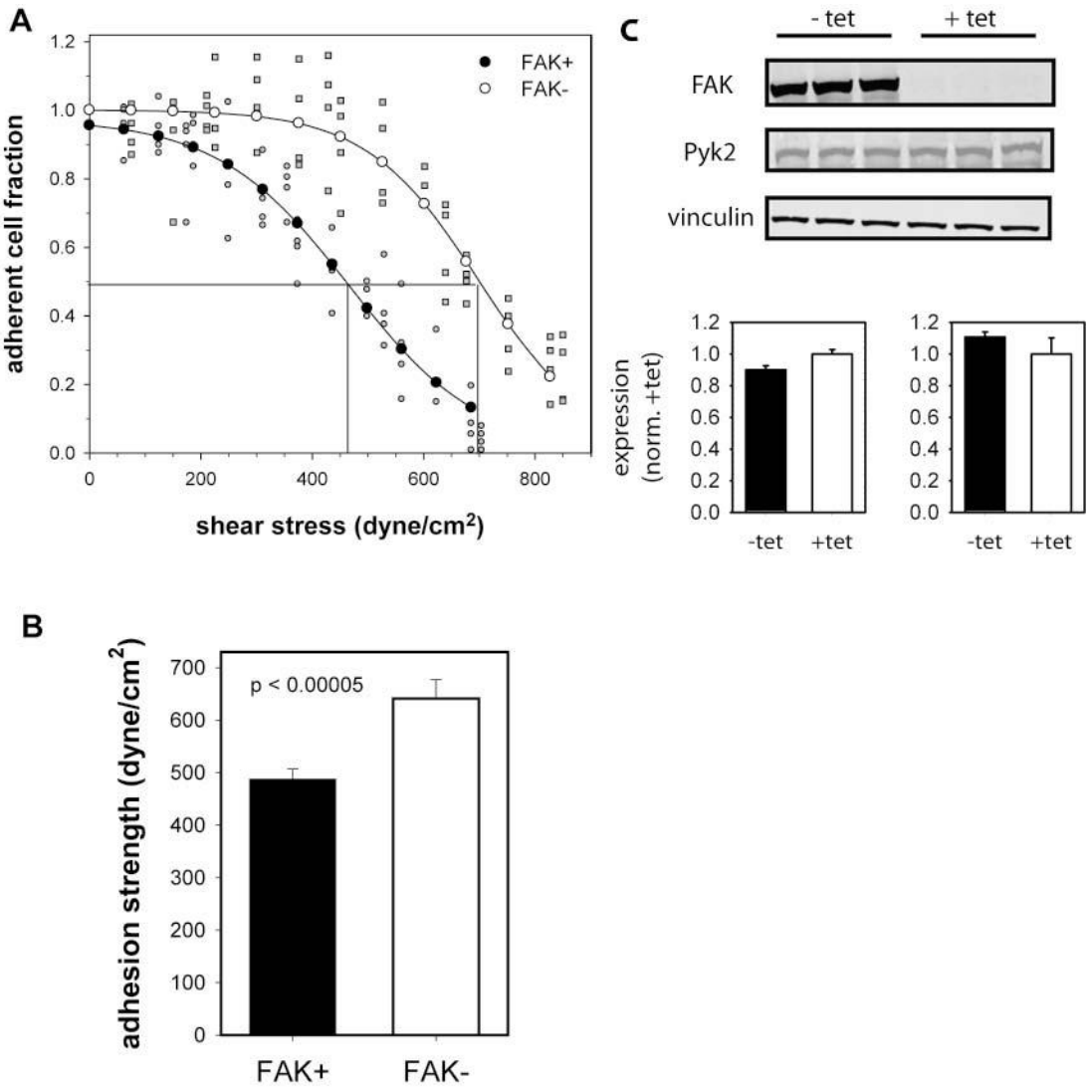

Figure 3.1. FAK modulates steady-state levels of adhesion forces. (A) Adhesive profiles showing the fraction of adherent cells as a function of applied shear stress for FAK-expressing (FAK+) and FAK-null (FAK-) cells. Experimental values (FAK+, grey circles; FAK-, grey squares) were fitted to a sigmoid curve (fit values: FAK+, filled circles; FAK-, empty circles) to obtain the shear stress for 50% detachment, indicated by vertical lines. (B) Mean adhesion strength values showing increased adhesive forces for FAK- cells (mean +/- S.D.). 1 dyne = 10^{-5}N. (C) Tetracycline-regulated expression of FAK in FAK-null cells. In the absence of tetracycline (-tet), FAK expression is activated. Addition of tetracycline to the culture media (+tet) represses FAK expression. No differences in expression levels for Pyk2 or vinculin were observed between tet conditions. Representative Western blots (top) and quantification of protein levels (normalized to FAK-null condition [+tet], bottom) are shown.

FAK modulates steady-state adhesive force via vinculin recruitment to the adhesive interface

The reduction in steady-state adhesion strength for FAK-expressing cells could arise from (i) a decrease in the number of integrin/ECM bonds, (ii) modified position/distribution of bonds, (iii) reduction in the coupling of integrin/ECM bonds to the cytoskeleton (e.g., focal adhesion assembly), or (iv) change in the conformation state of the bound integrins. We previously demonstrated that integrin α5β1 binding to fibronectin provided the dominant adhesion mechanism in this cellular system (Michael et al., 2009). Biochemical analyses of integrin binding revealed no differences in the numbers of bound integrin for FAK+ and FAK- cells at steady state, and no differences in integrin localization within the adhesive interface were observed by immunostaining (data not shown). In addition, we previously demonstrated that there were no differences in the activation state of β1 between FAK+ and FAK- conditions at steady-state (Michael et al., 2009). We therefore postulated that the differences in steady-state adhesive force arise from differences in focal adhesion assembly. We have demonstrated that focal adhesion assembly, independently from integrin binding, contributes significantly to adhesion strength (Gallant et al., 2005). Immunostaining for vinculin demonstrated localization of this cytoskeletal protein around the periphery of the micropatterned contact area for both FAK+ and FAK- cells (Fig. 3.2A). We conducted a comprehensive analysis of vinculin localization focusing on fractional area, intensity (density), and the product of intensity and area (Fig. 3.2A). FAK+ cells exhibited a significant (35%) reduction in the adhesive area occupied by vinculin compared to FAK- cells. There are no differences in mean intensity between FAK+ and FAK- cells. The differences in the

density & area product between FAK+ and FAK- are attributed to differences in focal adhesion area. Differences in recruitment to the adhesive area were specific for vinculin as no differences in staining were detected between FAK+ and FAK- cells for talin, tensin, and paxillin (Fig. 3.2B,C).

Recruitment of focal adhesion components to integrin clusters is expected to increase adhesive force by efficiently distributing mechanical loads among bound integrins. In fact, we previously demonstrated that vinculin recruitment to focal adhesions enhances adhesion strengthening by 30% in fibroblasts (Gallant et al., 2005). We therefore carried out RNAi knock-down experiments to determine the contributions of vinculin to steady-state adhesion strength in FAK+ and FAK- cells. Tet-FAK cells were co-transfected with a GFP plasmid and siRNA duplexes for either vinculin (VCL) or non-targeting control sequence (NT) via nucleofection. After 24 h, cells were sorted for GFP expression and cultured in the appropriate tetracycline condition for 48 h prior to cell adhesion analyses. siRNA VCL knock-down reduces vinculin levels by 80% in FAK+ and FAK- cells (Fig. 3.3A); the non-targeting control sequence has no effects on vinculin levels. Immunostaining analyses demonstrated that vinculin knock-down eliminates the differences in vinculin localization between FAK+ and FAK- cells at 24 h (Fig. 3.3B), whereas significant differences in vinculin localization are still evident between FAK+ and FAK- cells for the non-targeting control siRNA. Notably, vinculin knock-down abrogates differences in steady-state adhesion strength between FAK+ and FAK- cells (Fig. 3.3C). Interestingly, no significant differences in vinculin recruitment or adhesion strength were observed between siRNA-treated and control FAK+ cells. We attribute this finding to residual vinculin localization to focal adhesions since only 15-

20% of the total vinculin pool localizes to focal adhesions (Gallant et al., 2005). Vinculin exhibits a high affinity for localization to focal adhesions and other investigators have experienced difficulties in completely eliminating vinculin localization from focal adhesions via RNAi approaches (S.W. Craig, personal communication). Taken together, these results demonstrate that FAK regulates steady-state adhesive force by modulating vinculin localization to focal adhesions.

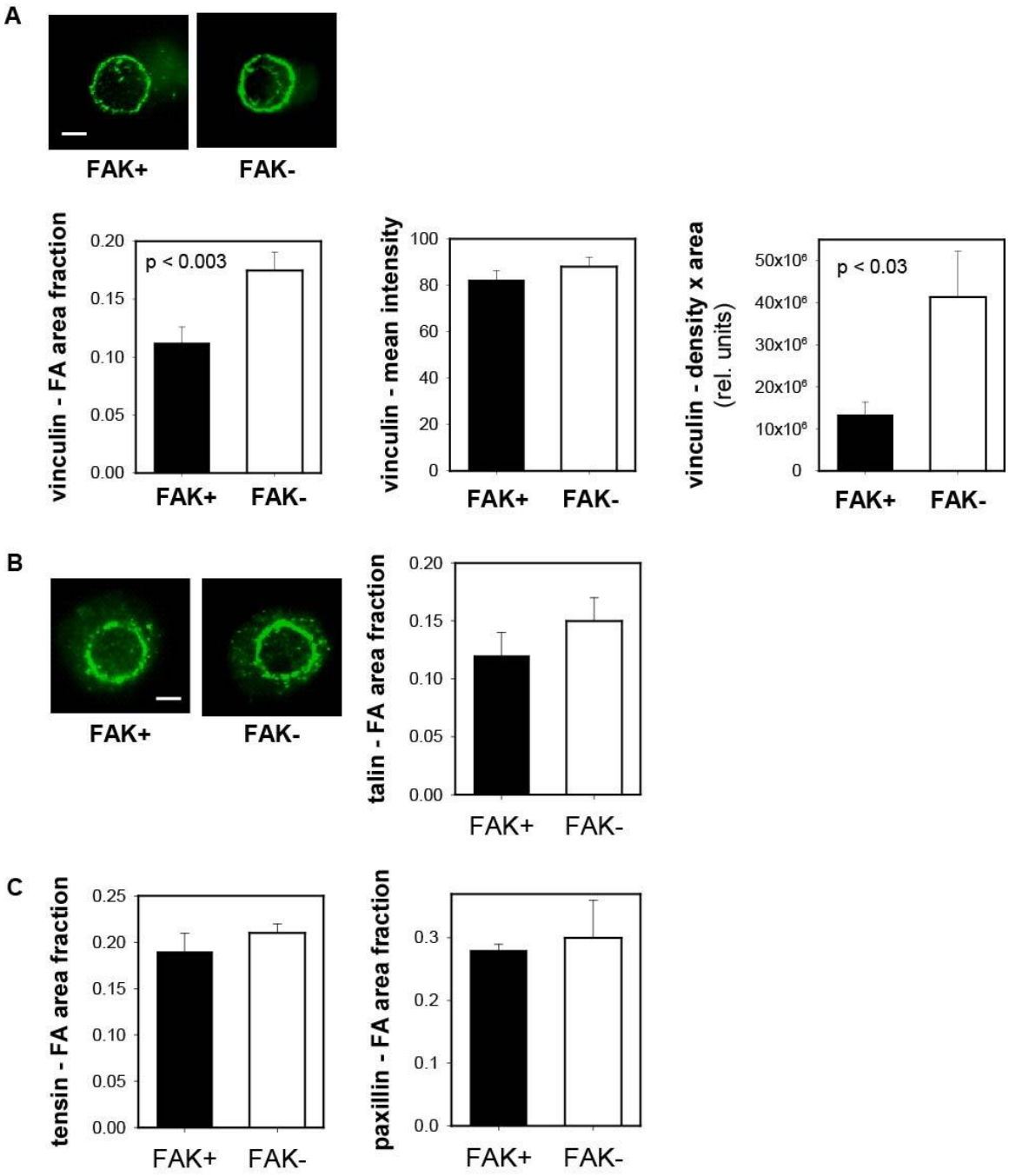

Figure 3.2. FAK modulates vinculin localization to the adhesive interface. (A) Immunostaining for vinculin recruitment to the micropatterned adhesive area, showing differences in the vinculin-containing focal adhesion area (scale bar, 2 μm). Quantification of vinculin-occupied adhesive area, intensity, and area-intensity product shown in the left, middle, and right panels, respectively. (B) Immunostaining (talin) and quantification of focal adhesions (FA) components recruited to micropatterned adhesive area, showing no difference between FAK+ and FAK- cells.

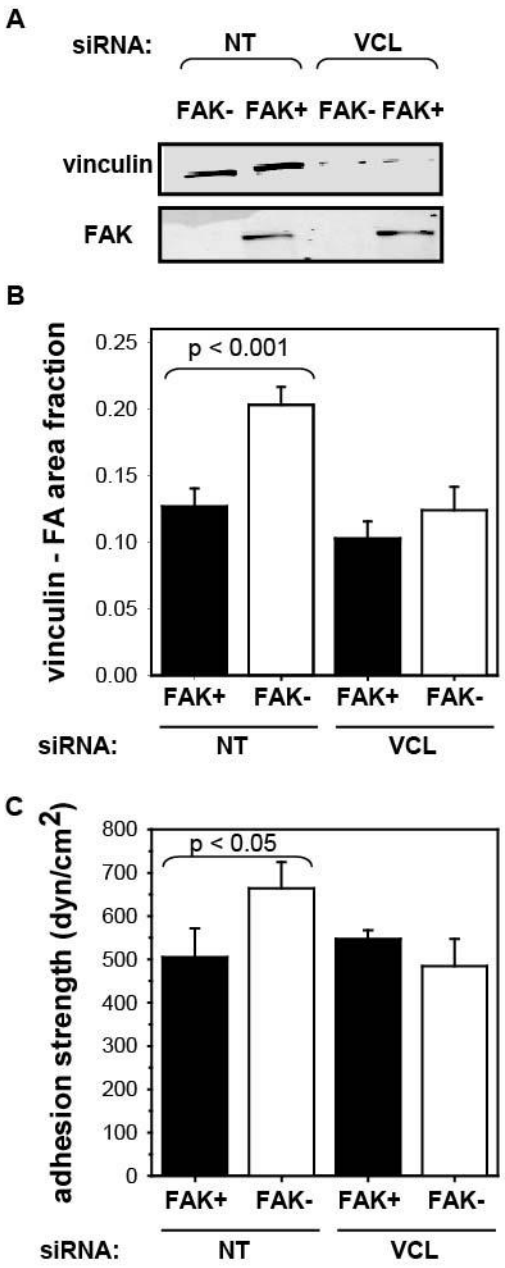

Figure 3.3. FAK regulates steady-state adhesive forces by modulating vinculin localization to focal adhesions. (A) RNAi knock-down reduced vinculin levels by 80% in FAK+ and FAK-. NT, non-targeting control. (B) Vinculin knock-down eliminated differences in steady-state vinculin recruitment to the adhesive area between FAK+ and FAK- cells. (C) Vinculin knock-down eliminated differences in steady-state adhesion strength between FAK+ and FAK- cells. 1 dyne $= 10^{-5}$N.

FAK knock-down in human dermal fibroblasts increases adhesive force and vinculin recruitment

We next examined the effects of FAK expression on adhesion strength and vinculin recruitment in primary fibroblasts to rule out any artifacts associated with the Tet-FAK cells. Human dermal fibroblasts were transduced with FAK siRNA-puromycin or control puromycin retrovirus, and puromycin-resistant cells were selected. Fibroblasts transduced with FAK siRNA retrovirus exhibited a 95% reduction in FAK expression compared to control cells, whereas vinculin and Pyk2 levels remained unchanged (Fig. 3.4A).

Measurements of adhesion strength for micropatterned cells showed 35% higher levels for fibroblasts with knocked-down FAK expression compared to control cells (Fig. 3.4B). This relative increase in adhesion strength is in excellent agreement with the results for the Tet-FAK cells. Furthermore, consistent with our observations for Tet-FAK cells, FAK knock-down enhances vinculin, but not talin, localization to the adhesive area (Fig. 3.4C).

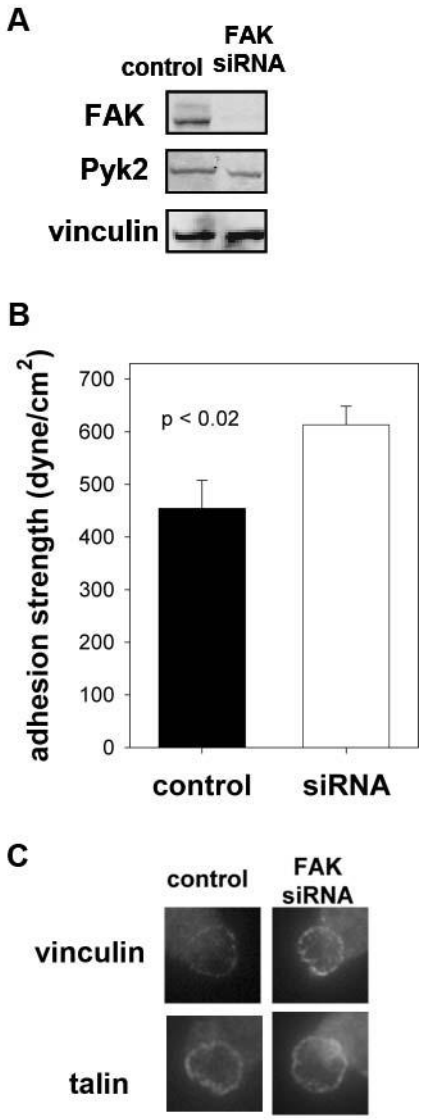

Figure 3.4. FAK knock-down in human dermal fibroblasts modulates adhesive forces. (A) FAK siRNA-puro retrovirus efficiently reduced FAK levels compared with control. No significant differences in Pyk2 or vinculin expression levels were detected. (B) Knock-down of FAK increases cell adhesion strength. (C) FAK knock-down enhances vinculin, but not talin, recruitment to the adhesive interface. 1 dyne = 10^{-5}N.

Discussion

We demonstrate that FAK reduces steady-state adhesive force via vinculin localization to focal adhesions. Vinculin localization to the adhesive interface most likely modulates adhesive force by altering the local distribution of forces at the adhesive

interface (Gallant et al., 2005; Gallant and Garcia, 2007). This work provides new insights into the role of FAK in the generation of adhesive forces involved in mechanical interactions between a cell and its environment. We recently demonstrated that during the early stages of adhesion FAK enhances the adhesion strengthening rate by upregulating integrin activation to enhance integrin binding (Michael et al., 2009). These FAK-dependent changes in integrin activation and binding and adhesive force generation were only observed in the early stages (<1-2 hour) of the adhesion process. In the present study, we demonstrate that, as the adhesive process reaches steady-state, FAK has an opposite effect in adhesive forces by reducing adhesion strength. This down-regulation in adhesive force arises from a separate mechanisms involving vinculin localization to focal adhesions. Once localized to focal adhesions, vinculin is proposed to be the primary functional link between focal adhesions and the actin cytoskeleton (Humphries et al, 2007). Taken together, these results indicate that FAK plays a multi-faceted, time-dependent role in adhesive force generation. These time-dependent, mechanism-distinct roles for FAK in adhesive force generation may be related to the biochemically distinct stages in cell adhesion to fibronectin recently established by Sheetz and colleagues (Zhang et al., 2008). Whereas we demonstrate significant contributions for FAK in adhesive force generation, previous studies with deformable substrates did not reveal a role for FAK in the development of traction forces (Wang et al., 2001; Pirone et al., 2006). We attribute these seemly contradictory observations to fundamental differences among cellular forces. We propose that mechanical interactions between a cell and its environment involve diverse force components (e.g., traction/propulsive, contractile,

tensile, adhesive). Importantly, these factors are not equal and should therefore be considered as distinct entities that together comprise cellular forces.

The mechanism by which FAK regulates the steady-state levels of vinculin localization to the adhesive area has recently been shown to be dependent on FAK-mediated paxillin phosphorylation (Pasapera et al., 2010). Specifically, myosin II activity enhances FAK-mediated phosphorylation of paxillin on tyrosines 31 and 118 and enhances vinculin recruitment to focal adhesions. Importantly, phospho-memetic mutations of paxillin enhance vinculin recruitment in a myosin-II independent manner. That fact that, in our system, FAK-null cells increase adhesion strength by enhancing vinculin recruitment to focal adhesions at first seems contradictory to the Pasapera finding. A closer examination of the Pasapera data reveals that FAK Y397 phosphorylation is not solely responsible for paxillin phosphorylation, and thus, vinculin recruitment to focal adhesions (Pasapera et al., 2010). Interestingly, in a separate study, fluorescence recovery after photobleaching experiments demonstrated that vinculin exchange dynamics within focal adhesions are directly coupled to phosphorylation of tyrosine 1065 ((Mohl et al., 2009)). Specifically, phosphorylation of vinculin decreases as focal adhesions mature and stabilize. We postulate that, in addition to phospho-paxillin-enhanced recruitment, it is possible that FAK phosphorylation of vinculin modifies the dynamics of vinculin in focal adhesions.

CHAPTER 4

CONTRACTILIY MODULATES CELL ADHESION STRENGTH THROUGH FOCAL ADHESION KINASE AND ASSEMBLY OF VINCULIN-CONTAINING FOCAL ADHESIONS*

Abstract

Actin-myosin contractility modulates focal adhesion assembly, stress fiber formation, and cell migration. We analyzed the contributions of contractility to fibroblast adhesion strengthening using a hydrodynamic adhesion assay and micropatterned substrates to control cell shape and adhesive area. Serum addition resulted in adhesion strengthening to levels 30% higher than serum-free cultures. Inhibition of myosin light chain kinase or Rho-kinase blocked phosphorylation of myosin light chain to similar extents and eliminated the serum-induced enhancements in strengthening. Blebbistatin-induced inhibition of myosin II reduced serum-induced adhesion strength to similar levels as those obtained by blocking myosin light chain phosphorylation. Reductions in adhesion strengthening by inhibitors of contractility correlated with loss of vinculin and talin from focal adhesions without changes in integrin binding. In vinculin-null cells,

*Modified from
(1) Dumbauld DW[1], Shin HN[1], Gallant ND, Michael KE, Radhakrishna H, García AJ. *Contractility modulates cell adhesion strengthening through focal adhesion kinase and assembly of vinculin-containing focal adhesions.* J Cell Physiol. 2010.
[1] – authors contributed equally to this work

inhibition of contractility did not alter adhesive force, whereas controls displayed a 20% reduction in adhesion strength, indicating that the effects of contractility on adhesive force are vinculin-dependent. Furthermore, in FAK-null mouse embryonic fibroblasts engineered to express FAK, inhibitors of contractility reduced serum-induced adhesion strengthening as well as eliminated focal adhesion assembly. In contrast, in the absence of FAK, these inhibitors did not alter adhesion strength or focal adhesion assembly. These results indicate that contractility modulates adhesion strengthening via FAK-dependent, vinculin-containing focal adhesion assembly.

Introduction

Integrin-mediated cell adhesion to the extracellular matrix (ECM) plays central roles in various cellular processes including survival, cell cycle progression, and the expression of tissue-specific phenotypes (Danen and Sonnenberg, 2003; Hynes, 2002). Cell adhesion comprises the coordinated evolution of binding of integrin receptors to adhesive domains in ECM ligands, integrin clustering, interactions with the actin cytoskeleton, and focal adhesion assembly (Geiger et al., 2001; Sastry and Burridge, 2000). Focal adhesions are discrete adhesive plaques that contain numerous structural (e.g., vinculin, talin, and α-actinin) and signaling elements (e.g., FAK, Src, paxillin, and p130CAS). Focal adhesions have emerged as putative mechanosensors for extracellular stimuli (Riveline et al., 2001; Wang et al., 2001). For example, external forces exerted on integrins enhance focal adhesion assembly and increase the strength and rigidity of the linkage between integrins and the actin cytoskeleton (Choquet et al., 1997; Geiger et al., 2009; Riveline et al., 2001; Wang et al., 1993). Moreover, focal adhesion assembly plays a key role in the generation of strong traction forces. Following initial integrin binding,

recruitment of focal adhesion components, such as vinculin and talin, result in graded increases in traction forces (Balaban et al., 2001; Galbraith et al., 2002; Tan et al., 2003). Focal adhesion assembly also contributes to cell adhesion strengthening by distributing bond forces along the cell-substrate interface (Gallant et al., 2005; Lotz et al., 1989). Nevertheless, the specific contributions of focal adhesion size and distribution to adhesion strength, independently from integrin-ligand bond strength and cytoskeletal architecture, remain poorly understood.

Contractile forces generated inside the cell regulate migration, neurite extension, cytokinesis, muscle cell contraction, cell cycle progression, angiogenesis and differentiation (Griffin et al., 2004; Mammoto et al., 2009; Mammoto et al., 2004; McBeath et al., 2004; Parizi et al., 2000; Polte et al., 2004; Tanaka and Sabry, 1995; Wozniak et al., 2003). Contractility results from dynamic interactions between actin filaments and myosin, which are regulated via phosphorylation of myosin light chain (MLC) (Kaibuchi et al., 1999; Worthylake and Burridge, 2003). Rho GTPases control the formation of stress fibers and focal adhesion assembly by modulating MLC phosphorylation and generating actin-myosin contractility (Amano et al., 1997; Chrzanowska-Wodnicka and Burridge, 1996; Totsukawa et al., 2000). When activated by serum factors, such as lysophosphatidic acid (LPA), Rho acts through its effector Rho-kinase (also termed ROCK), to enhance the contraction of smooth muscle cells as well as nonmuscle cells by either inactivation of myosin phosphatase (Kimura et al., 1996) or direct phosphorylation of MLC (Totsukawa et al., 2000). Contractile forces can also be modulated by MLC kinase (MLCK), which promotes assembly of actin-myosin filaments and MLC phosphorylation (Gallagher et al., 1997).

The equilibrium of forces within a cell represents a balance of internal contractile forces and anchoring forces to the underlying substrate (Ingber, 2003; Zhu et al., 2000). This complex and dynamic balance is governed by the size and distribution of cell-substrate adhesive structures, cytoskeletal architecture, and spatiotemporally-regulated internal contractile forces. The contributions of actin-myosin contractility to adhesive interactions have been characterized primarily in spreading and migration assays. While these functional measurements have identified key roles for actin-myosin contractility in focal adhesion assembly, stress fiber formation, and migratory forces (Amano et al., 1997; Chrzanowska-Wodnicka and Burridge, 1996; Worthylake and Burridge, 2003), relatively little is known about how actin-myosin contractility and focal adhesion assembly regulate cell adhesive forces. This lack of quantitative understanding of adhesion strengthening limits the interpretation of functional studies of structural and signaling focal adhesion components. Cell spreading and migration assays do not provide direct measurements of adhesion strength and generally serve as implicit indicators of adhesion strength due to the complex spatiotemporal relationships between migration/spreading and adhesion strength. For instance, cell migration speed exhibits a biphasic dependence on adhesion strength (Palecek et al., 1997). In the present study, we used a robust quantitative cell adhesion assay in combination with micropatterned substrates to control adhesive area in order to examine the role of actin-myosin contractility in cell adhesion strengthening.

Materials and Methods

Reagents

Human plasma fibronectin and Dulbecco's phosphate buffered saline (PBS) were obtained from Invitrogen (Carlsbad, CA). Bovine serum albumin, mouse anti-talin and anti-biotin antibodies, and H-7 were purchased from Sigma (St. Louis, MO). Mouse antibody against glyceraldehyde-3-phosphate dehydrogenase (GAPDH), rabbit anti-paxillin, and rabbit anti-α5 antibodies were obtained from Chemicon (Temecula, CA). Biotin-conjugated donkey anti-rabbit and donkey anti-mouse antibodies were obtained from Jackson ImmunoResearch (West Grove, PA). Rabbit anti-FAK and mouse anti-vinculin antibodies were purchased from Upstate Biotechnology (Lake Placid, NY). Rabbit anti-myosin light chain (MLC) 2 (Santa Cruz Biotechnology, Santa Cruz, CA) and rabbit anti-phospho-MLC (Abcam, Cambridge, MA) antibodies were also used. Hoechst 33258, AlexaFluor 488-conjugated antibody against mouse IgG, ethidium homodimer, and rhodamine phalloidin were purchased from Molecular Probes (Eugene, OR). Poly(dimethylsiloxane) (PDMS) elastomers and curing agents were obtained from Dow Corning (Midland, MI). Inhibitors (Y-27632, HA-1077, blebbistatin, and cytochalasin D (CD)) were purchased from Calbiochem (La Jolla, CA). 3,3´-Dithiobis(sulfosuccinimidylpropionate) (DTSSP) was purchased from Pierce Chemical (Rockford, IL). Tri(ethylene glycol)-terminated alkanethiol ($HO(CH_2CH_2O)_3$-$(CH_2)_{11}SH$) was purchased from ProChimia Surfaces (Sopot, Poland). All other reagents including hexadecanethiol ($H_3C(CH_2)_{15}SH$) were purchased from Sigma.

Micropatterned Substrates

Micropatterned arrays of adhesive islands within a non-adhesive background were prepared by microcontact printing of self-assembled monolayers of alkanethiols on gold-coated glass coverslips . A master template featuring circular holes (10 μm diameter) with a 75 μm center-to-center spacing was prepared on a Si wafer. UV light was exposed to a photoresist-coated Si wafer through an optical mask (Gallant and Garcia, 2007a)with the desired pattern. The UB-exposed area was then etched away, leaving a template mold of recessed wells of the pattern. The template was coated with (tridecafluoro-1,1,2,2,-tetrahydrooctyl1)-1-trichlorosilane under vacuum for 30 minutes to facilitate removal of the template from a PDMS stamp following the curing process. PDMS precursors (Slygard 186:184, 10:1) and curing agents were vigorously mixed at 10:1 ratio, poured over the template in a 100 mm diameter glass Petri dish, placed under vacuum for 30 minutes to remove air bubbles, and cured overnight at 65°C. Following curing, the PDMS stamp was peeled from the master template and sonicated in 70% ethanol for 30 minutes. Glass coverslips were cleaned in O_2 plasma using a plasma etcher (Plasmatic Systems, North Brunswick, NJ) for 4 min and coated with Ti (100 Å) followed by Au (150 Å) using an electron beam evaporator (Thermonics, San Leandro, CA). For stamping, the PDMS stamp was sonicated in 70% ethanol for 15 minutes, dried, and placed onto a glass slide for rigid backing. The Au-coated glass coverslip was cleaned under a stream of N_2 and laid down on a glass slide. The patterned face of the PDMS stamp was brushed with 1.0 mM hexadecanethiol (in absolute ethanol) using a cotton swab, blown dry under a stream of N_2 and overlaid onto the Au-coated glass coverslip for 20 seconds. Conformal contact of the stamp with the Au substrate generated CH_3-

terminated circular patterns on the glass coverslip that readily allow protein adsorption and cell adhesion. The coverslip featuring hexadecanethiol islands was subsequently incubated in 1.0 mM ethanolic solution of ($HO(CH_2CH_2O)_3$-$(CH_2)_{11}SH$) for 4 hours to create non-fouling domains around the cell-adhesive islands. The micropatterned substrate was then rinsed twice with 70% ethanol and PBS, coated with fibronectin (20 μg/mL) for 30 minutes, then blocked with heat-inactivated serum albumin (1% w/v) for 30 minutes, and incubated in PBS overnight to elute non-specifically adsorbed fibronectin from non-adhesive regions (Capadona et al., 2003).

Cell Culture and Inhibitor Treatment

Murine NIH3T3 fibroblasts (CRL-1658) were purchased from the American Type Culture Collection (Manassas, VA) and cultured in DMEM containing 10% newborn calf serum, penicillin (100 unit/mL), and streptomycin (100 μg/mL). Vinculin-null and vinculin +/+ mouse embryo fibroblasts were a kind gift from Eileen Adamson and have been previously described (Xu et al., 1998a). Vinculin-/- and vinculin+/+ mouse embryo fibroblasts were cultured in DMEM supplemented with 10% FBS, sodium pyruvate (1 mM), penicillin (100 units/mL), streptomycin (100 μg/mL), and non-essential amino acids (1 mM). Tet-FAK fibroblasts were engineered to express FAK under a tetracycline-regulated promoter have been previously described (Owen et al., 1999). In the presence of tetracycline, FAK expression is repressed, whereas in the absence of tetracycline, high FAK levels are induced. Tet-FAK cells were cultured in DMEM supplemented with 10% FBS, sodium pyruvate (1 mM), penicillin (100 unit/mL), streptomycin (100 μg/mL), amphotericin B (0.25 μg/mL), and non-essential amino acids (1mM) in the absence or presence of tetracycline (1.0 μg/mL) for two days prior to cell

seeding. Cells were enzymatically lifted from the culture dish using trypsin/EDTA and seeded onto micropatterned substrates at 225 cells/mm^2. Cell cultures were maintained for 16 hours in serum-containing media prior to analysis of steady state adhesion (Gallant et al., 2002). For pharmacological treatments, cultures were incubated for 30 minutes prior to analysis in Y-27632 (50 μM), H-7 (500 μM), HA-1077 (50 μM), blebbistatin (250 μM), and CD (1 μM). For serum-free studies, cells were cultured in DMEM supplemented with 1% serum albumin and 0.1% ITS.

Adhesion Assay

Adhesion strength was measured using our spinning disc system. Micropatterned substrates with adherent cells were spun in PBS+2mM dextrose for 5 minutes at constant speed. The applied shear stress (τ) is given by the formula

$$\tau = 0.8r\sqrt{\rho\mu\omega^3}$$

where *r* is the radial position from the center and ρ, μ, ω are the fluid density, viscocity, and rotational speed, respectively. In some experiments, the spinning buffer was supplemented with 5% dextran to increase the fluid viscosity. After spinning, cells were fixed in 3.7% formaldehyde, permeabilized in 1% Triton X-100, stained with ethidium homodimer-1 (Invitrogen) and counted at specific radial positions using a 10X objective lens in a Nikon TE300 microscope equipped with a Ludl motorized stage, Spot-RT camera and Image-Pro 6.3 analysis system. A total of 61 fields (80-100) cells per field before spinning were analyzed and cell counts were normalized to the number of cells in the center of the disk. The fraction of adherent cells (*f*) was then fitted to a sigmoid curve

$$\boldsymbol{f = \frac{1}{(1 + e^{[b(\tau - \tau_{50})]})}}$$

where τ_{50} is the shear stress for 50% detachement and *b* is the inflection slope. τ_{50} characterizes the mean adhesion strength for a population of cells.

Protein Expression and Phosphorylation Levels

Cultures were rinsed in PBS and lysed for 20 min at room temperature in RIPA buffer (150 mM NaCl, 1% Triton X-100, 1% deoxycholate, 0.1% SDS, 150 mM Tris, pH 7.2) containing Na_3VO_4 (0.04% w/v) and protease inhibitors (10 μg/mL leupetin, 10 μg/mL aprotinin, and 350 μg/mL PMSF). The protein content of total cell lysates was determined by microBCA assay (Pierce, Rockford, IL). Identical amounts of cell lysates were mixed in sample buffer (50 mM Tris-HCl pH 6.8, 100 mM DTT, 2% SDS, 10% glycerol, and 0.1% bromophenol blue) and separated by SDS-PAGE (8% or 16% gels). After transferring to nitrocellulose membranes, proteins were visualized by incubating in primary and secondary antibodies and ECF substrate (Pierce, Rockford, IL). Relative amounts of proteins were quantified by image analysis.

Focal Adhesion Assembly

For immunostaining of focal adhesion proteins, adherent cells were rinsed with PBS, fixed in ice-cold formaldehyde (3.7% in PBS) for 3 min, permeablized for 15 minutes in cold 0.5% Triton X-100 containing protease inhibitors (20 μg/mL aprotinin, 1 μg/mL leupeptin, and 350 μg/mL PMSF). After incubating in blocking buffer (5% FBS, 0.1% Tween 20, 0.02% NaN_3 in PBS) for 1 h at 37°C, samples were incubated in primary antibodies for 1 h at 37°C, followed by AlexaFluor488-conjugated secondary antibody, rhodamine phalloidin, and Hoechst 33258 for 1 h at 37°C. For quantification of proteins localized to focal adhesions, micropatterned cells were analyzed by a modified wet

cleaving method (Keselowsky and Garcia, 2005). Briefly, cultures were rinsed with PBS (Ca^{2+}/Mg^{2+} free) containing protease inhibitors. A dry nitrocellulose sheet (PROTRAN BA85, Schleicher & Schuell) was then overlaid onto the cells for 1 min and rapidly removed to isolate cell bodies from basal cell membranes containing focal adhesions. Remaining adhesive structures on surfaces were scraped into sample buffer (100 μL). Western blotting was used for quantitative analysis of recovered focal adhesion proteins.

Integrin Binding

Integrin binding was quantified via a cross-linking/extraction/reversal procedure (Garcia et al., 1999; Keselowsky and Garcia, 2005). After rinsing cultures three times with PBS, DTSSP (1.0 mM in cold PBS + 2 mM dextrose) was incubated for 30 minutes to cross-link integrins to their bound ligands. The cross-linking reaction was quenched by addition of Tris (50 mM in PBS) for 15 minutes. Uncross-linked cellular components were then extracted in 0.1% SDS containing 10 μg/mL leupeptin, 10 μg/mL aprotinin and 350 μg/mL PMSF. Cross-linked integrins to their bound ligands were visualized by immunostaining with α_5 integrin-specific antibodies. Alternatively, bound integrins were quantified by Western blotting following cleaving of the cross-linker in 50 mM DTT and 0.1% SDS for 30 minutes at 37°C.

Statistics

Data are reported as mean ± standard deviation. ANOVA was used with a 95% confidence interval (SYSTAT 8.0, SPSS, Chicago, IL). If ANOVA detected significant differences, Tukey HSD multiple comparison tests were performed to establish treatment effects.

Results

Acto-myosin contractility regulates adhesion strength

Cells were plated on fibronectin-coated micropatterned substrates with dimensions smaller than a cell diameter in order to control adhesive area and cell shape. This approach allows isolation of focal adhesion assembly from changes in cell spreading/shape and provides for direct comparisons among experimental groups. We previously reported that NIH3T3 fibroblasts remained viable for several days when adhering to micropatterned circular islands with dimensions ranging from 2 to 20 μm diameter (Gallant et al., 2005). Cells maintained a round morphology (Fig. 4.1A), and their contact area and focal adhesions were constrained to the micropatterned domain. The 75 μm center-to-center spacing of islands restricted a single cell to occupy one adhesive island, preventing interactions with neighboring cells. To further validate our cell patterning system, we compared the adhesion strength of unpatterned, spread cells with those constrained to 10μm adhesive islands in the presence or absence of serum and LPA (Fig. 4.2A). No significant differences were detected between the patterned and unpatterned cells and their respective treatment groups.

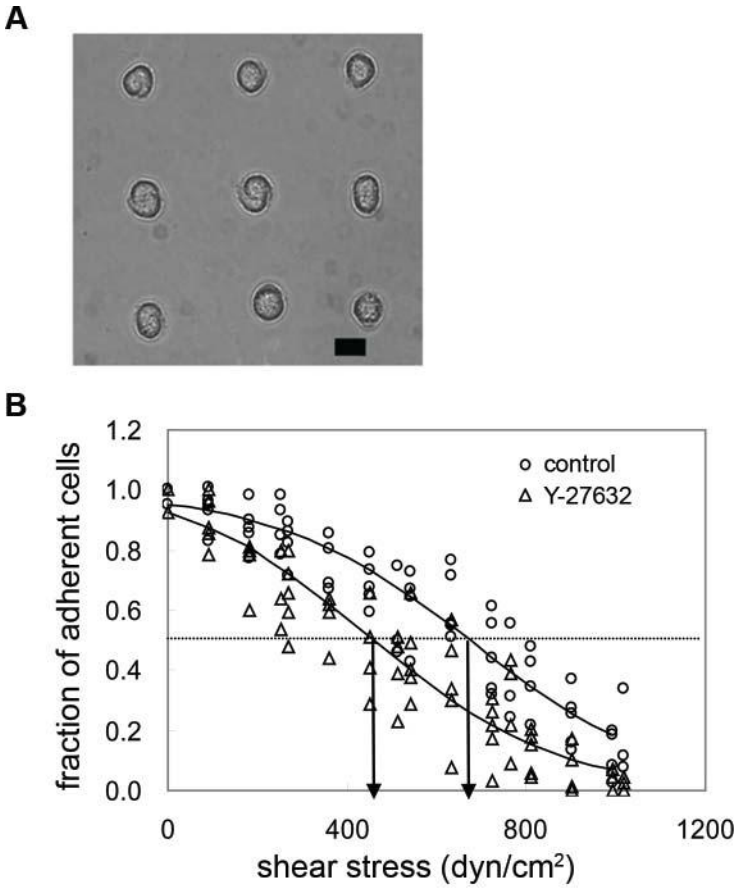

Figure 4.1. (A) Phase contrast image of adherent NIH 3T3 cells cultured for 16 h on micropatterned substrate (scale bar: 10μm). (B) Characteristic detachment profiles showing the fraction of adherent cells (*f*) versus applied shear stress (τ). The shear stress for 50% detachment (indicated by arrows in the profile), τt_{50}, represents the mean adhesion strength. Adhesion strength is 632dyne/cm^2 for untreated control cells, and is shifted left-ward to 451dyne/cm^2 for cell treated with Y-27632 (50μM).

We measured adhesion strength using a spinning disk device that applies a range of well-defined hydrodynamic shear forces to adherent cells (Garcia et al., 1998). For a particular sample, the fraction of adherent cells (*f*) is plotted as a function of the applied shear stress (τ). From this detachment profile, the shear stress for 50% detachment (τ_{50}), which represents the mean cell adhesion strength, is determined. Fig. 4.1B depicts typical detachment profiles showing the fraction of adherent cells vs. applied shear stress. We chose a 16 hour culture time point for analysis of long-term adhesion strength

because it was previously demonstrated that the adhesion strength of NIH3T3 fibroblasts on micropatterned substrates reached constant values by 4 h and remained constant for up to 16 hours (Gallant et al., 2005). Equivalent levels of adhesion strength were observed in serum- and LPA-treated cultures (640 ± 55 dyne/cm^2) (Fig. 4.2A). These values are 30% higher than those for cells cultured under serum-free conditions (450 ± 80 dyne/cm^2).

Because actin-myosin contractility is driven by phosphorylation of MLC, which is regulated by MLCK and Rho-kinase (Gallagher et al., 1997), we used pharmacological inhibitors that impair phosphorylation of MLC to examine the contributions of contractility to adhesion strength. Y-27632 is a specific inhibitor of Rho-kinase (Narumiya et al., 2000). H-7 inhibits phosphorylation of MLCK, which in turn potently blocks phosphorylation of MLC (Volberg et al., 1994). HA-1077 has a broad negative influence on both Rho-kinase and MLCK activity (Yanase et al., 2003). Inhibitor dosage and exposure time were selected from published reports and preliminary experiments showing no gross adverse effects. To examine the contributions of actin-myosin contractility inhibitors to cell adhesion strengthening, we measured adhesion strength of cells exposed to contractility inhibitors for 30 minutes prior to spinning. In general, inhibitors of Rho-kinase and MLCK significantly reduced adhesion strength for cells adhering in the presence of serum as demonstrated by a left-ward shift in the detachment profile (Fig. 4.1B). Adhesion strength values for each inhibitor (409 ± 845 dyne/cm^2 for Y-27632, 468 ± 80 dyne/cm^2 for H-7, and 473 ± 84 dyne/cm^2 for HA-1077) were 30-35% lower than those for untreated controls in the presence of serum (640 ± 55 dyne/cm^2) (Fig. 4.2B). Although Y-27632 and HA-1077 are known inhibitors of Rho-

kinase and actin-myosin contractility, Rho-kinase has other targets and, therefore, may alter cell-matrix adhesion by a mechanism not directly related to contractility (Amano et al., 2000). As an alternative to inhibiting MLC phosphorylation, additional experiments were performed in the presence of blebbistatin, a specific inhibitor of myosin II activity that acts via a distinct mechanism (Kovács et al., 2004). Blebbistatin also reduced serum-induced cell adhesion strength to similar levels (480 ± 110 dyne/cm^2) as the agents that reduce MLC phosphorylation via inhibition of Rho-kinase and MLCK (Fig. 4.2B). Additional experiments under serum-free conditions revealed that these contractility inhibitors do not reduce adhesion strength below levels for untreated, serum-free samples (Fig. 4.2B). Taken together, these results show that actin-myosin contractility accounts for the increases in adhesion strength resulting from serum stimulation. Finally, treatment with cytochalasin D (CD) was included for comparison as CD is expected to modulate adhesion strength via a different mechanism, namely disruption of actin filament polymerization. Cells treated with CD exhibited significantly lower adhesion strength (270 ± 36 dyne/cm^2) than cells treated with any of the contractility inhibitors or cells cultured under serum-free conditions.

Following treatment with these inhibitors, phosphorylation of MLC was analyzed by Western blotting. For equivalent total MLC levels, relative amounts of phosphorylated MLC in cells treated with inhibitors were significantly decreased compared to untreated controls (Fig. 4.2C). There were no differences in MLC phosphorylation levels among inhibitor treatments as determined by quantification of the Western blots in Figure 4.2C . These results confirm essential roles of MLCK and Rho-kinase in MLC phosphorylation. In addition, since all inhibitor treatments reduced MLC

phosphorylation to the same level despite distinct mechanisms of action in blocking actin-myosin contractility, this result suggests that cell adhesion strength is regulated by overall levels of phosphorylated MLC rather than specific effects of Rho-kinase or MLCK.

To elucidate the mechanism by which cell detachment occurred on 10μm islands of fibronectin under the applied forces, cells were spun and stained for vinculin, F-actin, and DNA. For control untreated samples, cells at the center of the disk, which experience low detachment forces, stained positive for vinculin and F-actin (not shown) in a manner similar to unstressed cells. However, at the periphery of the substrate where detachment forces are highest, minimal traces of vinculin (Fig. 4.2D) and F-actin were observed. This negative staining indicates that cell detachment took place at the junction between focal adhesions and the underlying substrate, resulting in removal of the entire cell without gross failure. Similar staining patterns were observed for cells treated with contractility inhibitors (Fig. 4.2D). In contrast, cultures treated with CD displayed significant cytoskeletal debris and vinculin at the periphery of the sample following detachment (Fig. 4.2D). This residual cytoskeletal debris indicates gross cell failure at points above focal adhesions due to loss of cellular integrity arising form impaired actin polymerization. Taken together, these results indicate that inhibition of MLC phosphorylation and contractility does not reduce adhesion strength by compromising cellular integrity and that cell detachment under these conditions occurs at the focal adhesion-substrate interface.

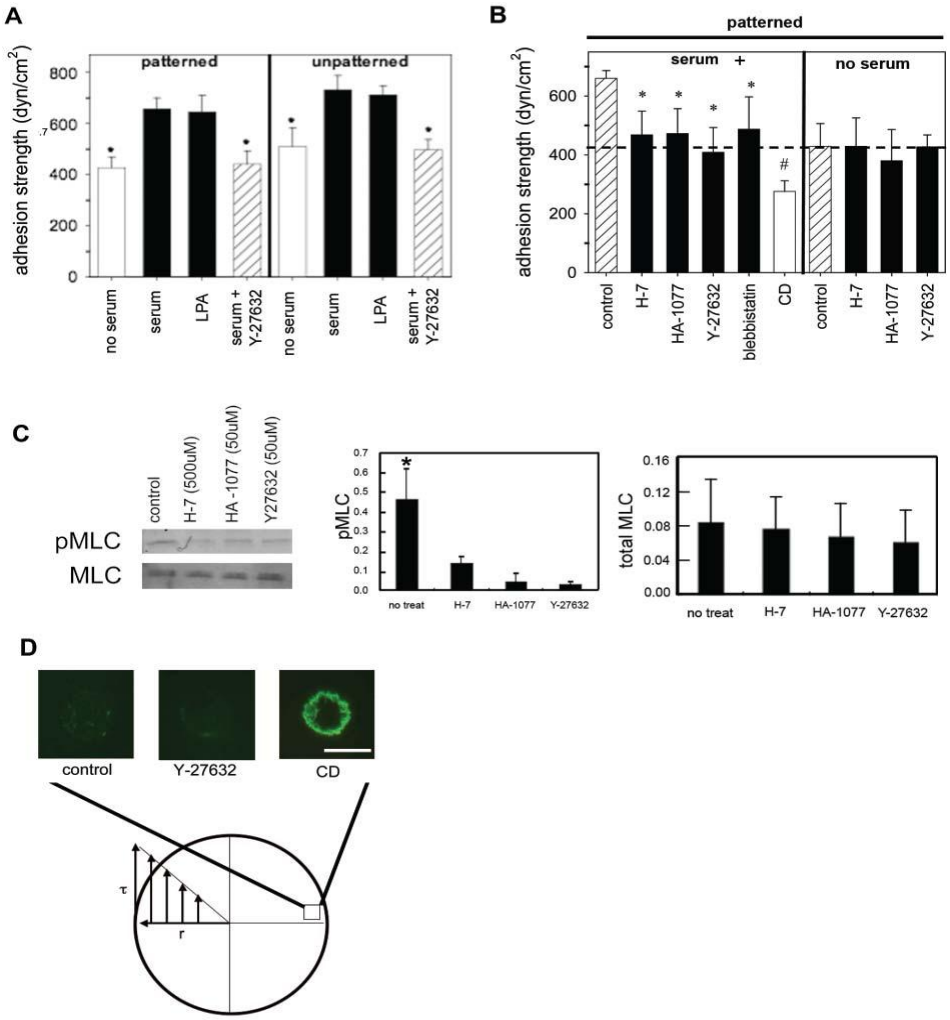

Figure 4.2: Adhesion strength for patterned and spread (unpatterned) NIH 3T3 fibroblasts cultured under serum-containing or serum-free conditions, and treated with LPA and serum supplemented with Y-27632 (50μM) for 30min. Adherent cells were spun and analyzed to determine adhesion strength. *P < 0.04 relative to serum containing controls (mean ± standard deviation, n=3–5). (B) Adhesion strength for micropatterned NIH 3T3 fibroblasts cultured under serum-containing or serum-free conditions, and treated with pharmacological agents for 30min: Y-27632 (50μM), H-7 (500μM), HA-1077 (50μM), blebbistatin (250μM), or CD (1μM). Adherent cells were spun and analyzed to determine cell adhesion strength. *P < 0.05 and #P < 0.01 relative to no treatment controls (mean±standard deviation, n=3–5). Dashed line represents adhesion strength for cells cultured under serum-free conditions. (C) Western blotting (left) for MLC and phosphorylated-MLC in cells cultured in serum-containing media on micropatterned substrates for 16 h and treated with Y-27632 (50μM), H-7 (500μM), and HA-1077 (50μM) for 30min and quantification (right) of protein levels (n=3). (D) Immunostaining for vinculin on adherent cells on micropatterned islands (10mm diameter) of fibronectin located on the periphery of the disk following application of detachment forces. Cells on edge of disk are exposed to maximal detachment force.
Cells treated with vehicle, Y-27632 (50μM), or CD (1μM) (scale bar: 10μm).

Reduction in cell adhesion strength correlates with dissolution of focal adhesions independently of changes in integrin binding

The reduction in adhesion strength as a result of inhibiting MLC phosphorylation is consistent with the role of MLC-mediated contractility in focal adhesion assembly and stress fiber formation. Two mechanisms have been proposed for the regulation of focal adhesion assembly by contractility (Balaban et al., 2001). Tension generated by actin-myosin contractility on adhesion sites may regulate recruitment and assembly of focal adhesion components. Alternatively, contractile forces may trigger changes in integrin binding affinity or bond density within the focal complex. To explore these two possibilities, we first determined whether actin-myosin contractility modulates integrin binding to ECM. We have previously shown that NIH3T3 adhesion to these micropatterned FN islands is mediated by integrin $\alpha_5\beta_1$ (Gallant et al., 2005). Immunofluorescence staining confirmed that bound $\alpha_5\beta_1$ integrins were present throughout the contact area with a preferential localization to the periphery of the adhesive area (Fig. 4.3A). Equivalent staining patterns were observed between control and cells treated with contractility inhibitors, suggesting no differences in integrin intensity or distribution. To confirm these observations, bound integrins were quantified using a biochemical cross-linking/extraction method that isolates integrins bound to fibronectin (Garcia et al., 1999; Keselowsky and Garcia, 2005). Following recovery of bound integrins by cleaving the cross-linker and analysis by Western blotting, no differences in bound $\alpha_5\beta_1$ integrins were detected among control and experimental groups (Fig. 4.3B). These results indicate that integrin binding activity is not altered by changes in actin-myosin contractility.

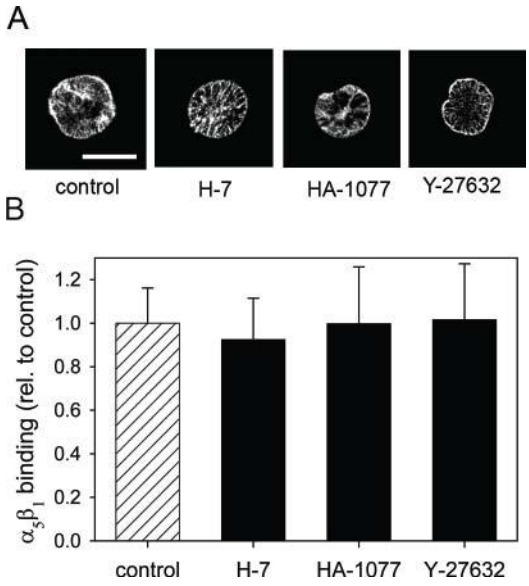

Figure 4.3 Inhibitors of MLC phosphorylation do not alter integrin binding to micropatterned substrates. Cells were cultured on micropatterned substrates for 16 h and treated with inhibitors: Y-27632 (50μM), H-7 (500μM), HA-1077 (50μM), blebbistatin (250μM) for 30min. Bound integrins were cross-linked with DTSSP. After extracting cells, the bound integrins were recovered and analyzed by Western blotting. (A) Immunofluorescence staining for α5 integrin subunit following the cross-linking/extraction showing localization of integrins mostly at the periphery of the substrate. Counter-staining with Hoechst 33258 and rhodamine–phalloidin confirmed complete extraction of unbound cellular components (not shown) (scale bar: 10μm). (B) Relative amounts of bound α5 were quantified by Western blotting and image analysis.

To investigate the recruitment and localization of focal adhesion components to adhesive plaques in response to changes in actin-myosin contractility, two independent but complementary approaches were used. Immunostaining for vinculin showed that untreated cells on micropatterned substrates formed discrete focal adhesion clusters throughout the adhesive island (Fig. 4.4A). Vinculin was spatially segregated and constrained to the circular adhesive domain of micropatterned islands, which was consistent with the localization of F-actin (data not shown). In the absence of inhibitors, the localization of vinculin also corresponded to that of bound $\alpha_5\beta_1$ integrins. These adhesive structures were similar to those previously observed for the same cells cultured

on micropatterned substrates (Gallant et al., 2005). In general, treatment of cells with inhibitors of MLC phosphorylation resulted in disassembly of focal adhesions (Fig. 4.4A). Treatment with Y-27632 and HA-1077 resulted in minimal vinculin clustering in the center of the micropatterned (Fig. 4.4A). Treatment with H-7 inhibited formation of vinculin-containing focal adhesions at both the center and the periphery of the adhesive area. Similar changes in the localization of the structural protein talin were also observed (Fig. 4.4A). In control, untreated cells, talin localized to punctuate structures constrained to the circular adhesive island with a preferential distribution toward the periphery of the adhesive domain. Inhibitors of MLC phosphorylation disrupted talin clustering to various degrees with the most significant effects elicited by Y-27632. Consistent with the dissolution of focal adhesions containing vinculin and talin, inhibitors of Rho-kinase and MLCK also blocked stress fiber formation. The dissolution of focal adhesions by inhibitors of MLC phosphorylation was also confirmed by internal reflection microscopy (IRM) in cells adhering to FN-coated glass substrates. In IRM, areas of 'close' (> 15 nm) cell-substrate contact appear as dark patches (Izzard and Lochner, 1976, 1980). Untreated NIH3T3 cells spread and formed close contacts with the substrate, as demonstrated by the dark line structures (Fig. 4.4B). In contrast, cells treated with Y-27632 for 30 minutes lacked areas of close contacts between the cell membrane and the glass substrate (Fig. 4.4B). These results indicate that, upon addition of inhibitors of MLC phosphorylation, focal adhesions disassemble. To further characterize the changes in focal adhesions, we used a wet-cleaving biochemical technique in which basal cell membranes containing focal adhesive structures are mechanically isolated and analyzed by Western blotting (Gallant et al., 2005; Keselowsky and Garcia, 2005). Inhibitors of MLC phosphorylation

dramatically reduced the localization of vinculin and talin to focal adhesions compared to control cells (Fig. 4.4C and D). There were no differences in protein levels for either vinculin or talin in whole cell lysates, demonstrating that the decreases in vinculin and talin arise from dissolution of focal adhesions. These results are in excellent agreement with our immunostaining observations. These findings indicate that inhibitors of MLC phosphorylation reduce adhesion strength via dissolution of focal adhesions independently of changes in integrin binding.

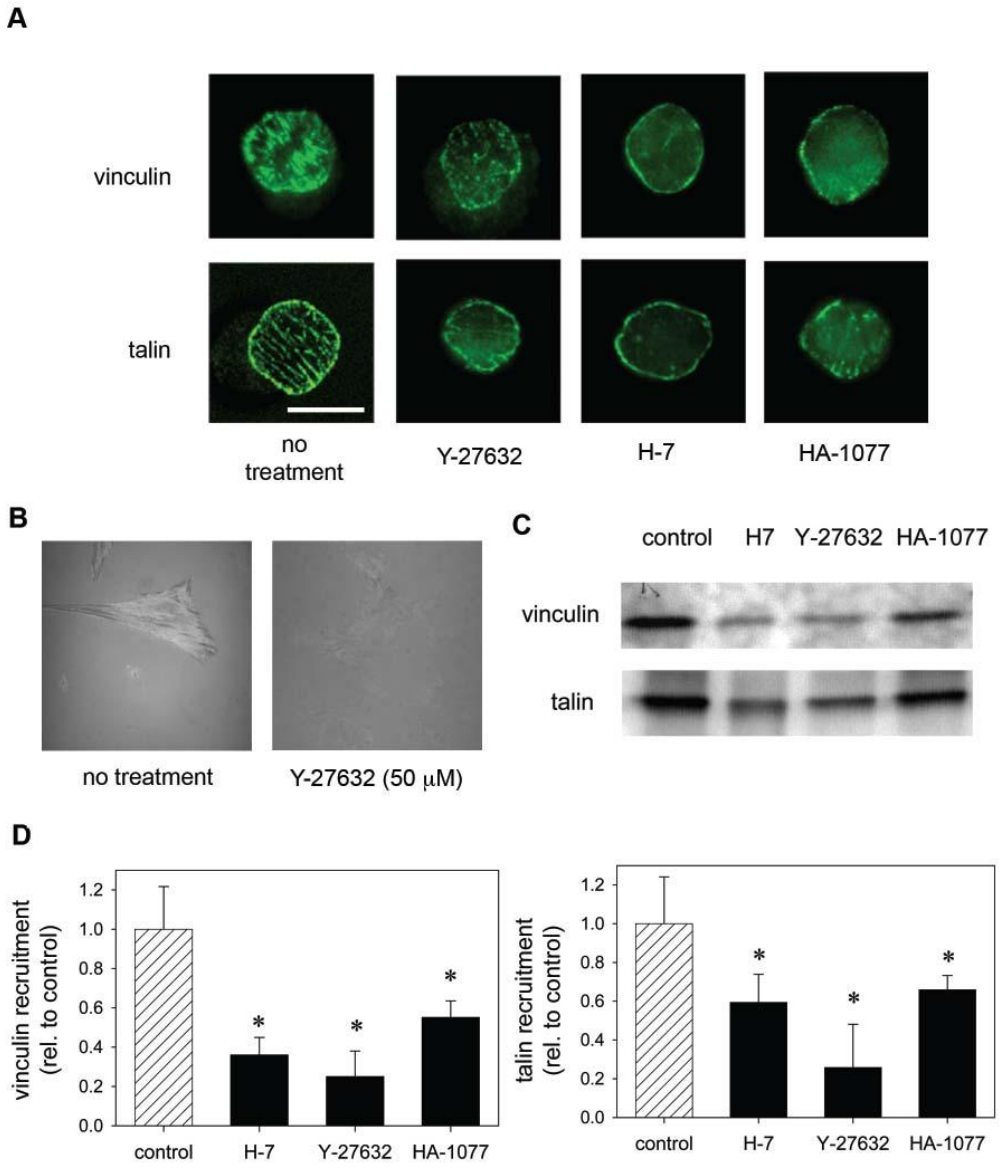

Figure 4.4 Inhibitors of MLC phosphorylation modulate recruitment of vinculin and talin to adhesive structures onmicropatterned substrates. Fibroblasts were cultured on micropatterned substrates for 16 h and treated with Y-27632 (50μM), H-7 (500μM), and HA-1077 (50μM) for 30 min. Controls received fresh media without inhibitors. The cells were then fixed, extracted, and stained for vinculin, talin, or actin (scale bar: 10μm). (B) Inhibition of MLC phosphorylation reduces focal adhesion formation. Fibroblasts were cultured overnight on glass substrates coated with10μg/ml FN and treated with indicated condition 30min before IRM imaging. (C) Inhibitors of contractility modulate recruitment of vinculin and talin to focal adhesions. Western blotting for vinculin and talin recruited to focal adhesions as analyzed by wet-cleaving method. (D) Relative amounts of localized vinculin and talin were analyzed by Western blotting (mean±standard deviation, n=3 from two independent experiments). *P < 0.05
relative to no treatment controls, which received fresh media without inhibitors.

We next examined the role of vinculin in contractility-induced increases in adhesion strength. Vinculin binds between the actin cytoskeleton and integrins and has been implicated in modulating focal adhesion turnover and transmitting mechanical forces (DeMali, 2004; Humphries et al., 2007; Mierke et al., 2008). Using vinculin-null (vinc-/-) and vinculin-expressing (vinc+/+) mouse embryonic fibroblast cells (MEFs), we investigated the role of vinculin in contractility-mediated adhesive force generation. First, we confirmed that the spinning disk detachment profiles for these cells were consistent with those of the NIH3T3 cell lines (Fig. 4.5A). Next, we analyzed the effect of the MLC phosphorylation inhibitor Y-27632 on adhesion strength. Consistent with our data for NIH3T3 cells, vinculin-expressing MEFs showed a 20% reduction in adhesion strength upon exposure to Y-27632 for 30 minutes compared to untreated controls (Fig. 4.5B). In contrast, vinculin-null MEFs showed no decrease in adhesion strength upon exposure to Y-27632 for 30 minutes (Fig. 4.5B). In addition, there were no differences in adhesive force between vinculin-expressing cells treated with Y-27632 and vinculin-null cells. Immunofluorescence staining showed that bound $\alpha_5\beta_1$ integrins were present throughout the contact area with a preferential localization to the periphery of the adhesive area (Fig. 4.5C). Importantly, no differences in the intensity or localization of bound integrins could be detected between the treatment groups indicating that adhesion strength differences did not arise from differences in integrin binding. These findings indicate that vinculin expression is required for contractility-induced increases in adhesion strength.

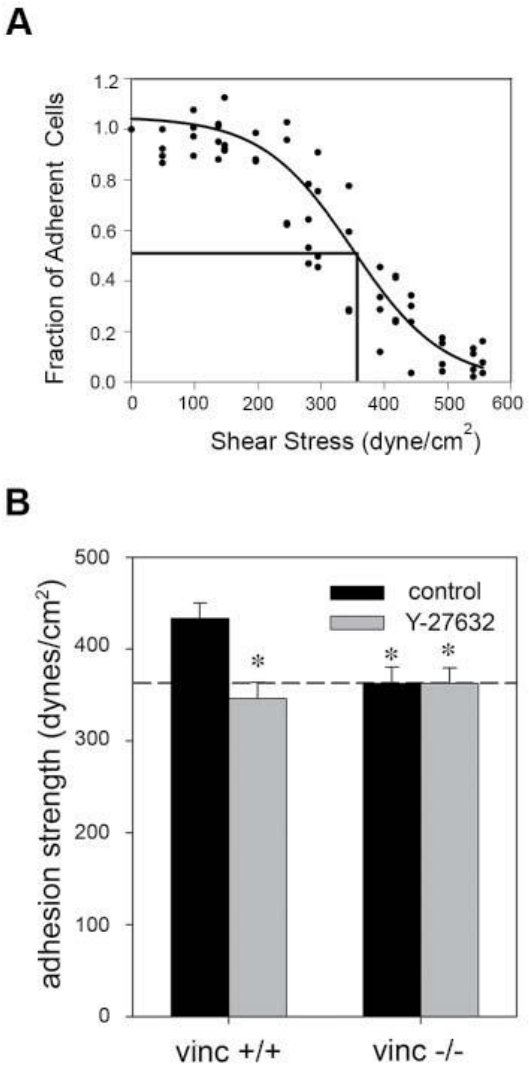

Figure 4.5 Loss of vinculin abolishes differences in adhesion strength because of contractility independent of bound integrin levels. (A) Characteristic detachment profile for vinculin +/+ and vinculin -/- MEFs showing the fraction of adherent cells (f) versus applied shear stress (t). These cells exhibit the same detachment profiles as the NIH3T3 cells. (B) vinculin+/+ and vinculin -/- MEFs were cultured for 16 h on micropatterned surfaces and treated with Y-27632 (50μM) for 30 min prior to spinning. The no-treatment group received fresh media without inhibitor. Addition of inhibitor resulted in a 20% decrease in adhesion strength for the vinculin +/+ cells. No differences in adhesion strength were detected for the vinculin -/- cells. *P < 0.03 relative to no treatment vinculin +/+ MEFs. (C) Immunoflourescence staining for α5 integrin subunit following cross-linking/extraction showing localization of integrins mostly at the periphery of the substrate (scale bar: 10μm). Treatment with Y-27632 (50μM) for 30min did not significantly alter integrin binding.

Effects of MLC phosphorylation on cell adhesion strength are FAK-dependent

FAK is a central regulator of focal adhesions and adhesive interactions (Hanks et al., 1992; Ilic et al., 1995). Furthermore, it is well established that inhibition of contractility reduces tyrosine phosphorylation of focal adhesion components, including FAK (Chrzanowska-Wodnicka and Burridge, 1996). In addition, we recently demonstrated that FAK regulates the early stages of the adhesion strengthening process via changes in integrin activation (Michael et al., 2009). To examine the effects of contractility on FAK phosphorylation in micropatterned cells, protein and phosphorylation levels in the presence of inhibitors of MLC phosphorylation were analyzed by Western blotting. Consistent with the effects on MLC phosphorylation and adhesion strength, all contractility inhibitors tested reduced phosphorylation of FAK at the autophosphorylation site Y397 compared to untreated controls with no differences in total FAK levels (Fig. 4.6). These results are in excellent agreement with previous observations for spread cells (Chrzanowska-Wodnicka and Burridge, 1996).

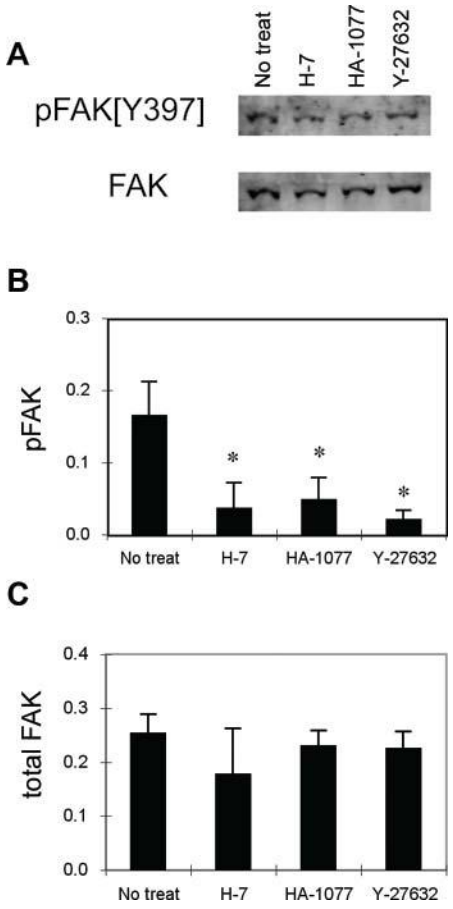

Figure 4.6 FAK phosphorylation is regulated by inhibitors of MLC phosphorylation. Cells were cultured on micropatterned substrates for 16 h and treated with inhibitors for 30min. (A) Western blotting for pFAK [Y397] and total FAK. Relative amounts of (B) pFAK [Y397] and (C) total FAK. The results represent two independent experiments with mean±standard deviation (n=3). *P < 0.05 relative to no treatment controls that received fresh media without inhibitors.

The role of FAK in contractility-mediated adhesion strengthening was examined using Tet-FAK cells. Tet-FAK cells are stable clones derived from FAK-/- mouse embryo fibroblasts engineered to express FAK under a tetracycline-responsive promoter (Owen et al., 1999). In the presence of tetracycline, FAK expression is repressed and these cells have no FAK (FAK–); removal of tetracycline from the culture media results in expression of FAK (FAK+) to similar levels as wild-type fibroblasts (Fig. 4.7A). This inducible system allows examination of the effects of FAK in the same cell population,

without non-specific effects from dominant-negative constructs or clonal variation. Tet-FAK cells, induced and non-induced to express FAK, adhered to fibronectin-coated micropatterned substrates in a similar fashion as NIH3T3 fibroblasts. Consistent with our observations with NIH3T3 fibroblasts, the Rho-kinase inhibitor Y-27632 reduced MLC phosphorylation for Tet-FAK cells in the presence and absence of FAK without changing levels of total MLC (Fig. 4.7B). Higher Y-27632 concentrations were required to reduce MLC phosphorylation in cells without FAK, consistent with higher expression levels of Rho-kinase in these cells (Chen et al., 2002). Adhesion strength in the presence and absence of inhibitors of contractility was determined using the spinning disk assay. In FAK+ cells, treatment with Y-27632 reduced adhesion strength by 30% compared to untreated cells (Fig. 4.7C). Furthermore, treatment with Y-27632 also reduced localization of vinculin to focal adhesions (data not shown). The decrease in adhesion strength and reduced localization of vinculin to focal adhesions are in excellent agreement with the 35% decrease in adhesion strength observed in NIH3T3 fibroblasts (Fig. 4.2A) and reductions in vinculin localization to focal adhesions (Fig. 4.4D). Remarkably, in FAK– cells, inhibition of MLC phosphorylation by Y-27632 did not reduce cell adhesion strength (Fig. 4.7C) or alter focal adhesion assembly (data not shown). We note that the FAK- and FAK+ control conditions are normalized values, not meant for direct comparison. These results indicate that the contractility-mediated cell adhesive forces require FAK expression.

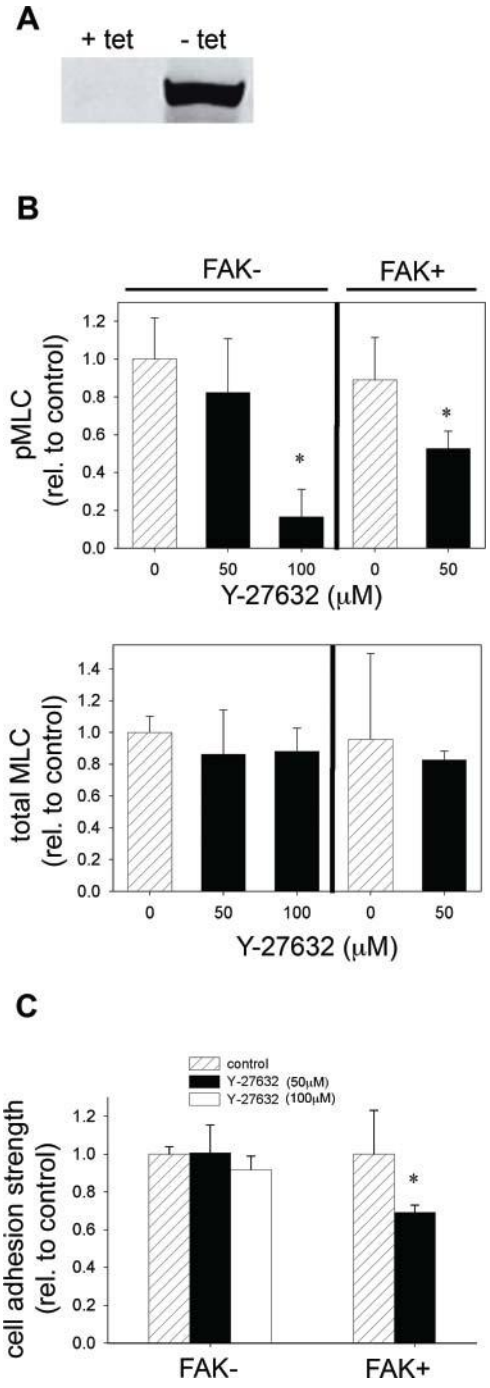

Figure 4.7 Rho-kinase modulates cell adhesion strength via FAK. (A) Tet-FAK cells with inducible FAK expression. In the absence of tetracycline (tet), FAK expression is induced at high levels, while expression is repressed in the presence of tet. Tet-FAK cells expressing FAK (FAK+) and cells without FAK (FAK-) were cultured on micropatterned surfaces for 16 h and treated with Y-27632 (50 or 100μM) for 30min. (B) Inhibitor of Rho-kinase reduced adhesion strength in the presence of FAK, but adhesion strength was not altered in the absence of FAK. *P < 0.05 relative to untreated controls of corresponding FAK condition.

Discussion

We tested the hypothesis that actin-myosin contractility regulates cell adhesion strengthening via modulation of focal adhesion assembly. While previous reports have shown that Rho-mediated actin-myosin contractility drives focal adhesion assembly and regulates cells spreading and migration (Arthur and Burridge, 2001; Chrzanowska-Wodnicka and Burridge, 1996), the specific contributions of contractility to cell adhesion strengthening are not well understood. Recent evidence supports a complex relationship between the state of contractility in a cell and its adhesion to the underlying matrix (Griffin et al., 2004). Moreover, it is not clear how localized, directional traction forces involved in migration are integrated to regulate overall levels of adhesion strength. Although the size of focal adhesion structures shows correlation to the level of traction force generated (Balaban et al., 2001; Galbraith et al., 2002; Tan et al., 2003), focal adhesion size does not solely control adhesion strength (Tan et al., 2003), as integrin-ligand bond strength, actin cytoskeleton architecture, and the spatiotemporal distribution of focal adhesions also regulate adhesion strength (Gallant et al., 2005). In order to control cell adhesive area and position as well as cell shape, we examined adhesion strength for cells cultured on micropatterned substrates. This approach allows for direct comparisons of adhesive force among experimental groups by eliminating differences in adhesive area/distribution and cell morphology. Adhesions strength was quantified using a hydrodynamic detachment assay that applies a wide range of forces and provides sensitive measurements of adhesion strength (Garcia et al., 1999). Equivalent levels of adhesion strength were observed between serum- and LPA-treated cultures (data not shown). These values are 30% higher than those for cells cultured under serum-free

conditions. Since LPA induces Rho-dependent contractility (Chrzanowska-Wodnicka and Burridge, 1996), this result suggests that activation of contractility enhances adhesion strength. To impair actin-myosin contractility, cells were treated with pharmacological agents that inhibit either Rho-kinase (Y-27632) or MLCK (H-7 and HA-1077). Due to their high specificity and our ability to precisely control timing and concentration of dosage, we use chemical inhibitors of contractility throughout this study. We note that several previous studies have relied exclusively on the use of these same inhibitors (Chen et al., 2002; Chrzanowska-Wodnicka and Burridge, 1996; Delanoe-Ayari et al., 2004; Totsukawa et al., 2000). Treatment with any of these inhibitors eliminated the serum-induced enhancements in adhesion strength by >95% to levels indistinguishable from serum-free cultures. Furthermore, these inhibitors did not reduce adhesion strength for cells cultured in the absence of serum, indicating that the effects of serum stimulation on adhesion strength were regulated by actin-myosin contractility. Moreover, blocking myosin II activity with blebbistatin, which acts through a different mechanism, had equivalent effects on adhesion strength. These results demonstrate that actin-myosin contractility is responsible for serum-induced enhancements in adhesion strength. Despite distinct mechanisms of action in blocking actin-myosin contractility (Rho-kinase vs. MLCK vs. myosin II activity), all inhibitors tested reduced adhesion strength to similar values. Since all inhibitor treatments reduced MLC phosphorylation to the same levels, this result suggests that cell adhesion strengthening arising from serum or LPA stimulation is regulated by overall levels of phosphorylated MLC. Consistent with our observations, Chrzanowska-Wodnicka and Burridge showed that inhibition of MLC phosphorylation via different mechanisms leads to inhibition of Rho-induced focal

adhesion assembly and stress fiber formation (Chrzanowska-Wodnicka and Burridge, 1996).

Treatment with these inhibitors of contractility also resulted in the dissolution of focal adhesions as indicated by reduced localization of vinculin and talin to adhesion structures, in agreement with previous reports (Chrzanowska-Wodnicka and Burridge, 1996). Both inhibitors of Rho-kinase and MLCK reduced recruitment of talin and vinculin to adhesive plaques to similar levels, consistent with their effects on adhesion strength. Although distinct roles and spatial activities for Rho-kinase and MLCK in spread fibroblasts have been reported (Totsukawa et al., 2000), we observed no significant differences between these two regulators of MLC phosphorylation, possibly due to the constrained micropatterned adhesive domains. Because no differences in integrin binding in response to treatment with contractility inhibitors were observed, we attribute the contractility-mediated differences in adhesive force to changes in focal adhesion assembly. Indeed, experiments with vinculin-null cells demonstrated that vinculin was required for the contractility-dependent differences in adhesive force. Recruitment of vinculin and other structural components to adhesion plaques enhances adhesion strength by increasing the local membrane stiffness thereby modulating bond stressing in the contact area (Gallant and Garcia, 2007b; Gallant et al., 2005; Goldmann and Ingber, 2002; Wang et al., 1993). Interestingly, inhibition of MLC-driven contractility did not alter integrin binding, in terms of bound density and distribution, to the ECM. In contrast to our observations, Friedland et al. recently reported that $\alpha_5\beta_1$ integrins do not cross-link to FN when cells were serum-starved overnight and exposed to inhibitors of contractility (Friedland et al., 2009). The differences between this study and

the present findings may be attributed to differences in available adhesive area (fully spread vs. micropatterned) and the duration of exposure to both serum-free conditions and inhibitors. Taken together, our results indicate that actin-myosin contractility modulates recruitment of cytoskeletal elements to adhesion plaques independently of integrin binding. A possible mechanism for this recruitment is that contraction-driven forces applied to the adhesion plaque concentrates or "focuses" cytoskeletal elements (e.g., vinculin, talin) into clusters (Palecek et al., 1997; Wolfenson et al., 2009). Alternatively, application of forces to integrins or integrin-associated elements may lead to conformational changes favorable to the recruitment of focal adhesion proteins, such as vinculin (del Rio et al., 2009; Hytonen and Vogel, 2008). In contrast to our observations, Chrzanowska-Wodnicka and Burridge reported that contractility also modulates integrin distribution in spread fibroblasts (Chrzanowska-Wodnicka and Burridge, 1996). The discrepancy between this study and the present findings may be attributed to differences in available adhesive area (fully spread vs. micropatterned cells).

Inhibitors of contractility also down-regulated tyrosine phosphorylation of FAK, consistent with previous reports (Chrzanowska-Wodnicka and Burridge, 1996; Gallagher et al., 1997; Wozniak et al., 2003). Given the central role of FAK in focal adhesion turnover (Ilic et al., 1995; Webb et al., 2004), we examined the role of FAK in contractility-mediated adhesion strengthening using cells with inducible expression of FAK. In the presence of FAK, inhibitors of contractility reduced serum-induced adhesion strengthening as well as eliminated focal adhesion assembly, in excellent agreement with our observations for NIH3T3 fibroblasts. In the absence of FAK, however, these inhibitors did not alter adhesion strength or focal adhesion assembly.

These results indicate that actin-myosin contractility modulates adhesion strengthening via FAK-dependent organization of focal adhesions. While it is well established that FAK plays central roles in modulating focal adhesion turnover and cell motility (Ilic et al., 1995; Ren et al., 2000; Webb et al., 2004), this is the first report demonstrating a direct role for FAK in serum-dependent increases in steady-state adhesive force. This finding contrasts with the view that modulation of FAK activity (phosphorylation) is a downstream event following contractility-driven focal adhesion assembly (Chrzanowska-Wodnicka and Burridge, 1996). Our results implicate FAK in regulating adhesion strengthening via focal adhesion assembly. This function is distinct from the role of FAK in modulating focal adhesion turnover (Webb et al., 2004) and promoting directional persistence in motility and reorientation in response to mechanical forces (Wang et al., 1993). Furthermore, the FAK-dependent effects of contractility on adhesion strengthening contrast the actions of FAK and contractility on cell spreading and migration. Chen et al. reported that inhibition of Rho-kinase by Y-27632 in FAK-/- fibroblasts induced spreading and enhanced cell motility with concomitant reorganization of focal adhesions (Chen et al., 2002). These authors concluded that Rho-kinase leads to formation of actin-myosin filaments at the periphery of FAK-/- cells, which generate contractile forces that reduce cell migration. These results are consistent with the observation that FAK suppresses Rho activity to promote focal adhesion turnover (Ren et al., 2000). The distinct effects of the interplay of contractility and FAK on migration and adhesion strengthening highlight the complex interactions in these two adhesive processes. Finally, we note that we recently established a role for FAK in the modulation of initial adhesive forces via changes in integrin activation (Michael et al., 2009). The

role of FAK in the contractility-mediated changes in steady-state focal adhesion assembly and adhesion strengthening described in the present study appears to be distinct from these earlier adhesive processes.

In summary, we demonstrate that actin-myosin contractility controls serum-dependent cell adhesion strengthening. Phosphorylation of MLC, either via Rho-kinase or MLCK, was central to the strengthening process by modulating focal adhesion assembly and required vinculin to achieve maximum adhesion strength. Notably, the effects of MLC phosphorylation on adhesion strengthening were mediated by FAK, implicating this adhesion kinase in the generation of strong adhesive forces.

CHAPTER 5

CONTRIBUTIONS OF VINCULIN HEAD AND TAIL DOMAINS TO INTEGRIN BINDING, FOCAL ADHESION ASSEMBLY, AND ADHESION STRENGTH

Abstract

Vinculin, a 116 kDa focal adhesion (FA)-associated protein, plays an essential role in various cellular processes including migration, adhesion, and mechanotransduction. Vinculin-dependent regulation of FA dynamics requires a conformational change involving release of strong binding between the head and tail domains of the protein. Once activated, vinculin regulates FA dynamics by binding to talin with its head domain and F-actin with its tail domain. While significant progress has been made in identifying how vinculin modulates its interactions with its numerous binding partners, little is known about how the protein contributes to the generation of adhesion force. Using vinculin-null cells expressing wild-type and mutant vinculins under an inducible tetracycline promoter, we analyzed the role of vinculin in the generation of steady-state adhesive forces using micropatterned substrates and a hydrodynamic adhesion assay. Vinculin expression increased adhesion strength by an average 25% in two separate vinculin-null fibroblast cell lines. Mutations inhibiting strong head-tail interactions (T12), resulting in a constitutively open vinculin

conformation, increased adhesions strength by 50% over null controls. Surprisingly, expression of tail-less vinculin (VH) increased adhesion strength to the same level as wild-type vinculin, suggesting that vinculin localization to FA, independently from binding to actin, contributes significantly to adhesive force. It also indicates, however, that interactions of the tail domain with the actin cytoskeleton are required for maximal vinculin enhancements to adhesive force. Analysis of fibronectin (FN)-bound integrins showed that both T12 and VH mutations increased the area of integrin staining by 200% compared to WT vinculin and null controls. T12 and VH mutations also increased the amount of talin and vinculin localization to micropatterned islands over both WT and null controls indicating that vinculin modulates adhesion strength by increasing both integrin binding and focal adhesion assembly. Adhesion strength comparisons among cells transiently transfected with head, tail, or a combination of head and tail demonstrated that the physical linkage between the head and tail domains of vinculin is critical for achieving maximum adhesion strength. These findings provide new insights into the role of vinculin in regulating mechanical interactions between the cell and the extracellular matrix.

Introduction

Cell adhesion to extracellular matrix (ECM) provides adhesive forces mediating migratory processes, tissue structure and organization, and mechanotransduction responses (Danen and Sonnenberg, 2003; Fu et al., 2010; Hynes, 2002). Adhesion to ECM components such as fibronectin and laminin, is primarily mediated by the integrin family of heterodimeric αβ receptors (Hynes, 2002). Integrin-mediated adhesion is a highly coordinated process initiated by activation and binding of the integrin to its ECM

ligand (Choquet et al., 1997; Faull et al., 1993; Friedland et al., 2009). Once bound, integrins rapidly cluster together and generate linkages to the actin cytoskeleton mediated by the supramolecular structures termed focal adhesions (FA) (Geiger et al., 2001). Morphologically, FAs are long, flat structures typically located near the periphery of the cell. There, they mediate strong adhesion to the ECM by modulating force transfer between integrins and the actin cytoskeleton (Gallant et al., 2005; Riveline et al., 2001; Tan et al., 2003)(Vogel and Sheetz, 2006). In addition to their structural role, FAs serve as signaling platforms that control various functions including differentiation, proliferation, and apoptosis (Sastry and Burridge, 2000). Focal adhesions are highly dynamic structures that are actively remodeled in response to external and stimuli including growth factors and cues from the extracellular matrix (Greenwood et al., 1998; Ridley and Hall, 1992; Riveline et al., 2001) These supramolecular structures constitute a central hub in the mechanostranduction machinery, exhibiting force-responsive changes in shape, size, and composition (Bershadsky et al., 2006).

Vinculin, a 116 kDa F-actin binding protein, is an important regulator of FA dynamics (Cohen et al., 2006; Humphries et al., 2007). In order to associate with FA, a conformational change in the vinculin must occur. This change constitutes release of strong binding between the head and tail domains of the protein, revealing a talin binding site on the head domain and an F-actin binding site on the tail (Cohen et al., 2006). Importantly, the head and tail of the vinculin molecule are connected via a pro-line rich strap which spatially constrains the two portions of the protein to close proximity of each other, giving rise, in part, to the strong association constant between the two domains (Bakolitsa et al., 2004; Cohen et al., 2005). The exact mechanism of head and tail

separation has yet to be fully elucidated (Cohen et al., 2005; Cohen et al., 2006; Izard et al., 2004). Once activated, vinculin regulates FA dynamics by binding to talin with its head domain and F-actin with its tail domain (Chen et al., 2005; Humphries et al., 2007). Activated vinculin is only found in FA (Chen et al., 2005). Once localized to FAs, the molecule can transmit force between talin and F-actin (Grashoff et al., 2010). It is important to note while no detectable strain is applied to the protein when it lacks a tail (Grashoff et al., 2010), this does not imply that this same protein cannot contribute to adhesion strength. As our lab as shown (Gallant et al., 2005), only 30% of adhesion strength comes from focal adhesion assembly. The other 70% is matrix-bound integrins (Gallant et al., 2005). The spatial localization of the FA within the cell modulates the level of mechanical tension across the molecule as well as its dynamics with the adhesion (Grashoff et al., 2010; Wolfenson et al., 2009). Despite extensive characterization of the structure of vinculin and its role in cellular processes including regulating FA dynamics and cell migration, the contribution of vinculin to the generation of adhesive forces has yet to be fully characterized. For instance, previous work has shown that talin binding is critical for vinculin activation and localization to FAs (Cohen et al., 2006), however, how this integrin-talin-vinculin complex, independent from binding the actin cytoskeleton, modulates adhesion strength is unknown. The functional importance of vinculin tail binding to the cytoskeleton is complex. On one hand the integrin-talin complex, by itself, can bind the actin cytoskeleton directly, potentially minimizing the importance of vinculin connection (Critchley, 2004). On the other, experimental work has demonstrated that the retrograde flow of FAs is dependent on the ability of vinculin to bind both talin and the contractile cytoskeleton (Humphries et al., 2007), suggesting that

the mechanical coupling of vinculin between integrin-talin complex and the cytoskeleton is important for proper focal adhesion function.

In the present study, we use a robust, quantitative cell adhesion assay in combination with micropatterned substrates to control adhesive area along with cells engineered to express wild-type vinculin to characterize the contribution of vinculin to adhesion strength. Structural mutants of the protein were used in combination with various biochemical techniques to characterize the functional contributions to adhesion strength of the head and tail domain of the protein. We demonstrate that both the head and tail domain of vinculin contribute to the generation of adhesive forces and that the physical connection between the two in required for generation of maximum adhesion strength.

Materials and Methods

Cells and reagents

Mouse embryonic fibroblasts (MEF1 and MEF2) were a kind gift from Eileen Adamson (Burnham Institute, La Jolla, CA). Monoclonal antibodies against vinculin (clone V284; Millipore), talin (clone 8d4; Sigma) were used for immunostaining and Western blotting. Monoclonal antibody against extracellular domain of β1-integrin (9EG7, Millipore) was used for integrin binding study. Polyclonal antibody against β1-integrin (ab1950, Chemicon) was used for adhesion blocking study (note this antibody is no longer available). Poly(dimethylsiloxane) (PDMS) elastomers and curing agents were obtained from Dow Corning (Midland, MI). Dithiobis(sulfosuccinimidylpropionate) (DTSSP) was purchased from Pierce Chemical

(Rockford, IL). Tri(ethylene glycol)-terminated alkanethiol ($HO(CH_2CH_2O)_3$-$(CH_2)_{11}SH$) was purchased from ProChimia Surfaces (Sopot, Poland). All other reagents including hexadecanethiol ($H_3C(CH_2)_{15}SH$) were purchased from Sigma. Human plasma fibronectin was purchased from Invitrogen (Carlsbad, CA). VH-CFP and vinT-YFP constructs were a kind gift from Christoph Ballestrem (The University of Manchester, UK).

Retroviral vectors for eGFP-vinculin expression

Retroviral plasmids pTJ66-tTA and pXF40 were previously described (Gersbach 2006). eGFP-C1 WT, T12, VH vinculin plasmids were a kind gift from Susan Craig (Johns Hopkins School of Medicine, Baltimore, MD). One AgeI restriction site was inserted into the multiple cloning site of pXF40, the retroviral expression vector. The oligonucleotides 5'-AGCTTGTCAGCTACCGGTGCTACTGCA-3' and 5'-AGCTTGCAGTAGCACCGGTAGCTGACA-3' (AgeI sequences underlined) were annealed together, creating HindIII-compatible overhands at each end. This product was then ligated into a linearized pXF40 vector which had been digested with HindIII. Finally, the eGFP- vinculin constructs were digested from the pEGFP-C1 with AgeI and SalI and ligated into the SalI and AgeI-digested pXF40 vector. The pXF40-eGFP-Vinculin vectors transcribe the eGFP-vinculin gene from the tetracycline-inducible promoter (Fig. 5.1A). All vectors were verified by sequencing the ligation points.

Retroviral Transduction with eGFP-Vinculin into Vinculin-null Mouse Embryonic Fibroblasts

Retroviral stocks were produced by transient transfection of helper virus-free Phoenix amphotropic producer cells with plasmid DNA as previously described (Byers, 2002). Vinculin-null mouse embryonic fibroblasts (cell lines 1 & 2) were cultured and plated on tissue culture polystyrene at 2 $x10^4$ cells/cm^2 24 h prior to retroviral transduction. Cells were transduced with 0.2 ml/cm^2 of equal parts pTJ66-tTA and pXF40-eGFP-Vinculin retroviral supernatant supplemented with 4 μg/ml hexadimethrine bromide (Polybrene) and 10% fetal bovine serum, and centrifuged at 2500 r.p.m. (1200 g) for 30 min in a Beckman model GS-6R centrifuge with a swinging bucket rotor. Retroviral supernatant was replaced with growth media (DMEM, 10% fetal bovine serum, 100U/ml penicillin G sodium, 100 μg/ml streptomycin sulfate, 1% non-essential amino acids, 1% sodium pyruvate). Five days after transduction, eGFP expressing cells were FACS sorted, expanded, and either used for experimentation or cyropreserved in liquid nitrogen for later use. Expression of vinculin constructs was verified by Western blot and immunofluorescence microscopy.

Micropatterned substrates

Micropatterned substrates were generated by microcontact printing of self-assembled monolayers of alkanethiols on gold (Gallant et al., 2002). Arrays of CH_3-terminated alkanethiol [$HS-(CH_2)_{11}-CH_3$] circles were stamped on to Au-coated glass coverslips using a PDMS stamp (Sylgard 184/186 Elastomer-kit). The remaining exposed areas were functionalized with a tri(ethylene glycol)-terminated alkanethiol [$HS-(CH_2)_{11}-(CH_2CH_2O)_3-OH$]. Patterned substrates were coated with human plasma fibronectin (2 μg/mL), blocked with 1% heat-denatured BSA. This process results in an

array of fibronectin-coated circular islands 5μm in diameter spaced 75μm apart to promote single cell attachment to each island.

Adhesion Strength Assay

Adhesion strength was measured using our spinning disc system (Gallant et al., 2005; Garcia et al., 1997; Garcia et al., 1998). Micropatterned substrates with adherent cells were spun in PBS + 2mM dextrose for 5 minutes at constant speed. The applied shear stress (τ) is given by the formula

$$\tau = 0.8r\sqrt{\rho\mu\omega^3}$$

where *r* is the radial position from the center of the patterned coverslip and ρ, μ, ω are the fluid density, viscosity, and rotational speed, respectively. In some experiments, the spinning buffer was supplemented with 5% dextran to increase the fluid viscosity. After spinning, cells were fixed in 3.7% formaldehyde, permeabilized in 1% Triton X-100, stained with ethidium homodimer-1 (Invitrogen) and counted at specific radial positions using a 10X objective lens in a Nikon TE300 microscope equipped with a Ludl motorized stage, Spot-RT camera and Image-Pro 6.3 analysis system. A total of 61 fields (80-100) cells per field before spinning were analyzed and cell counts were normalized to the number of cells in the center of the disk. The fraction of adherent cells (*f*) was then fitted to a sigmoid curve

$$f = \frac{1}{(1 + e^{[b(\tau - \tau_{50})]})}$$

where τ_{50} is the shear stress for 50% detachment and *b* is the inflection slope. τ_{50} characterizes the mean adhesion strength for a population of cells.

Integrin Binding

Integrin binding was quantified via a cross-linking/extraction procedure (Garcia et al., 1999; Keselowsky and Garcia, 2005). After rinsing cultures three times with PBS, DTSSP (1.0 mM in cold PBS + 2 mM dextrose) was incubated for 30 minutes to cross-link integrins to their bound ligands. The cross-linking reaction was quenched by addition of Tris (50 mM in PBS) for 15 minutes. Uncross-linked cellular components were then extracted in 0.1% SDS containing 10 μg/mL leupeptin, 10 μg/mL aprotinin and 350 μg/mL PMSF. Cross-linked integrins to their bound ligands were visualized by immunostaining with β_1 integrin-specific antibodies.

Focal Adhesion Assembly

For staining of focal adhesion components, cells were permeabilized in cytoskeleton-stabilizing buffer (0.5% Triton X-100: 10 mM PIPES buffer, 50 mM NaCl, 150 mM sucrose, 3mM $MgCl_2$, 0.5% (v/v) Triton X-100, 1 mM PMSF, 1 μg/mL leupeptin, 1 μg/mL aprotinin, 1 μg/mL pepstatin) for 10 min, fixed in 3.7% formaldehyde for 5 min, blocked in 5% goat serum, and incubated with primary antibodies against focal adhesion components followed by AlexaFluor-labeled secondary antibodies (Invitrogen). Images were captured using a Nikon Eclipse E400 equipped with a 60X APO (1.4 NA) TIRF objective and Spot RT Camera/Software. Focal adhesion area fractions were quantified using a custom MATLAB image analysis script. Briefly, original images of

immunostained cells were first background subtracted and then pixel intensity thresholded to determine focal adhesion area.

Transient Transfection of Vinculin-eGFP constructs

MEF1 cells were transfected using a Nucleofector II (Amaxa). For each sample, 2 million cells were resuspended in 100 µl of nucleofector solution MEF 2 with 2.5 µg of plasmid DNA coding for indicated vinculin-eGFP construct. Plasmid containing cell suspension was loaded into Nucleofector cuvette and transfected with program T-20. Immediately after transfection, cells were transferred to 1.5mL centrifuge tube containing 500 µL of pre-warmed RPMI 1640 (Invitrogen) and incubated for 15 minutes to minimize cell death. Cells were then transferred into 100 mL plates containing normal growth media (1% P-S, 1% NEAA, 1% Sodium Pyruvate, 10% fetal bovine serum, Dulbecco's Modified Eagle Medium). Cells were fluorescence active cell sorted (FACS) 72 hours after transfection for eGFP expression and seeded onto micropatterned surfaces. The next day, the spinning disk assay and immunostaining were performed.

Adhesion Blocking

Cells were trypsinized from dish, quenched in serum containing media, pelleted, and resuspended in appropriate blocking antibody or isotype control for 15 minutes with gentle rocking. Cells were seeded on micropatterned substrates for 15 min prior to visualization.

Western blotting

Cells were washed with PBS and lysed in cold radioimmunoprecipitation assay (RIPA) buffer (1% Triton X-100, 1% sodium deoxycholate, 0.1% SDS, 150 mM NaCl, 150 mM Tris-HCl pH 7.2, 350 μg/ml phenylmethylsulfonyl fluoride, 10 μg/ml leupeptin, 10 μg/ml aprotinin, and 1 mM sodium orthovanadate) for 20 min. Lysates were pipette up and down ~25 times to shear the DNA and then clarified by centrifugation at 10,000g for 10 min. Protein concentration was then determined using a Micro BCA protein assay kit (Pierce, Rockford, IL). Equal amounts of protein (25 μg) were boiled in Laemmli sample buffer (2% SDS, 10% glycerol, 100 mM DTT, 60 mM Tris-HCl pH 6.8, and 0.001% bromophenol blue) for 10 min and separated by SDS-PAGE. Proteins were transferred by electrophoresis onto nitrocellulose membranes and blocked with Blotto (5% non-fat dry milk, 0.02% sodium azide, 0.2% Tween 20 in PBS w/o Ca^{2+}/Mg^{2+}) overnight at 4ºC. Membranes were then incubated with appropriate antibodies in Blotto for 1 h at room temperature under gentle rocking. Membranes were washed in TBS-Tween (20 mM Tris HCl pH 7.6, 137 mM NaCl, 0.1% Tween 20) for 30 min and incubated in near-infrared conjugated-secondary antibodies (LiCor Biosciences, Lincoln, NE) for 30 minutes followed by 30 min washing in TBS-Tween. Membranes were imaged with a LiCor Odyssey Imager (LiCor Biosciences, Lincoln, NE).

Statistical Analysis

Non-linear regression analysis was performed using SigmaPlot 2001 software (SPSS). Analysis of variance (ANOVA) statistical analyses were performed using SYSTAT 11 software.

Results

Inducible retroviral system for vinculin-eGFP expression

Because of the central role of vinculin in regulating adhesive interactions, we developed an inducible expression retroviral system to express wild-type and mutant vinculins in vinculin-null cells. Our inducible system is based on the well-characterized tetracycline inducible promoter (Gossen et al., 1994). In the absence of anhydrotetracycline (aTc), a more potent version of tetracycline, the tetracycline-controlled transactivator (tTA) binds the tet operon and activates transcription of the gene of interest. However, in the presence of sub-toxic levels of aTc, the antibiotic binds tTA, blocking binding of the tet operon and subsequent transactivation. Two independent vinculin-null mouse embryonic fibroblast cell lines were transduced simultaneously with pTJ66-tTA and pXF40-WT-Vinculin-eGFP retroviral supernatants (Fig. 5.1A). A significant advantage of this system is that it allows for direct comparison of the effects of vinculin in the same cell population. Vinculin-eGFP positive cell populations were enriched by fluorescence-activated cell sorting for a minimum of three sequential rounds (data not shown). Western blotting using vinculin specific antibodies confirmed expression of vinculin-eGFP constructs in both lines of transduced vinculin-null MEFs (Fig. 5.1B). Culturing MEF2 cells in the presence of anhydrotetracycline (aTc, 100ng/mL) significantly lowered the levels of vinculin-eGFP expression. . We next examined proper localization of vinculin-eGFP to focal adhesions by fluorescence microscopy (Fig. 5.1C). Briefly, MEF1 and MEF2 cells were seeded overnight on fibronectin (FN) coated coverslips. The following day, cells were fixed with 4% paraformaldehyde, mounted on glass slides and visualized using a fluorescence

microscope equipped with an eGFP-specific filter cube (Fig. 5.1C). MEF1 cells are smaller, migrate faster, and replicate more rapidly than MEF2 cells (data not shown). In addition, the general morphology of MEF1 cells is more fibroblastic than MEF2 cells. In both cell lines, eGFP-vinculin properly localized to FA.

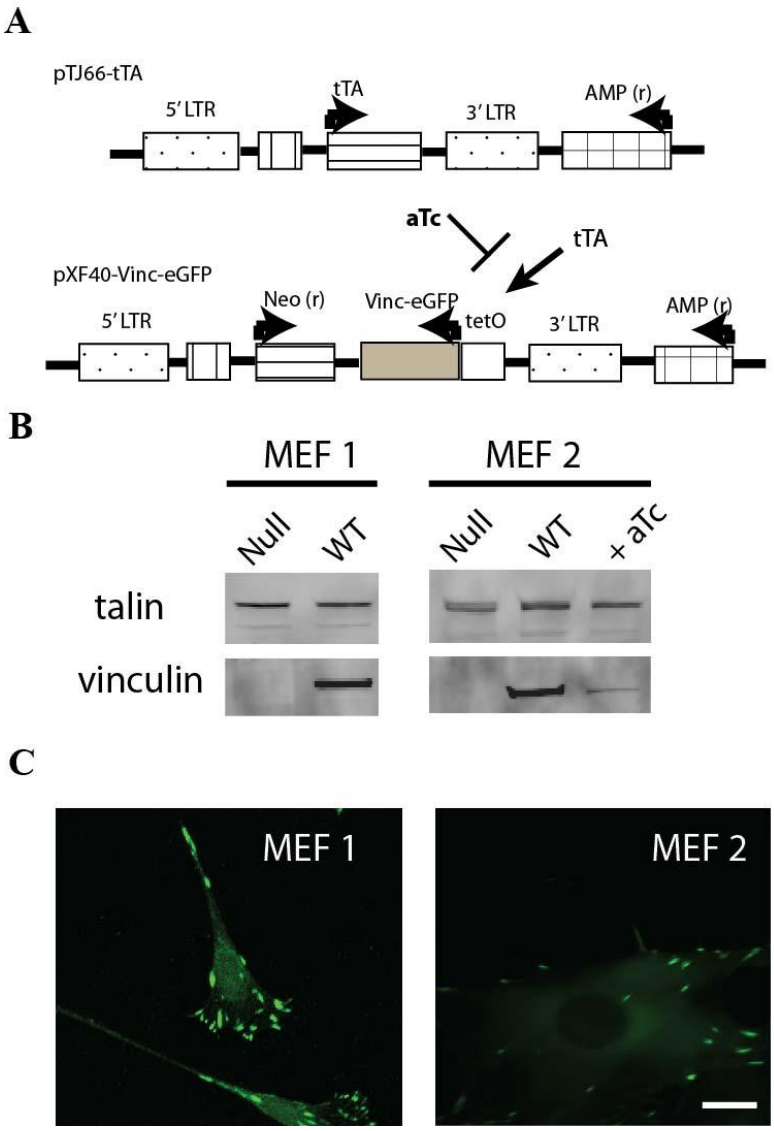

Figure 5.1 Development of retroviral vinculin expression system . (A) Retroviral vectors. The tetracycline-controlled transactivator (tTA) is constitutively expressed by pTJ66-tTA. Vinculin-eGFP expression is controlled via the tet operon of pXF40-Vinc-eGFP. (B) Western blot of expression for talin and vinculin in two separate vinculin-null mouse embryonic fibroblast (MEF) lines. MEFs were tranduced and a stable population expressing vinculin-eGFP was selected. (C) Vinculin-eGFP properly localizes to focal adhesions in spread MEFs on fibronectin-coated glass substrates (scale, 10μm).

Micropatterned substrates to control adhesive area and cell shape

FN-coated micropatterned substrates with dimensions smaller than a cell diameter in order to control adhesive area and cell shape were produced using micropatterned self-assembled monolayers of alkanethiols on gold using standard procedures (Fig. 5.2A) ((Gallant et al., 2002)). First, a PDMS stamp was created by casting PDMS pre-polymer and curing agent into a rigid mold with recessed features. Following heat-induced curing, the PDMS stamp is released from the mold. Next, the stamp is inked with methyl-terminated alkanethiol and then brought into conformal contact with an Au-coated glass coverslip. Once in contact, the methyl-terminated alkanethiol molecules transfer from the stamp to the Au-surface to form a patterned self-assembled monolayer (SAM). Non-printed areas of the Au-substrate are backfilled with tri(ethylene glycol)-terminated alkanethiol to create a protein adsorption resistant SAM. The entire substrate is washed and incubated with FN, which preferentially adsorbs to the patterned, methyl-terminated SAMs (Fig. 5.2B, inset 1). This approach allows isolation of focal adhesion assembly from changes in cell spreading/shape and provides for direct comparisons among experimental groups. We previously reported that NIH3T3 fibroblasts remained viable for several days when adhering to micropatterned circular islands with dimensions ranging from 2 to 20 μm diameter (Gallant et al., 2005). Vinculin-null MEF1 cells, re-expressing vinculin-eGFP maintained a round morphology, and their contact area and focal adhesions were constrained to the micropatterned domain of 10 μm diameter circles (Fig. 5.2B, inset 2). The 75 μm center-to-center spacing of islands restricted a single cell to occupy one adhesive island, preventing interactions with neighboring cells.

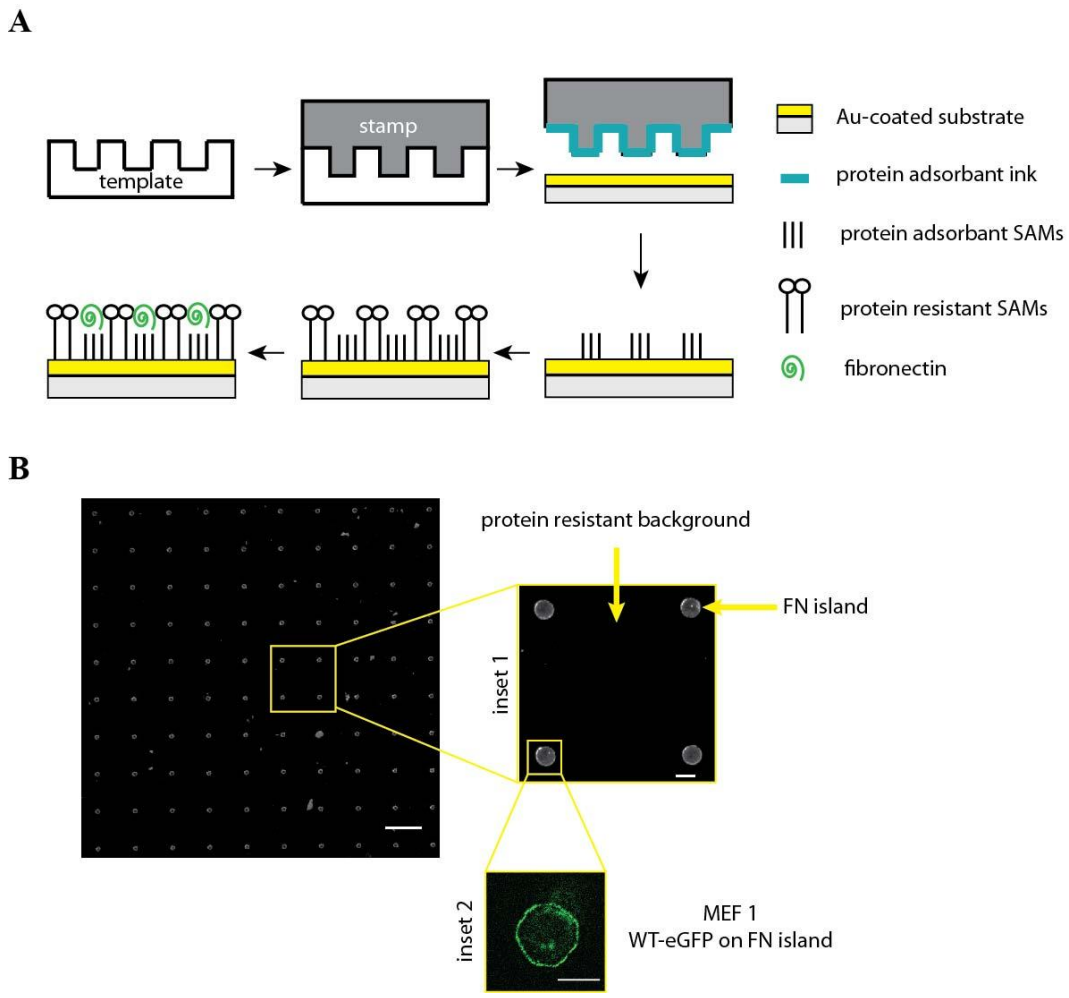

Figure 5.2 Micropatterned substrates for control of cell shape, spacing, and area. (A) Workflow for generating islands of fibronectin (FN) in cell adhesion-resistant background. PDMS (1:10, 186:184) is cast into a silicon template to create stamp. Stamp is inked with protein adsorption-promoting alkanethiol and transferred to the surface of an Au-coated substrate, forming a patterned self-assembled monolayer (SAM). Non-printed areas are backfilled with tri(ethylene glycol)-terminated alkanethiol to create a protein resistant SAM. Finally, FN is passively adsorbed to surface to promote cell adhesion. (B) Islands of FN promote controlled cell adhesion. Anti-FN antibody was used to visualize FN localized to microcontact printed circular islands (10μm in diameter, spaced 75 μm apart) (scale 75μm). (Inset 1) FN adsorbs specifically to patterned islands with undetectable amounts of protein in between (scale bar, 10μm). (Inset 2) Vinculin-eGFP localized to FN-coated islands (scale bar, 10μm).

Vinculin increases steady-state adhesion strength over vinculin-null controls

We measured the steady-state adhesion strength of MEF1 and MEF2 cell expressing vinculin variants using a spinning disk device that applies a range of well-

defined hydrodynamic shear forces to adherent cells (Garcia et al., 1998) (Fig. 5.3A). For a particular sample, the fraction of adherent cells (*f*) is plotted as a function of the applied shear stress (τ). From this detachment profile, the shear stress for 50% detachment (τ_{50}), which represents the mean cell adhesion strength, is determined (Fig 5.3B). MEF1 and MEF2 cells were seeded overnight on 15 μm-diameter islands of FN. The following day, adhesion strength of measurements were made using the spinning disk apparatus. Re-expression of vinculin-eGFP in vinculin-null MEF1 cells increased adhesion strength by 22% over the null controls. Expression of vinculin-eGFP in vinculin-null MEF2 cells increased adhesion strength by 27%. We verified that these increases in adhesion strength were due to vinculin expression by culturing stably expressing vinculin-eGFP MEF2 cells in 100 ng/mL of anhydrotetracycline to inhibit expression (Fig 5.1B). Under these conditions, adhesion strength of MEF2 cells returned to the level of vinculin-null MEF2 control cells (Fig. 5.3C). This result is consistent with previous results in our lab demonstrating that vinculin attributes approximately 25% to cell adhesion strength in NIH3T3 cells (Gallant et al., 2005).

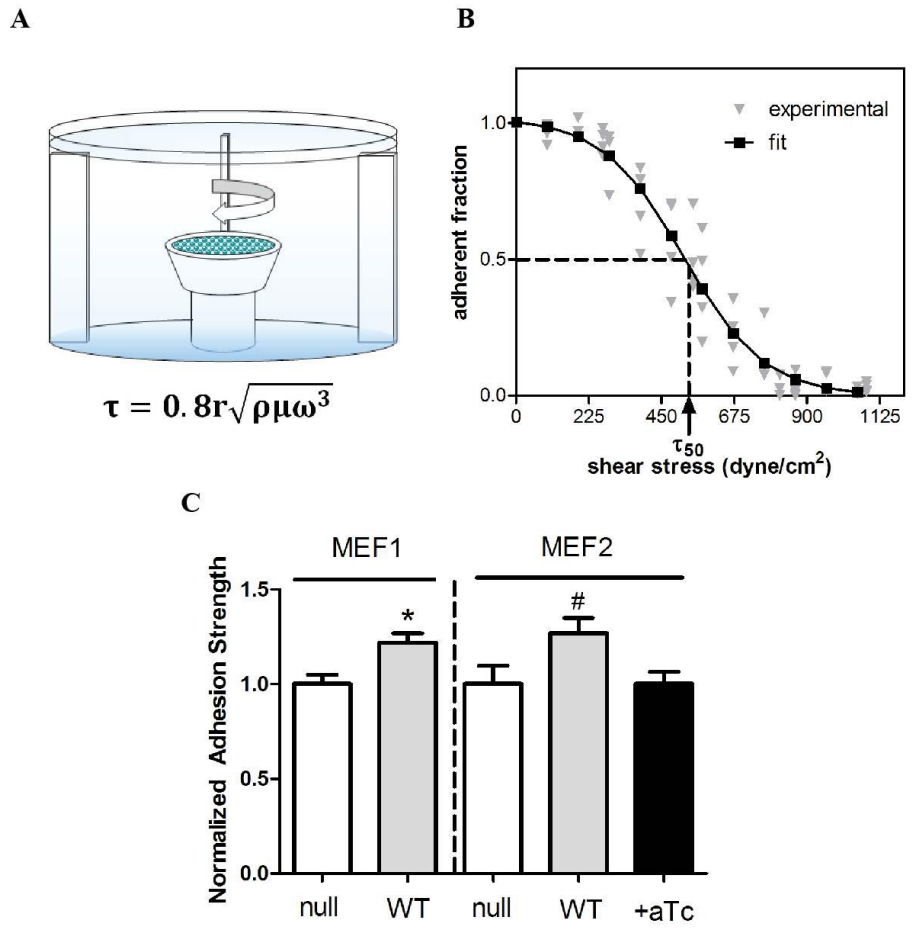

Figure 5.3. Re-expression of vinculin-eGFP in vinculin-null fibroblast increases steady-state adhesion strength. (A) Spinning disk assay for adhesion strength measurements. Cells seeded onto micropatterned substrates (Figure 5.2) are loaded into spinning disk machine and subjected to fluid-induced shear stress. The applied shear stress (τ) is given by the formula in figure where *r* is the radial position from the center and ρ, μ, ω are the fluid density, viscocity, and rotational speed, respectively. (B) Characteristic detachment profile generated by spinning disk machine. Cell numbers at difference radial positions (inverted triangles) are quantified using a motorized microscope stage and image analysis system. The fraction of adherent cells is calculated by dividing the number of cells in each field by the total number of cells at the center of the disk, where negligible forces are applied. The detachment profile (cell adherent fraction versus shear stress τ) is then fit (black squares connected by line) to a sigmoid curve to obtain the shear stress for 50% detachment, which represents the mean adhesive force. (C) Re-expression of vinculin-eGFP in vinculin-null MEFs increases adhesion strength by 22% and 27% in MEF 1 and MEF2, respectively (* $p < 0.04$, # $p<0.05$). Addition of 100ng/mL of aTc reduces adhesion strength.

MEF1 adhesion to FN-coated micropatterned islands is β1-integrin mediated

Previous work in our lab examining NIH3T3 fibroblast adhesion to FN-coated micropatterned islands demonstrated that the $\alpha_5\beta_1$-integrin receptor mediated adhesion in our system (Gallant et al., 2005). We confirmed this result with our vinculin-eGFP expressing MEF1 cells. Specifically, vinculin-eGFP MEF1 cells were trypsinized, quenched in serum containing media, and resuspended in DPBS supplemented with 2mM dextrose and 100 μg/mL of β1-specific blocking antibody or isotype control. Cells were incubated in suspension with antibodies under gentle rocking conditions for 15 minutes. Cells were then seeded in serum-free media for 15 min before visualization (Fig. 5.4). No attached cells were visible on surfaces in the presence blocking antibody whereas isotype control exhibited extensive numbers of attached cells to FN-coated islands (Fig. 5.4).

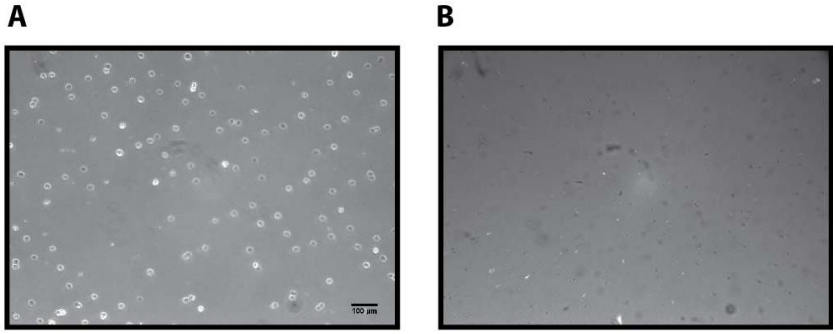

Figure 5.4 Adhesion of MEFs on FN coated substrates is $\alpha_5\beta_1$ integrin specific. Cells were trypsinized from dish, quenched in serum containing media, pelleted, and resuspended in appropriate antibody for 15 minutes with gentle rocking. (B) Blocking $\alpha_5\beta_1$ integrin binding to fibronectin coated islands eliminated cell attached to micropatterned islands (15μm diameter) compared to isotype control (A). scale bar, 100μm.

Disruption of vinculin head-tail interaction to constitutively open conformation increases steady-state adhesion strength

Vinculin exists in the cytoplasm in a closed, inactive conformation (Fig. 5.5A). The 880amino acid, talin-binding head domain of the protein is tightly bound (K_d 10^{-9}) to the F-actin binding tail (Chen et al., 2005; Cohen et al., 2006) (Fig. 5.5A). Once localized to sites of focal adhesions, the molecule opens via separation of the head and tail domain by a yet-to-be-determined mechanism. This activated vinculin molecule binds several structural and signaling FA molecules including talin and paxillin. Mutations to specific residues on the tail domain reduce the binding strength of the head-tail interaction by 100-fold (Cohen et al., 2006) (Fig.5.5A). To examine the contributions of the open conformation of vinculin on adhesive forces, we generated vinculin-null MEF1 cells stably re-expressing head-tail interaction mutant-vinculin (T12-eGFP). We seeded wild-type vinculin-eGFP (WT-eGFP) and T12-vinculin-eGFP (T12-eGFP) MEF1 cells on glass coverslips coated with FN overnight. The following day, cells were fixed and mounted onto microscopy slides for visualization of vinculin molecules. T12-eGFP expressing cells exhibited increased number and size of FAs compared to WT-eGFP expressing cells, consistent with previous reports (Cohen et al., 2006; Humphries et al., 2007) (Fig. 5.5B). We measured the steady-state adhesion strength of WT-eGFP and T12-eGFP cells on micropatterned substrates. Compared to vinculin-null parental control cells, expression of WT-eGFP increased adhesion strength by 25% whereas T12-eGFP increased adhesion strength by 50% over null control cells (Fig. 5.5C). This result indicates that the head-tail autoinhibitory interaction between the head and tail domain is critical for proper modulation of cell adhesion strength. The increase in adhesion strength over WT could be due to increases in total amounts of integrin-talin complexes or higher association of T12 with integrin-talin complexes.

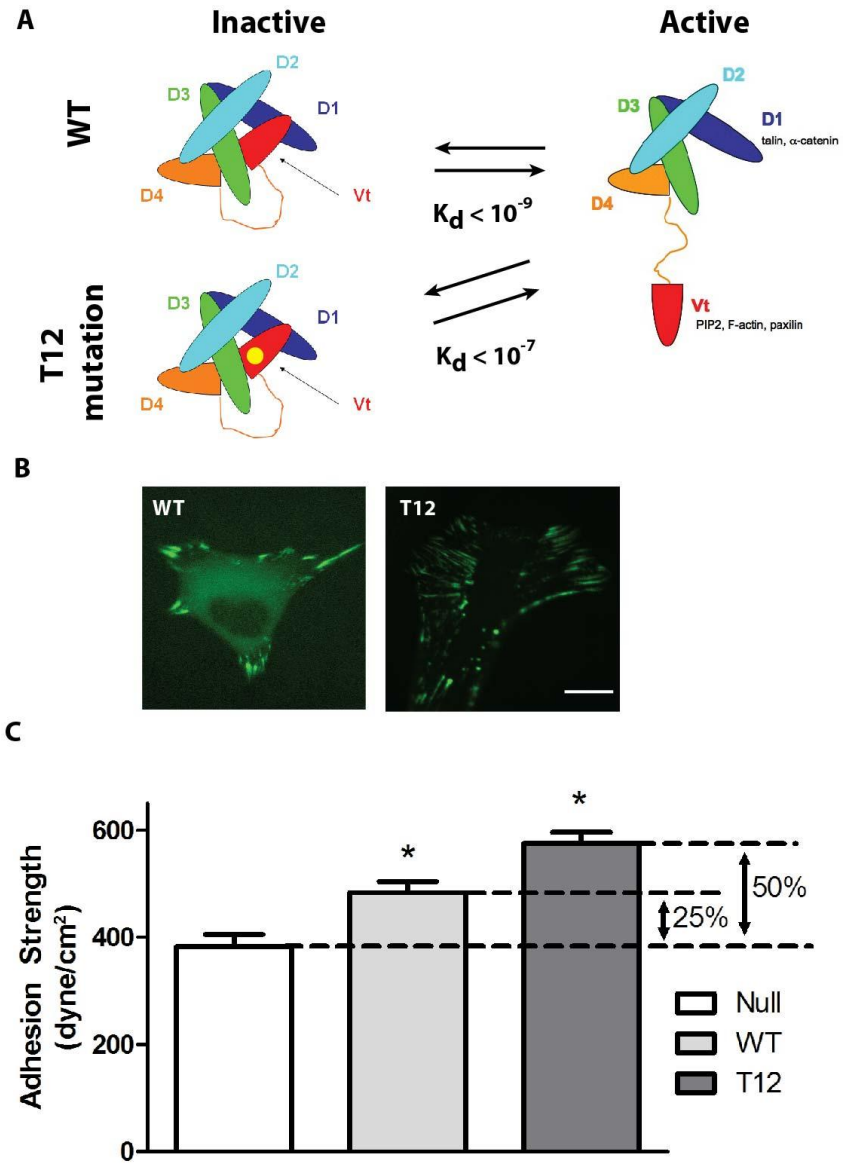

Figure 5.5. Disruption of vinculin head-tail interaction leads to increase in number of focal adhesions and cell adhesion strength. (A) Cartoon depiction of vinculin inactive (closed) and active (open) state and the dissociation constant associated between each condition. Notice the T12 mutant (yellow dot represents area of tail-domain containing mutations) has 100-fold decrease head-tail interaction (B) WT-eGFP and T12-eGFP constructs expressed in MEF1 vinculin-null fibroblasts seeded on FN-coated (10ug/mL) FN (scale bar, 10µm). (C) Steady-state adhesion strength of cells on 15µm-diameter islands. WT-eGFP increases adhesion strength 25% compared to null while T12-eGFP increases adhesion strength 50% over null (* $p < 0.05$ compared to null).

Vinculin head domain, independent of interactions with the cytoskeleton, increases adhesion strength

When localized to focal adhesions, vinculin is in an open, active confirmation allowing it to transfer force (Grashoff et al., 2010). Removal of the F-actin binding tail-domain of vinculin eliminated force transferring ability of molecule (Grashoff et al., 2010), presumably because the molecule needs to be anchored to binding partners at both the N-terminal head and C-terminal tail. We generated vinculin-null MEF1 cells stably re-expressing head only-vinculin (VH-eGFP) for analyzing the effect of tail-less vinculin on cell adhesion strength (Fig. 5.6A). We seeded VH-eGFP MEF1 cells on glass coverslips coated with FN overnight. The following day, cells were fixed and mounted onto microscopy slides for visualization of vinculin molecules. Similar to T12-eGFP (Fig. 5.5B), VH-eGFP expressing cells exhibited increased number and size of FAs compared to WT-eGFP expressing cells, consistent with previous reports (Humphries et al., 2007) (Fig. 5.6B). We measured the steady-state adhesion strength of VH-eGFP cells on micropatterned substrates. Compared to vinculin-null parental control cells, expression of WT-eGFP and VH-eGFP both increased adhesion strength by 25% (Fig. 5.6C). This result is surprising because it suggests that a significant amount of vinculin-mediated adhesion force is directly attributable to binding the integrin-talin-complex and is not dependent on direct interaction with the actin cytoskeleton. Furthermore, these results underscore the importance of connection to the cytoskeleton for full adhesion strength gains to be achieved. Stated differently, the ability of VH to form higher numbers of FAs does not increase adhesion strength over the WT molecule. However,the T12 head-tail interaction deficient mutant increases adhesion strength by 25% over VH despite having similar, increased numbers of FAs, implicating the tail domain of vinculin is critical for cell adhesion strength. Taken together, these results demonstrate, for the

first time, the critical importance of vinculin head binding to the talin-integrin complex, independent of vinculin interaction with the cytoskeleton, in the generation of adhesive forces.

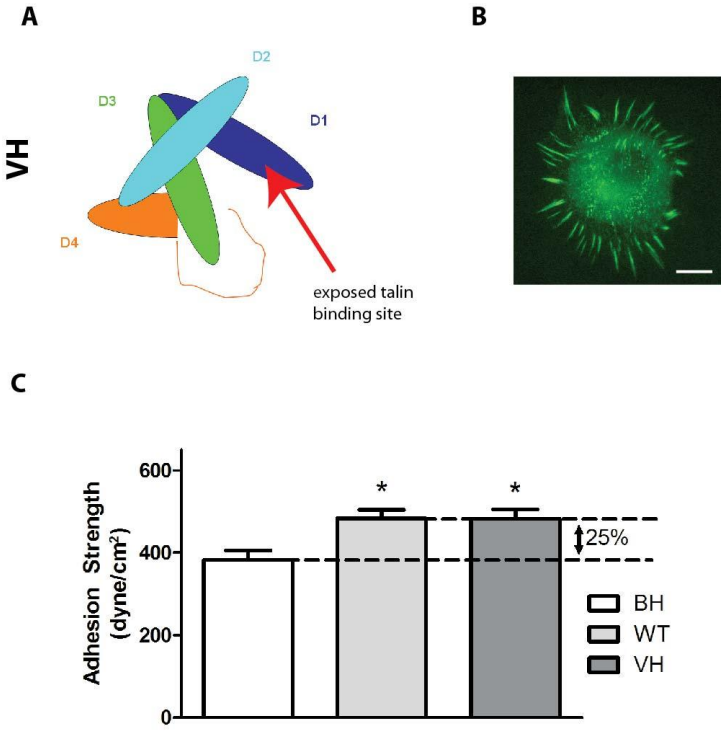

Figure 5.6. Disruption of vinculin head-tail interaction leads to hypertrophied focal adhesions and increase in cell adhesion strength. (A) Cartoon depiction of vinculin head domain (VH) only (1-880) which lacks the F-actin binding domain. VH mutant does not exhibit autoinhibitory behavior and can always bind talin. (B) VH-eGFP constructs expressed in MEF1 vinculin-null fibroblasts seeded on FN-coated (10ug/mL) FN (scale bar, 10µm). (C) Steady-state adhesion strength of cells on 15µm-diameter islands. VH-eGFP increases adhesion strength 25% compared to null which is same increase as WT-eGFP (* $p < 0.05$ compared to null).

Vinculin-dependent increases in adhesion strength correlate with both increases in integrin binding and focal adhesion assembly

Two potential methods by which vinculin increases adhesion strength are (1) by changing the integrin bond numbers, distribution or clustering and (2) by modulating the recruitment and assembly of focal adhesions. To explore these two possibilities, we

first determined if vinculin and vinculin mutants modulated integrin binding and localization to the extracellular matrix (ECM). Previous work in our lab demonstrated that, in our micropatterned system, approximately 70% of steady-state adhesion strength is attributable to α5β1-integrin receptors binding to FN (Gallant et al., 2005). FN-bound integrins were visualized using a cross-linking and extraction method(Keselowsky and Garcia, 2005) to covalently cross-link bound integrins to FN using the cell impermeable bifunctional reagent sulfo-DTSSP. After detergent extraction of uncross-linked cellular components, immnostaining for β1 integrin was performed. We previously demonstrated that this technique provides specific staining of bound integrin and shows equivalent localization of β1 integrin to focal adhesions as conventional immunostaining (Garcia et al., 1999; Keselowsky and Garcia, 2005), indicating that the cross-linking/extraction method does not alter integrin distribution. In addition, an advantage of this technique is that it removes non-specific nuclear staining that can impede visualization of the integrins on the micropatterned islands. Furthermore, our abilty to control cell shape allows us to compare the quantities of surface-bound integrins between cell treatment groups (Gallant et al., 2005; Michael et al., 2009). Immunostaining of FN-bound integrins demonstrated that T12 and VH vinculin mutants increase the area and intensity of integrin staining in compared to WT and null conditions (Fig. 5.7A). We quantified these increases in integrin area (Fig. 5.7B) and intensity (Fig. 5.7C). T12 and VH increased integrin area by over 200% compared to both WT and null controls. This result demonstrates that the head domain of vinculin modulates the quantity and localization of the integrin-talin complex. Similarly, the intensity of integrin staining of T12 and VH conditions was significantly higher than null control. Interestingly, while the area of integrin staining

between WT and null was the same, the intensity of WT integrin staining was greater than the null control (Fig. 5.7C). In addition, vinculin mutants modulated the distribution of integrin staining. FN-bound integrin localized to a narrow rim on the outer edge of the pattern for null and WT conditions. T12 and VH vinculin mutants exhibited a similar staining pattern on the rim of the adhesive area, while having a less predictable pattern of integrin staining in the inner portions of FN-coated islands. Vinculin modulates the assembly and disassembly kinetics of focal adhesions (Cohen et al., 2006; Wolfenson et al., 2009), and these mutants disrupt the physiologic interactions of vinculin for focal adhesions, leading to mislocalized FAs and FN-bound integrins (Humphries et al., 2007; Mohl et al., 2009). Taken together, these data suggest vinculin is an important modulator of the density and localization of FN-bound integrins.

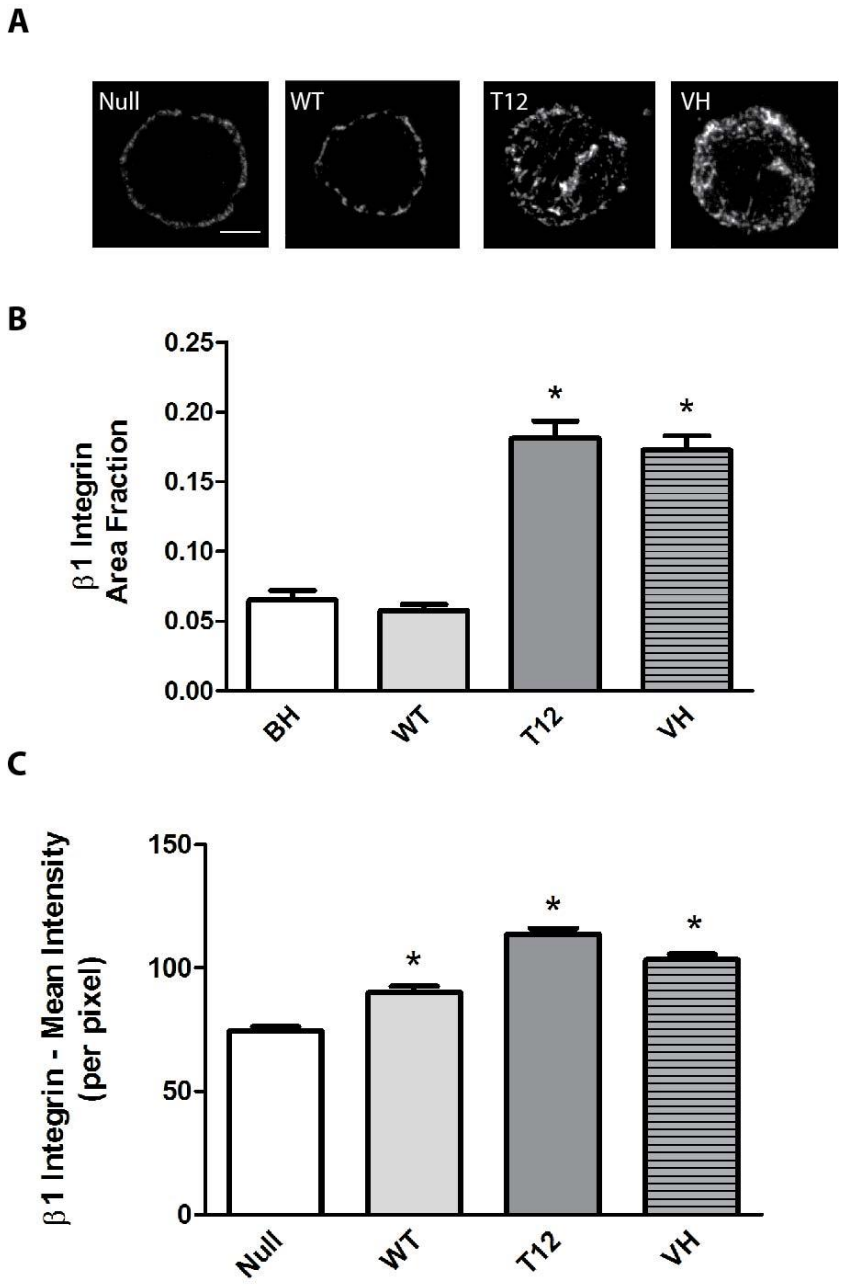

Figure 5.7. Vinculin modulates the spatial localization and intensity of surface-bound integrins. (A) Surface-bound integrins were visualized using a cross-linking and extraction technique, followed by immunostaining (scale bar, 5μm). (B) Integrin staining area-fraction was calculated by measuring the total area of pixels above a specific threshold (applied to all conditions) divided by the total cell area (n=60 cells for each condition). (C) In the same manner as (B), the mean intensity of the integrin-area fraction was calculated, (* $p < 0.05$ compared to null condition).

To investigate the recruitment and localization of focal adhesion components to the adhesive plaque, immunofluorescence staining was performed. It has been demonstrated that talin is required for vinculin to localize to focal adhesions (Zhang et al., 2008). In addition, a single amino-acid mutation in the talin binding head domain of vinculin (A50I) inhibits interaction with talin (Bakolitsa et al., 2004; Cohen et al., 2005). Furthermore, it has been suggested that vinculin directly modulates focal adhesion formation by directly interacting with talin (Cohen et al., 2006; Humphries et al., 2007). Therefore, we focused our analysis of focal adhesion components on talin and vinculin. MEF1 cells expressing the indicated vinculin molecule (WT, T12, and VH) were seeded overnight on FN micropatterned substrates. Immunostaining for talin showed that expression of WT, T12, and VH vinculin variants in vinculin-null cells increases the amount of talin localized to focal adhesions compared to vinculin-null controls (Fig. 5.8 A,B). Talin was spatially segregated and constrained to the circular adhesive area of the micropatterned islands. These adhesive structures were consistent with previous work in our lab using the same system (Gallant et al., 2005). Also consistent with previous findings (Cohen et al., 2006; Humphries et al., 2007), the exposed head domain of both VH and T12 vinculin mutants increased talin localization to the adhesive interface compared to WT. Spatial localization of vinculin strongly correlated with the talin localization results (Fig. 5.8 A,B). Both VH and T12 vinculin mutants increased vinculin localization compared to WT control. In addition, T12 mutant vinculin occupied a large percent of the patterned island than VH. Taken together, increases in integrin binding and focal adhesion assembly correlate well with the corresponding increases in adhesion strength.

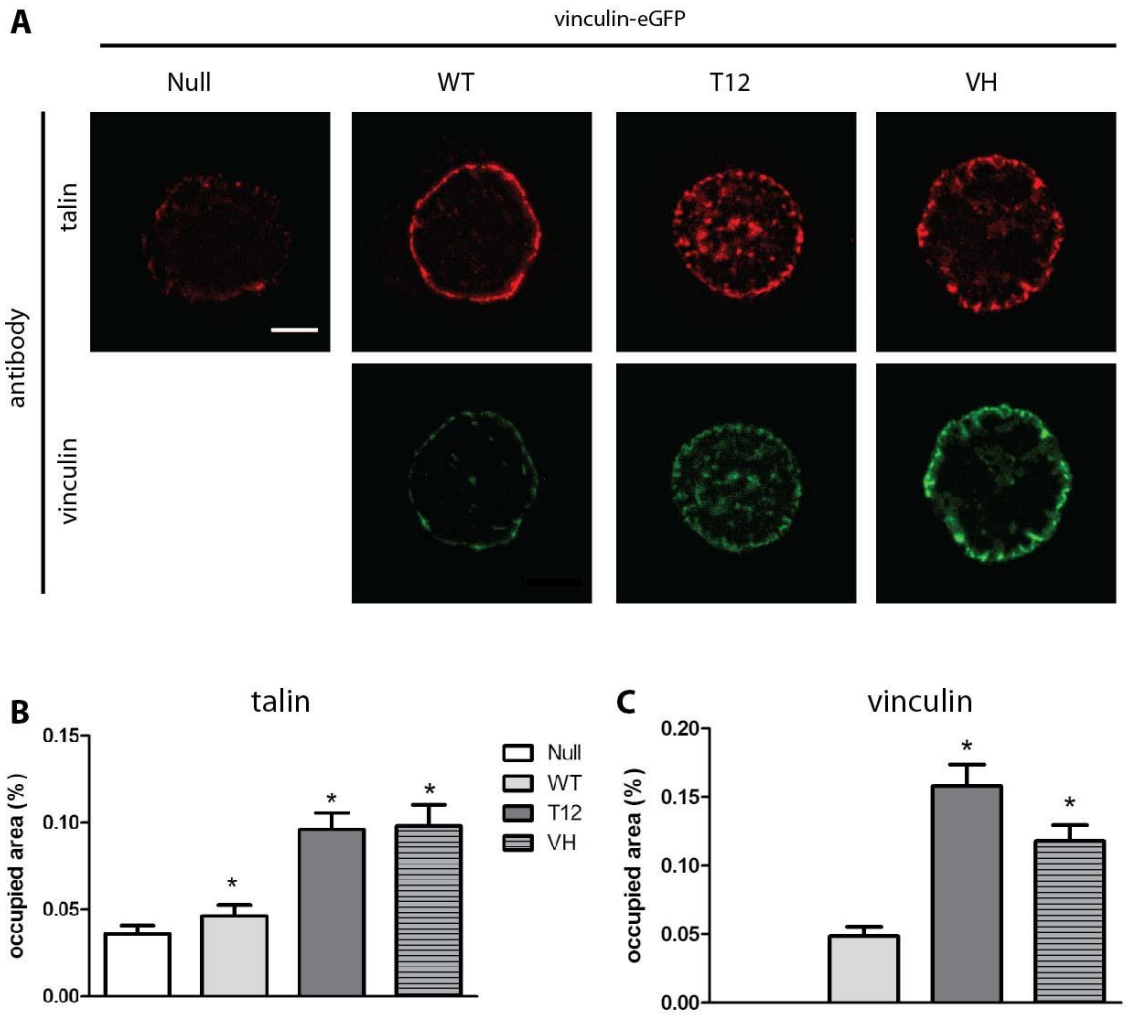

Figure 5.8. Vinculin modulates spatial localization and area of focal adhesions. (A) Immunofluorescence staining for talin (red, top row) and vinculin-eGFP in MEF1 fibroblasts seeded onto micropatterned substrates. (B) Area of talin staining as a percent of total cell area (* $p < 0.05$ compared to null). (C) Area of vinculin staining as a percent of total cell area (* $p < 0.05$ compared to WT).

Physical connection between the head and tail domain of vinculin is required for maximum adhesion strength

The head domain of vinculin modulates focal adhesion assembly via direct binding of talin (Cohen et al., 2006; Humphries et al., 2007). The tail domain is important for efficient linkage between the actin cytoskeleton and focal adhesions (Humphries et al., 2007). Our results indicate that the head-tail interaction mutant, T12,

results in the highest level of adhesion strength. Surprisingly, expression of F-actin binding deficient VH molecule results in adhesion strength comparable to WT, despite increases in focal adhesion assembly and integrin binding. This result suggests that vinculin must bind to the cytoskeleton in order to achieve maximum adhesion strength. Vinculin has recently been shown to transfer force between talin and F-actin in focal adhesions (Grashoff et al., 2010), suggesting that the physical linkage between the head and tail domain might be important for generating adhesion strength. We tested the hypothesis that the physical linkage between the head and tail domain of vinculin was required for maximum adhesion strength.

We transiently transfected the head domain (VH), head-tail binding deficient (T12), tail only (vinT) and a control eGFP vector into MEF1 vinculin-null cells (Fig. 5.9A). 72 hrs after transfection, fluorescent cells were enriched with FAC sorting and seeded on micropatterned islands. Fluorescence microscopy showed that vinculin mutants localized to FN-patterns in a similar way to those expressed in the retroviral system (Fig. 5.8A). We co-transfected the head (VH-CFP) and tail (vinT-YFP) and, 72hrs later, sorted for fluorescence expressing cells. Enriched cells were immediately seeded onto patterns (Fig. 5.9B). The VH-CFP and vinT-YFP molecules constitute the entire vinculin molecule, without the physical linkage between the head and tail domain. Fluorescence microscopy showed that the VH-CFP domain localizes to FN-micropatterns consistent with VH-eGFP (both transient and retroviral expression systems) (Fig. 5.9B). When co-expressed with VH-CFP, the tail domain (vinT-YFP) does not strongly co-localize with the VH-CFP protein. This finding is consistent with published results, as expression of the vinculin tail has been previously shown to decorate F-actin fibers and

does not strongly localize to focal adhesions (Humphries et al., 2007). Adhesion strength measurements were performed to quantify the contribution of these constructs to cell adhesion (Fig. 5.9C). Expression of tail only (vinT-YFP) increased adhesion strength to the same level of head only (VH-eGFP). This result is unexpected as the tail domain of vinculin does not directly connect to the integrin-tailin complex. Rather it was been shown to decorate F-actin filaments, but not to strongly localize to FAs or α-actinin rich lamellopida protrusions (Humphries et al., 2007; Kroemker et al., 1994; Menkel et al., 1994). Our own experiments with tail-only expression on a cell traction force measurement device indicate that even focal adhesions under high force cannot localize tail domain (Fig. 6.6). There are two possible explanations for this result. First, it is possible that the tail domain enhances actin cross-linking, thereby increasing the overall stiffness of the membrane, would more able to resist the peeling detachement mechanism inherent in our measurement assay (Gallant and Garcia, 2007a). An alternative explanation is that increases in actin bundling modulate the size, clustering, or distribution of the integrin-talin complexes.

These results implicate important roles for both the head and tail domain of vinculin. Independent expression of the vinculin head and tail constructs increases adhesion strength to those similar to WT levels. Surprisingly, VH accomplishes this independently of the action cytoskeleton, but rather, via enhancements in integrin binding and focal adhesion assembly. The tail domain, by contrast, cannot directly bind the integrin-talin complexes, and modulates adhesion strength via a separate mechanism. One possible explanation is that the tail domain increases membrane stiffness via enhanced bundling of the actin cytoskeleton (Mierke et al., 2008) (Le Clainche et al.,

2010) which improves resistant to the cell detachment by peeling, mechanism inherent our system, by more evenly distributing detachment forces (Gallant and Garcia, 2007a). An alternative explanation is that vinculin tail indirectly modulates the size, location, or density of the integrin-talin complexes. This is unlikely because there is little evidence to suggest that tail localizes to focal adhesions (Humphries et al., 2007).

The head and tail domains of vinculin are both important for the generation of adhesion strength, consistent with our earlier findings. In addition, expression of the head-tail binding mutant, T12-eGFP, showed the maximum adhesion strength (20% higher than tail-only and head-only). Interestingly, the co-expression of the head (VH-CFP) and tail domain (vinT-YFP) did not increase adhesion strength above those of head-only or tail-only. This result demonstrates that the physical connection between the head and tail domain represents an important functional domain of the vinculin molecule in adhesion force generation.

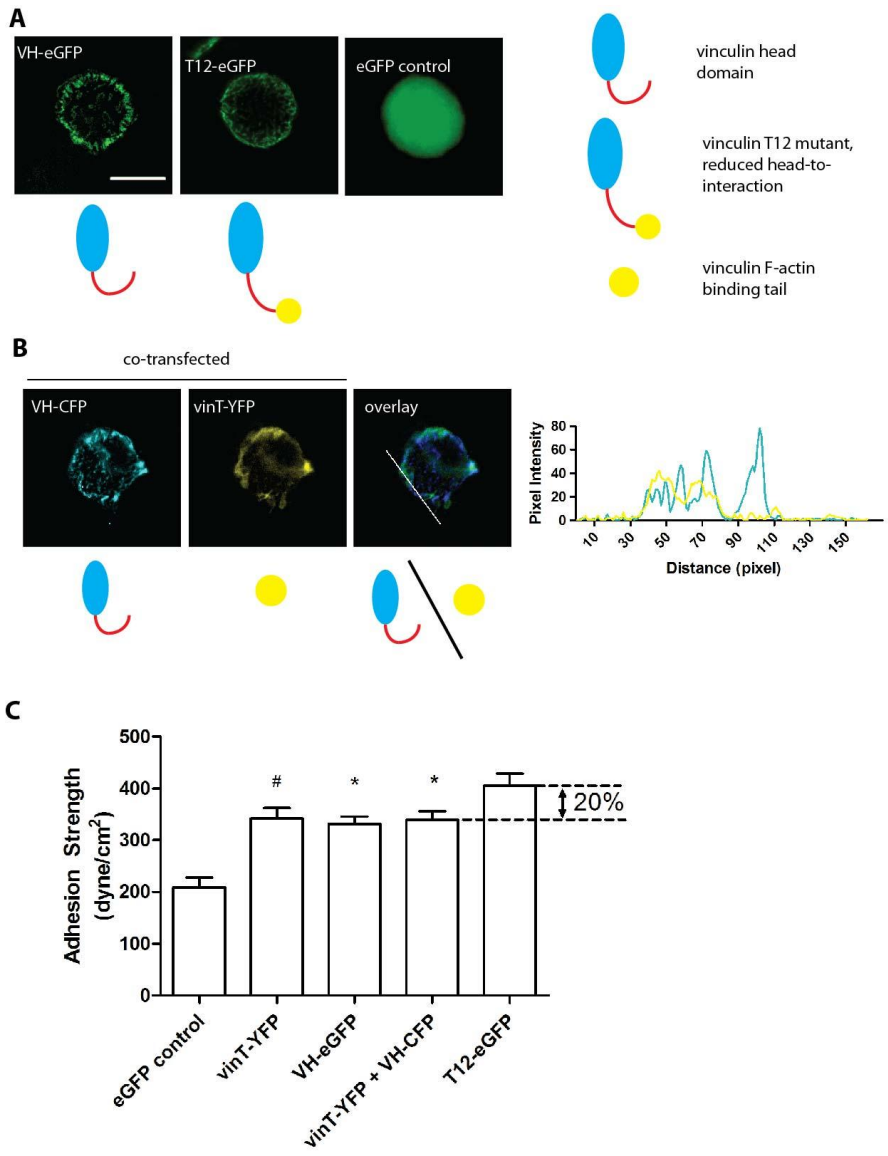

Figure 5.9. Physical linkage between the talin-binding head and F-actin-binding tail of vinculin is essential for maximum adhesion strength. (A) Indicated eGFP constructs were transiently transfected into MEF1 cells and seeded on micropatterned islands. Cartoon representation of vinculin constructs to show the physical linkage between the head and tail domains of vinculin. (B) Plasmids encoding for Head domain (VH-CFP) and tail domain (vinT-YFP) were co-transfected into MEF1 cells and seeded on micropatterned islands. Cartoon representation of the lack of physical connection between the head and tail domain. Line profile of VH-CFP and vinT-YFP overlay demonstrates that vinT does not strongly co-localize with FA-associated VH-CFP. (C) Adhesion strength of indicated constructs transfected in MEF1 cells (eGFP, 210 dyne/cm2; vinT-YFP, 342 dyne/cm2; VH-eGFP, 332 dyne/cm2; vinT-YFP + VH-CFP, 339 dyne/cm^2; T12-eGFP 405 dyne/cm2) (# $p < 0.9$ compared to T12-eGFP; * $p < 0.05$ compared to T12-eGFP).

Conceptual model of adhesive patch force combined with collective view of adhesion strength, integrin binding, and focal adhesion assembly data reveals importance of vinculin head and tail domains in force generation

To better understand the effects of vinculin on adhesion strength, we summarized the increases over the vinculin-null condition in adhesion strength, integrin area, and FA assembly in Table 5.1. Expression of the WT and VH domains increased adhesion strength by 25% each, while integrin area and focal adhesion assembly increased 167% and 172% for VH while remaining unchanged and 28% for WT, respectively. This result suggests that the talin-binding head domain, VH, increases adhesion strength both by increasing the number of bound integrin and focal adhesion assembly. It also suggests that vinculin modulates adhesion strength by its linkage to the cytoskeleton because WT has the same level of adhesion strength despite having lower amounts of integrin area and FA assembly. This result is supported by a comparison between T12 and VH. Specifically, when expressed in vinculin-null MEFs, T12 and VH vinculin mutants both increase integrin area and FA assembly to similar levels. T12 increases adhesion strength by 50% compared to vinculin-null controls, while VH increases by 25%, suggesting that the ability of the vinculin molecule to connect the integrin-talin-vinculin complex to the cytoskeleton is critical for full adhesion strength increases. This data also suggests that vinculin modulates adhesion strength by increasing the number of matrix-bound integrin, enhancing focal adhesion assembly, and increasing the connectivity of the integrin-talin-vinculin complex to the cytoskeleton.

Table 5.1. Effects of vinculin domains (percent increase over null)

	WT	T12	VH
adhesion strength	25%	50%	25%
integrin area	same	180%	167%
FA assembly (talin)	28%	167%	172%

In order to expand our understanding of the experimental results for vinculin-modulated adhesion strength, we present an engineering analysis of the dependence of adhesion strength generation on the number of bound integrins, focal adhesion assembly, and cytoskeleton connectivity. The model is based on previous work in our lab which demonstrated excellent agreement between predicted adhesion patch force data and experimental results (Gallant and Garcia, 2007a). Importantly, an advantage of the model is that it is based on parameters that can be measured experimentally, thus allowing for comparison between experimental results and model predictions.

We use a modified membrane peeling model that that assumes bond loading of matrix-bound integrin receptors is highly non-uniform and can thus be modeled by an exponential decay function with maximum bond forces generated at the perimeter of the cell which then rapidly decay towards the center (Fig. 5.10A). The total adhesive patch force is calculated by the sum of individual adhesive patches consisting of bound integrins (B) linked together by the fraction of bonds mechanically linked by focal adhesion assembly (χ). The model accounts for differences in membrane stiffness by modulating the sensitivity (κ) of the exponential dependence of segment loading (Fig. 5.10B). We populate the above parameters with a values derived from our own experimental data as well as data from the literature. Specifically, the number of bound integrins, B, used in the model (1600 for Null and WT, and 2500 for T12 and VH) were

chosen based on the integrin staining data presented in Fig. 5.7 as well as estimations of maximum amount of total bound integrins (3000) from Gallant 2005 (Gallant et al., 2005). Increases in cytoskeleton stiffness resulting from vinculin-mediated linkage of integrin-talin-vinculin complexes to the cytoskeleton were modeled by varying the exponential dependence of segment loading from 1 (no vinculin linkage, Null and VH) to 2 (vinculin linkage, WT and T12) (Table 5.2). Finally, we varied the levels of integrin bonds associated with FAs based on our experiment data of focal adhesion assembly (Fig. 5.8). Specifically, minimum amount of FA assembly requires one-third of integrins to be focal adhesion bound (Coussen et al., 2002), so we assigned this value (.33) to the vinculin-null condition (Table 5.2). We assigned a focal adhesion fraction of 0.5 to WT, T12, and VH vinculin constructs based on our experimental results showing increased assembly compared to null (Table 5.2).

The results of the conceptual model of adhesive patch force agree well with our experimental results of adhesion strength. The model predicts that expression of T12 vinculin increases the adhesive patch force by 99.8% over the vinculin-null condition while expression of vinculin WT and T12 increase adhesive patch force by 50.2% and 45.5%, respectively (Fig. 5.10C). Our own experimental results demonstrate that WT and VH increase adhesion strength over null by 25% while T12 increases adhesion strength by 50% (Fig. 5.10D). Comparing the predicted to the experimental results, we see good agreement in the relative gains in adhesion strength given by each vinculin construct over the vinculin-null condition. The conceptual model is useful for interpreting our experimental results as it predicts that vinculin can increase adhesive patch for by increasing the levels of bound integrin, increasing the percent of integrins

bound to FAs, and by increasing the stiffness of the cytoskeleton by linking it to the integrin-talin-vinculin complexes.

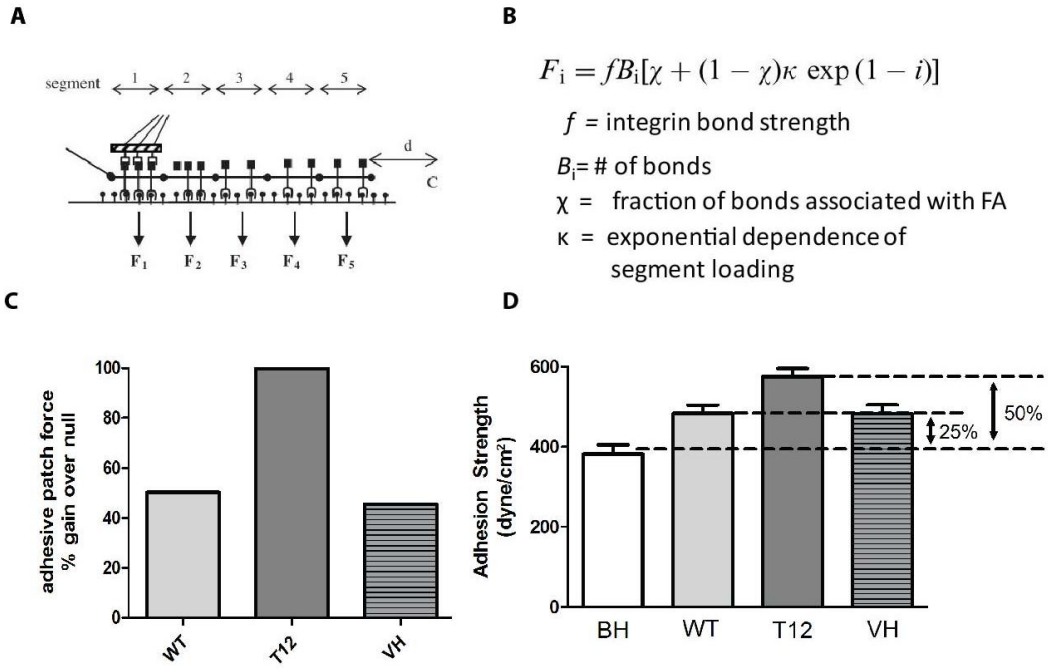

Figure 5.10. Conceptual model of adhesion strength. (A) Conceptual model of adhesive patch force generation. (B) Exponential dependence of adhesive patch force on individual integrin bond strength (*f*), number of integrin bonds (B), fraction of bonds associated with FAs (χ), and exponential dependence of segment loading (κ). (C) Predicted adhesive patch force gains as a percent over vinculin-null condition. (D) Experimentally determined adhesion strength values with percent gains over vinculin-null condition shown.

Table 5.2. Parameters for conceptual model of adhesion strength

	Null	WT	T12	VH
B	1600	1600	2500	2500
κ	1	2	2	1
χ	0.33	0.5	0.5	0.5

Discussion

We demonstrate that vinculin increases adhesion strength via enhancements in integrin binding/localization and focal adhesion assembly. Mutations reducing the head-tail interaction (T12) of the molecule result in additional increases of adhesion strength by further increasing the number of matrix-bound integrins as well as the assembly of talin and vinculin-containing focal adhesions. Importantly, vinculin mutants lacking the F-actin tail domain (VH) increase adhesion strength to levels of wild-type (WT), but fail to achieve the same adhesion strength of T12 mutants. This result is surprising because both VH and T12 exhibit similar levels of integrin binding and focal adhesion assembly, consistent with previous reports (Humphries et al., 2007). The major structural difference between the two mutants is that T12 retains the ability to bind actin while VH does not. This structural difference suggests that the binding of vinculin to the cytoskeleton is essential for maximum adhesion force generation, independent of integrin binding and focal adhesion assembly. High-resolution, 3-D imaging of the nanoscale architecture of the adhesive plaque demonstrated that vinculin head domain localizes to talin in the region sandwiched between with integrins below and the actin cytoskeleton above (Kanchanawong et al., 2010). While the authors did not directly measure the location of the tail domain of vinculin, it is reasonable to assume that the molecule orients itself such that the tail binds the actin cytoskeleton. The assumption is supported by direct evidence that vinculin tail is required for efficient linkage of adhesive complexes to the actin cytoskeleton (Humphries et al., 2007). In addition, vinculin tail efficiently cross-links and bundles actin filaments (Janssen et al., 2006; Menkel et al., 1994). Therefore, one possible explanation for our finding that the tail domain is required for

maximum adhesion strength is that discrete focal adhesions are mechanically coupled together by their vinculin-dependent linkage to the cytoskeleton. These mechanically coupled adhesions would thereby increase adhesion strength by requiring that all linked adhesions fail simultaneously. A similar model has been proposed to describe focal adhesion-induced increases in adhesion strength (Gallant and Garcia, 2007a). In this model, independent clusters of integrins adhesive patches are linked together by focal adhesions. Mechanically linked adhesive patches fail simultaneously, instead of individually, thereby increasing cell resistance to detach forces. Stated briefly, we hypothesize that vinculin is required for efficient coupling of the focal adhesions to the actin cytoskeleton and that this coupling to the cytoskeleton mechanically links discrete focal adhesions, thereby increasing the resistance to adhesion strength. Implicit in this model is the importance of the physical linkage between the head and tail domain of the vinculin molecule. Importantly, this simple model also explains why head adhesion strength to above null, but not the levels of actin-binding T12.

We therefore hypothesized that the proline-rich strap that physically links the talin-binding head and actin-binding tail is essential for achieving maximum adhesion strength. We directly tested this hypothesis by co-transfecting vinculin head and tail constructs. The constructs themselves represent the entire vinculin molecule in which the head and tail domains are not linked together. Consistent with our model, co-expression of head and tail constructs were not able to achieve the same level of achieve strength as the full-length, head-tail interaction mutant, T12. Importantly, transfecting cells with only the tail of vinculin increased adhesion strength compared to the null condition. This

result independently supports our view that the actin-bundling tail of vinculin is important for generating adhesion strength.

Finally, we employed the use of a previously validated (Gallant and Garcia, 2007a) conceptual model of adhesion force generation. Based on a modified membrane peeling model, it assumes bond loading of matrix-bound integrin receptors is highly non-uniform and can thus be modeled by an exponential decay function with maximum bond forces generated at the perimeter of the cell which then rapidly decay towards the center (Fig. 5.10A). The model considers the affects of numbers of bound integrins, extent of focal adhesion assembly, and cytoskeleton modulated membrane stiffness. Using parameters derived from our experimental data as well as the adhesion strength literature, the predicted adhesive patch force increases over null condition for each of the vinculin constructs (WT, T12, and VH) correlated strongly with our experimental results (Fig. 5.10C,D). The model predictions thus support our interpretation of the experimental data; namely, that vinculin increases adhesion strength by a combination of increasing the number of integrin-FN bonds, increasing FA assembly, and by physically linking the integrin-talin-vinculin complex to the cytoskeleton.

In conclusion, we have demonstrated that vinculin increases adhesion strength when expressed in vinculin-null cells. We showed that the gains in adhesion strength are attributable to increases in FN-bound integrins and focal adhesion assembly. Reduction in the strength of the head-tail interaction (T12) increases FN-bound integrins, focal adhesion assembly, and adhesion strength 25% higher than wild-type vinculin. Expression of the head domain only (VH) also increases FN-bound integrins and focal adhesion assembly, however, the adhesion strength is the same as wild-type. We

hypothesized that vinculin tail linkage to the cytoskeleton allows for maximum adhesion strength by mechanically linking independent focal adhesions. Adhesion studies with co-expression of independent head and tail domains support this model and demonstrate that the physical connection between the head and tail is essential for achieving maximum adhesion strength.

CHAPTER 6

Force-Dependent Dynamics of Vinculin Recruitment to Focal Adhesions

Abstract

The conversion of mechanical forces into chemical signals is a fundamental cellular process that occurs at supramolecular structures called focal adhesions (FAs). Integrin-mediated adhesion to the extracellular matrix gives rise to the assembly of force-sensing FAs. Despite considerable characterization of the structural and morphological changes to FAs in response to force, the exact molecular interactions that are responsible for the behavior remain unknown. Recent experimental and computational evidence has suggested that the binding interaction between talin and vinculin might be regulated by force. Direct evidence that force-induced binding interactions are relevant, *in-cellulo*, does not yet exist. Herein, we present a novel approach for characterizing the force-dependent dynamics of focal adhesion associated proteins. Using this system, we demonstrate that the dynamics of vinculin recruitment to FAs are linearly dependent on the level of force applied to the focal adhesion. Specifically, as force applied to the FA increases, so too does the stability of vinculin in the FA. This result supports a simple model in which cytoskeleton generated tension across vinculin modulates its binding interactions within FAs. However, we also provide surprising evidence to contradict this model by showing that the force applied to focal adhesions modulates the dynamic

recruitment of vinculin, independent of its interaction with the cytoskeleton. We therefore hypothesize that cytoskeleton generated force applied across talin exposes one or more vinculin binding sites (VBS) that are important for the force-dependent dynamics of recruitment of vinculin to FAs. Taken together, a model emerges wherein vinculin dynamics are dually regulated both by direct application of cytoskeleton generated force across vinculin and by force induced exposure of VBS on talin.

Introduction

Cells have the remarkable ability to detect and respond to their mechanical environment (Sastry and Burridge, 2000). Forces, both externally and internally generated, modulate cell behavior and structure. Apart from a few well characterized systems, how mechanical forces are converted into chemical signals remains largely undefined (Riveline et al., 2001). Focal adhesions are supramolecular structures that serve both as sites of force transfer between the extracellular matrix and cytoskeleton and as signaling platforms (Balaban et al., 2001; Riveline et al., 2001). These dynamic, complex structures link ECM-bound, transmembrane integrin receptors to the actin cytoskeleton. The processes by which FA grow, modulate shape and size, and control disassembly are all modulated by the stiffness of the underlying substrate (Sniadecki et al., 2007; Vogel and Sheetz, 2006). While it is clear that force modulates focal adhesions the structure and function of FAs, the manner in which they accomplish this is unclear.

The integrin-talin-vinculin complex serves as a critical force bearing linkage between the internal cytoskeleton and the extracellular matrix (Gallant et al., 2005; Humphries et al., 2007; Zhang et al., 2008). Previous work in our own lab has

demonstrated the importance of this complex to the generation of adhesion forces (Gallant et al., 2005). Importantly, all three of the individual proteins in the complex have been shown to respond to force. For example, integrin-ligand catch-bonds describe how integrins increase their affinity for ligands upon application of force (Kong et al., 2009). In addition, molecular dynamics of force application to both vinculin and talin have uncovered potential force-regulating binding pathways that could mediate interactions between the two proteins (Golji and Mofrad, 2010; Lee et al., 2008). By applying tensile force to individual talin molecules, del Rio et al provided physical evidence that cryptic vinculin-binding sites become exposed which promote binding of the vinculin head domain (del Rio et al., 2009). While these studies on isolated, single molecules provide insight into the potential force induced interactions of vinculin and talin, how these relationships unfold in the context of a living cell is unclear.

Herein we present a novel approach for measuring the force mediated, dynamic behavior of focal adhesion-associated proteins. We used micro post array deflections substrates to measure cell the force transferred across individual focal adhesions (Fu et al., 2010; Tan et al., 2003). Simultaneously, we measured the dynamic behavior of fluorescent vinculin molecules expressed in vinculin-null mouse embryonic fibroblasts using fluorescence recovery after photobleaching. This unique approach allowed us to characterize, for the first time, the force-dependent behavior of vinculin in focal adhesions. We show that vinculin turns over more rapidly in focal adhesions under low force compared to slower vinculin recovery at high forces. Importantly, we show that the relationship between applied focal adhesion force and vinculin recovery is linearly dependent. This result supports a simple model in which cytoskeleton generated tension

across vinculin modulates its binding interactions within FAs. However, we also provide surprising evidence to contradict this model by showing that the force applied to focal adhesions modulates the dynamic recruitment of vinculin, independent of any direct application of cytoskeleton generated force to the molecule. Combined, these results suggests a model by which the dynamic recruitment of vinculin to focal adhesions is, at least in part, modulated by force applied to other focal adhesions molecules.

Materials and Methods

Reagents

Human plasma fibronectin (FN), fetal bovine serum, Dulbecco's modified eagle's medium (high glucose) and Dulbecco's phosphate buffered saline (dPBS) were obtained from Invitrogen (Carlsbad, CA). Poly(dimethylsiloxane)(PDMS) elastomers and curing agents were obtained from Dow Corning (Midland, MI). Inhibitors (blebbistatin and calyculin-A) were purchased from Sigma-Aldrich (St. Louis, MO). 1,1'-dioleyl-3,3,3',3'-tetramethylindocarbocyanine methanesulfonate (Δ9-DiI) was purchased from Invitrogen. F127 Pluronic was purchased from Sigma-Aldrich (St. Louis, MO).

Fabrication Flow - Micro post array deflection substrates (mPADs)

mPAD devices were fabricated in accordance with the protocol developed by the laboratory of Chris Chen, University of Pennsylvania (Yang et al., 2011). PDMS molds were created by pouring 1:10 Sylgaurd 184 (Dow Corning) over the silanized mPAD silicon master (a kind gift from JP Fu lab, Univeristy of Michigan) and placed in a 110ºC convection oven for 1 hour. Molds were allowed to cool and then were peeled from the

masters and cut into individual device molds. These individual molds were then UVO cleaned (Jelight Model 342) for 10 minutes to promote the formation -OH groups on the surface of the mold. The molds were then transferred into a desiccator and 100 µL (two or three drops) of (tridecafluoro-1,1,2,2,-tetrahydrooctyl1)-1-trichlorosilane (Sigma) was placed onto a microscope slide. The desiccator was then placed under constant vacuum for 24 hours to promote the vapor phase silanization of the surface. After the molds were silanized, a drop of 1:10 PDMS was put on top of the each mold, and degassed for 30 minutes. During degassing, round 22mm coverslips were treated with atmospheric plasma to promote covalent bind to the coverslip prior to peeling. After the molds were sufficiently degassed to remove air bubbles, the molds were inverted onto the plasma treated coverslips and placed into a 110ºC convection oven for 20-24 hours. After full curing, the final device was created by peeling the mold, and inverting it into a bath EtOH followed by sonication to recover collapsed posts. Devices were dried under super-critical CO_2 (Tousimis PVT-3) to generate fully recovered mPAD devices. Detailed protocol can be found in Nature Protocols ((Yang et al., 2011)).

mPAD Device Prep Flow

A standard silicon wafer was silianized and 1:30 Sylguard 184 was cast on top and cured at 110ºC for minimum one hour. PDMS was peeled from the wafer and cut into square stamps smaller than the device area. Stamps were cleaned by sonication in EtOH for 5 min to remove loose PDMS flakes and debris. Under cell culture hood, stamps were dried under stream of N_2. Next, human plasma fibronectin (50 µg/mL) was adsorbed on the top surface of the stamps for 1 hour. Excess FN was removed by

submerging stamps in ultrapure diH2O. Stamps were removed and dried under a gentle stream of N_2. Fully recovered mPAD devices were then trimmed with razor blade to remove excess PDMS. mPAD devices were then treated with UVO cleaner for 10 min to prepare surface for microcontact printing. FN-coated, flat PDMS stamps, were then inverted onto the tops of mPAD devices (transfer of FN from flat stamp to top of the mPAD occurs within seconds). Without removing the FN stamp, mPAD devices were transfer into 100% EtOH, to allow for removal of the FN stamp without collapsing posts. Devices were then washed as follows: 1X 70% EtOH, 4X diH_2O, and transferred into 5µg/mL Δ9-DiI and incubated for 1 hour. Devices were then washed 2X in 100% H_2O followed by 1X rinse in dPBS (Ca^{2+} and Mg^{2+} free) and transferred to 1-2% Pluronics F127 (Sigma) and incubated for 30 minutes to block non-specific protein adsorption. Devices were rinsed 3X in 100% dPBS (Ca^{2+} and Mg^{2+} free) three times. Prepared devices were transferred into 6 well plates and seeded with cells at a density of 20,000 cells /cm^2. After waiting until the desired number of cells have seeded, non-seeded cells were washed off. Cells were allowed to spread on mPADs overnight.

Fluorescence recovery after photobleaching (FRAP)

A confocal microscope (Nikon C1) and an inverted microscope (Nikon TE 300) equipped with a Coherent Sapphire solid-state 488 laser under the control of Nikon EZ-C1 software were used for FRAP experiments. Cells were seeded overnight on FN-coated mPAD devices. Prior to imaging, devices were mounted into a on-stage incubator (LiveCell II, Pathology Devices, Westminster, MD) maintained 100% humidity and 5%

$C0_2$. A custom microscope enclosure was used to thermally stabilize the microscope at 37ºC.

FRAP experiments were performed as follows. Cell-seeded mPAD device was loaded into an Attofluor cell chamber (Invitrogen, Carlsbad, CA) and allow to equilibrate for >20 minutes. A 60X APO TIRF (1.49 NA) objective (Nikon) was used for imaging. Initial fluorescence intensity was measured using low laser power (1.5-2.5%) followed by photobleaching of a 0.85um-diameter circle inside FAs at 10% laser power for 1 zoomed pass (256x256 pixels inside of circle). The fluorescent recovery was monitored every 7-seconds (10 seconds for VH and T12) until plateau in recovery was reached (5 pre-bleach and 30 post-bleach images). Images were imported into MATLAB and background subtraction and bleaching correction were applied to data from the region of interest. Curves were fit to single exponential recovery model by assuming a reaction dominated system and disregarding any effects of diffusion.

The characteristic recovery time for a molecule under pure diffusion is given by:

$$\tau = \frac{r^2}{4D}$$

where τ, r, and D represent the first-order characteristic recovery time, radius of photobleached spot, and the diffusion constant of the molecule (Sprague and McNally, 2005). We used a bleach radius of 0.42μm which, for BSA (77kDa, D=66 $\mu m/s^2$), yields as recovery time of 0.001s. While vinculin (116 kDa) is larger than BSA, it is unlikely that the diffusion effects contribute to our recovery measurements. This assumption is supported by recent results showing similar recovery time for different size photobleached spots, indicating a reaction, not diffusion, dominated system (Wolfenson et al., 2009).

Post deflection measurements were taken immediately following FRAP recovery. Specifically, the top and bottom of the posts were sequentially captured. ImageJ (NIH, Bethesda, MD) was used to measure the center-to-center distance between the top and bottom of the tethered post. The resulting force was calculated using Euler-Bernoulli beam theory approximation where

$$F = \left(\frac{3}{64}\pi E \frac{D^4}{L^3}\right)\upsilon$$

in which F,E,D,L, and υ are the bending force, Young's modulus, pillar diameter, pillar height, and resulting deflection of the post (Yang et al., 2007).

For studies with chemical inhibitors, appropriate concentration (1μM blebbistatin and 0.1nM calyculin-A) were added to samples 30 minutes prior to measurements.

Retroviral vectors for eGFP-Vinculin WT

Retroviral plasmids pTJ66-tTA and pXF40 were previously described ((Gersbach et al., 2007)). eGFP-C1 WT vinculin and eGFP-C1 VH vinculin plasmids were a kind gift from Susan Craig. One AgeI restriction site was inserted into the multiple cloning site of pXF40, the retroviral expression vector. The oligonucleotides 5'-AGCTTGTCAGCTACCGGTGCTACTGCA-3' and 5'-AGCTTGCAGTAGCACCGGTAGCTGACA-3' (AgeI sequences underlined) were annealed together, creating HindIII- compatible overhands at each end. This product was then ligated into a linearized pXF40 vector which had been digested with HindIII. Finally, the eGFP-vinculin constructs were digested from the pEGFP-C1 with AgeI and SalI and ligated into the SalI and AgeI-digested pXF40 vector. The pXF40-eGFP-

Vinculin WT and VH vectors transcribe the eGFP-vinculin gene from the tetracycline-inducible promoter. All vectors were verified by sequencing the ligation points.

Retroviral Transduction of eGFP-Vinculin vectors into Vinculin-null Mouse Embryonic Fibroblasts

Retroviral stocks were produced by transient transfection of helper virus-free ΦNX amphotropic producer cells with plasmid DNA as previously described ((Byers et al., 2002)). Vinculin-null mouse embryonic fibroblasts, a kind gift from Eileen Adamson, were cultured and plated on tissue culture polystyrene at $2x10^4$ cells/cm^2 24 h prior to retroviral transduction. Cells were transduced with 0.2 ml/cm^2 of equal parts pTJ66-tTA and pXF40-eGFP-Vinculin retroviral supernatant supplemented with 4 μg/mL hexadimethrine bromide (Polybrene) and 10% fetal bovine serum, and centrifuged at 2500 r.p.m. (1200 g) for 30 min in a Beckman model GS-6R centrifuge with a swinging bucket rotor. Retroviral supernatant was replaced with growth media (DMEM, 10% fetal bovine serum, 100U/mL penicillin G sodium, 100 μg/mL streptomycin sulfate, 1% non-essential amino acids, 1% sodium pyruvate). Five days after transduction, eGFP expressing cells were FACS sorted, expanded, and either used for experimentation or cyropreserved in liquid nitrogen for later use. Expression of vinculin constructs was verified by Western blot and immunofluorescence microscopy (data not shown).

Results

Microfabriated post array detector system (mPADs) for cell traction force measurements

Cells continually sense, respond to, and modulate their mechanical environment. Physical cues from the extracellular matrix control cell behaviors such as migration, proliferation, and differentiation. Here, we use microfabricated post array detector systems (mPADs), originally developed by the laboratory of Chris Chen (U of Pennsylvania), to measure cell generated traction forces (Fu et al., 2010). The effective stiffness of each device can be tuned by changing the height of the individual pillars and there exists a well-characterized library of devices that are freely available (http://www.seas.upenn.edu/~chenlab/micropostform.html). We screened devices with three different spring constants (3.8, 11.5, 18.2 nN/μm) in order to determine the stiffness range that promoted optimal cell spreading and traction force generation with our vinculin-null mouse embryonic cells (MEF1) (data not shown). Based on these results, we chose mPADs with a post height of 6.1μm, post diameter of 1.83μm, and post-to-post spacing of 2μm, resulting in an effective spring constant of 18.2 nN/μm. We seeded vinculin-null MEF1 cells re-expressing vinculin-eGFP (Fig. 5.1) on FN-coated mPADs (Fig. 6.1A). Devices were mounted in an Attofluor cell chamber (Invitrogen), allowed to equilibrate for > 20 min on a Nikon TE300 equipped with an environmental chamber, and then imaged. Vinculin-eGFP co-localized to the tops of FN-coated posts (Fig. 6.1A) and showed preferential focal adhesion formation at the distal edges of the cell, consistent with MEF1 vinculin-eGFP on glass surfaces (Fig. 5.1C). An image of both the base and top of posts was captured and a composite image of post bottom (blue), post top (red), and vinculin-eGFP was created (Fig. 6.1B). Cell traction forces applied at each post were calculated by importing the image stack into a custom MATLAB code, kindly provided by Chris Chen (Fig. 6.1C). Consistent with previous results, maximum cell traction

forces occurred at the distal edge of the cell and were directed, in general, towards the center of the cell (Fu et al., 2010). Cells remained viable on mPADs for greater than 4 days.

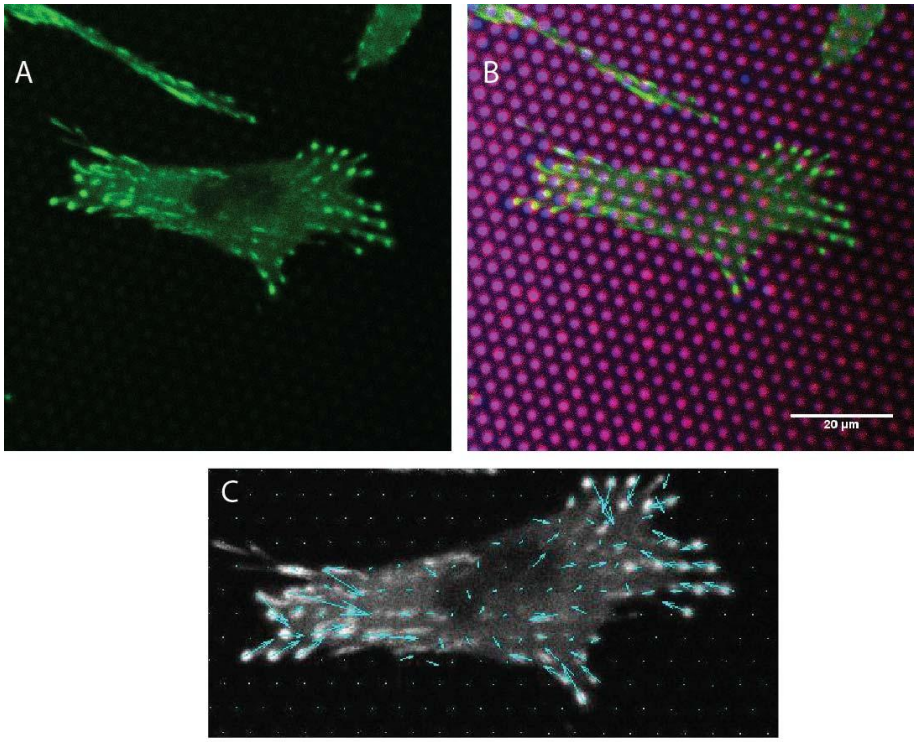

Figure 6.1. Microfabricated post array detector system (mPADs). (A) Vinculin-null MEF re-expressing WT-eGFP-vinculin spread on mPADs coated with 50µg/mL of fibronectin (FN). (B) Merged images of post bottom (blue), post top (red), spread cell expressing vinculin-eGFP. Notice how FAs localize with tops of posts. (scale bar, 20µm). (C) Blue arrows representing cell traction force applied to each post. Forces range for 0-20nN.

Fluorescent recovery after photobleaching measurements on mPADs

Focal adhesions (FAs) sense and respond to mechanical forces (Balaban et al., 2001). The exact molecular mechanism involved in this process, however, have yet to be determined. Vinculin exists in the cytoplasm in an inactive, autohibited conformation (Chen et al., 2005). At sites of focal adhesions, the protein adopts an open, active conformation and binds to talin and F-actin (Chen et al., 2005). The interaction between

talin and vinculin has recently been proposed as a potential force-sensing unit (Golji and Mofrad, 2010). Physical evidence for force-mediated interaction between vinculin and talin has recently been demonstrated (del Rio et al., 2009). In addition, fluorescence recovery after photobleaching has recently shown that the dynamic behavior of vinculin in focal adhesions is dependent on the spatial location of the adhesion (Wolfenson et al., 2009). Furthermore, a force sensing vinculin molecule demonstrated that vinculin experiences higher forces at the leading edge of migratory cells compared to the rear, retracting edge (Grashoff et al., 2010). To date, however, there exists no direct evidence that the dynamics of vinculin recruitment to FA are modulated by the force.

To address this issue, we combined fluorescent recovery after photobleaching (FRAP) with traction force measuring mPAD devices to characterize how the dynamics of vinculin recruitment to FA are modulated by force across focal adhesions. We measured the dynamics of vinculin-eGFP containing focal adhesions subjected to various levels of force (Fig. 6.2A). Vinculin-eGFP containing adhesions localized directly to the tops of individual posts. Importantly, only focal adhesions that were distinctly associated with a single post were analyzed, allowing for direct measurement of force applied across an adhesion (Fu et al., 2010). Arrowheads adjacent to the focal adhesion subjected to FRAP indicate the magnitude and direction of cell traction force (Fig. 6.2A). Raw images of time series FRAP recovery demonstrate minimal x-y-z stage drift and minimal focal adhesion rearrangement during recovery (Fig. 6.2A). Normalized percent recovery data was computed from raw images using custom MATLAB code. Normalize recovery curves demonstrated the capability of our technique to measure the dynamics of vinculin recruitment to FA independent of the amount of force applied to the post (Fig. 6.2B).

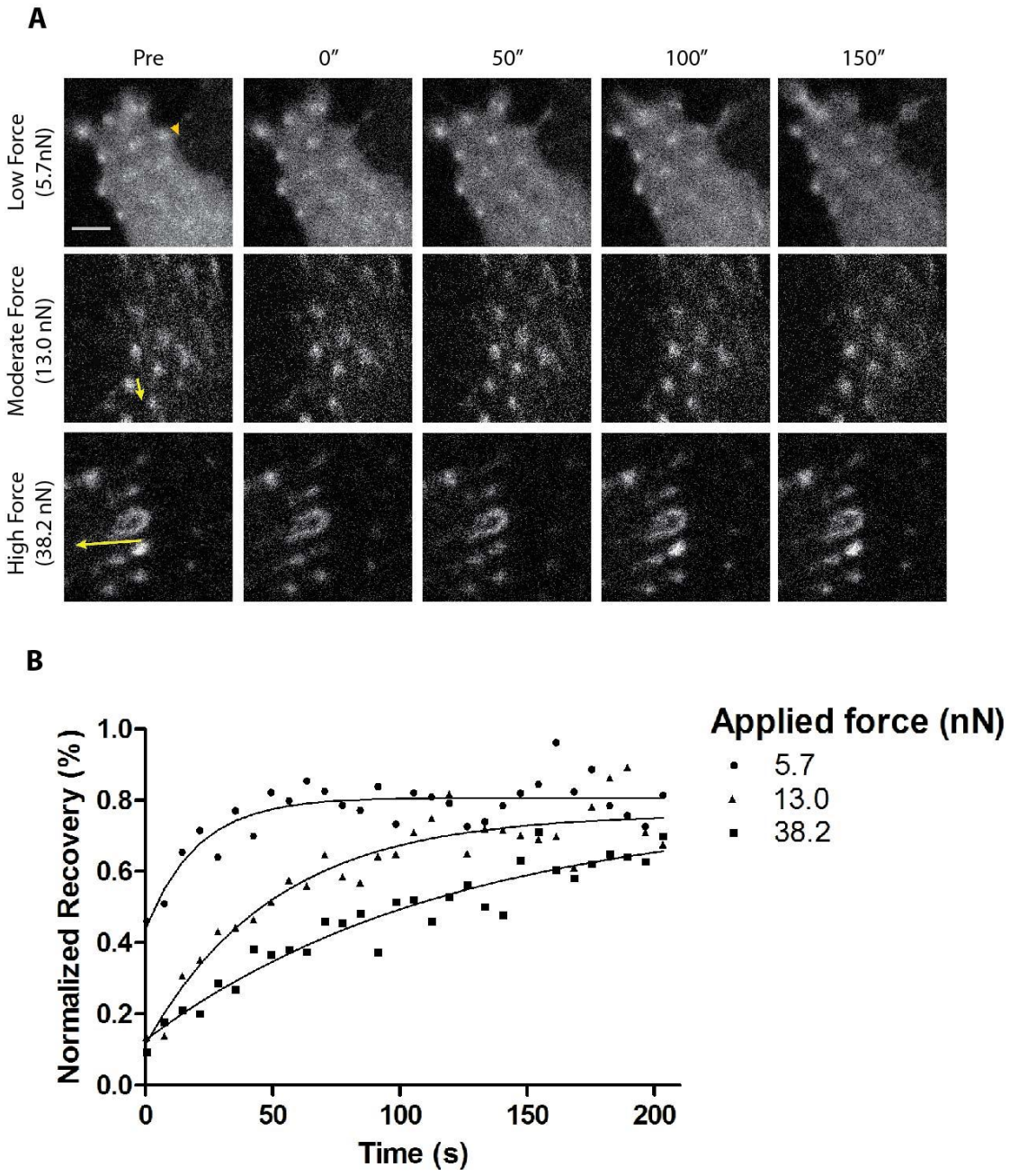

Figure 6.2. Fluorescence recovery of vinculin-eGFP on mPADs. (A) Time-lapse recovery of vinculin-eGFP focal adhesions on mPADs. FAs (arrow heads) were bleached and recovery was monitored (scale bar = 10μm). (B) Normalized recovery for low (5.7nN, filled circles), moderate (13.0nN, filled triangles), and high (38.2nN, filled squares) forces as measured by deflection of FA-associated post. Lines indicate first-order fit to respective data points.

Vinculin association with focal adhesions increases as force applied across focal adhesion increases

Using our novel technique of combining FRAP and traction-force measuring devices, we characterized the dynamics of vinculin in focal adhesions under different amounts of force. A total of 22 focal adhesions in three independent experiments were used to generate the force versus normalized recovery time in Fig. 6.3. We restricted our analysis to focal adhesions that were both located on the periphery of the cell and confined, geometrically, to only one post. In addition, we performed only one FRAP per cell in order to minimize any confounding effects resulting from exposure to the photobleaching laser power. This approach allowed for the most direct measurement of focal adhesion applied force. A linear least-squares fit was applied to the data describing the relationship between vinculin dynamics and applied force through a focal adhesion (slope significantly non-zero, $p < 0.0001$). At small forces, vinculin exhibits faster dynamics, while at higher forces, focal-adhesion associated vinculin exchanges more slowly.

We tested the force-dependent correlation of vinculin recovery by modulating the contractile state of the cytoskeleton. Specifically, we used well-characterized chemical inhibitors to modulate the amount of myosin II mediated cytoskeleton tension. First, vinculin-eGFP cells were exposed to a low concentration (1μM) of the myosin II ATPase inhibitor blebbistatin (Straight et al., 2003). This concentration relaxed cell generated contractile forces without complete abrogation of focal adhesions, thus allowing us to perform FRAP measurements (Fig. 6.4, blue dotted line). Importantly, previous reports in the literature have indicated that this concentration is sufficient to modulate cell

migration speed and adhesion strength (Gupton and Waterman-Storer, 2006). Vinculin-eGFP recovery times in cells exposed to blebbistatin demonstrated excellent agreement with our previous results. Next, cell traction force was increased by addition of low-levels of calyculin-A (100 pM), a potent type II phophatase inhibitor that blocks myosin II phosphatase, thus enhancing myosin II activity (Ishihara et al., 1989). A histogram of measured forces revealed that this concentration reduced the occurrence of low traction forces (Fig. 6.4A, red dotted line). The characteristic recovery time as a function of force closely matched our results in the absence of inhibitors (Fig. 6.4B). Taken together, the data indicate that the rate of vinculin dissociation in focal adhesion decreases as the amount of force applied across the adhesion increases. This result supports a simple model by which cytoskeleton generated tension across vinculin modulates its binding interactions within FAs.

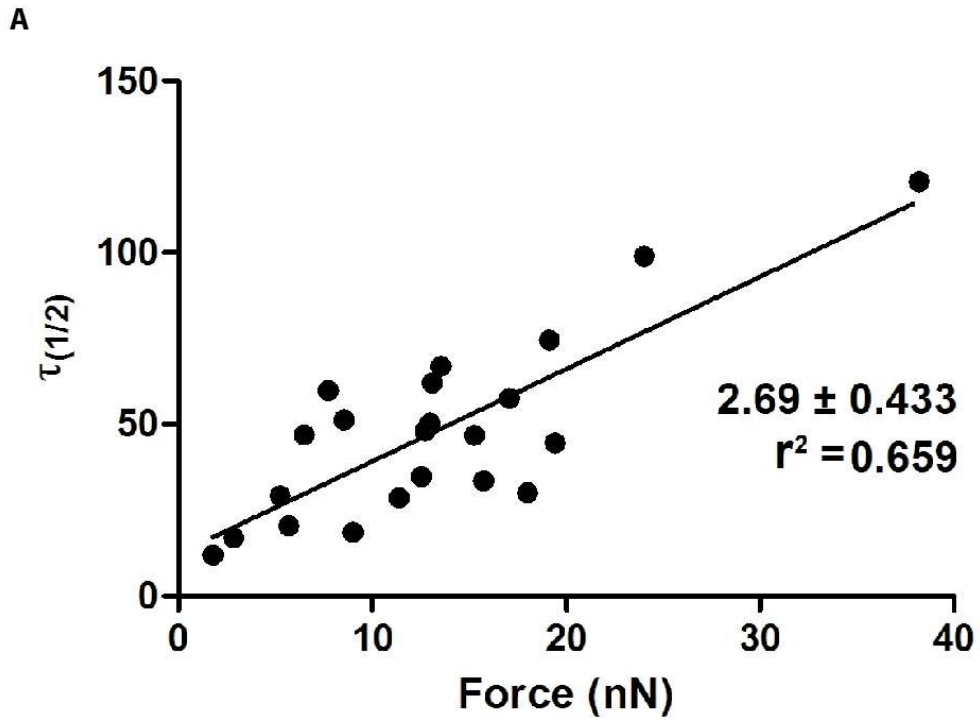

Figure 6.3. Disassociation of vinculin from focal adhesions slows as force applied to adhesion increases (A) Characteristic recovery time, $\tau_{(1/2)}$, plotted as a function of FA force. Each data point represents a single FA recovery in a cell. Fitted line is a linear least squares fit with the slope (s/nN) and r-squared values indicated. Slope is significantly non-zero, $p < 0.0001$.

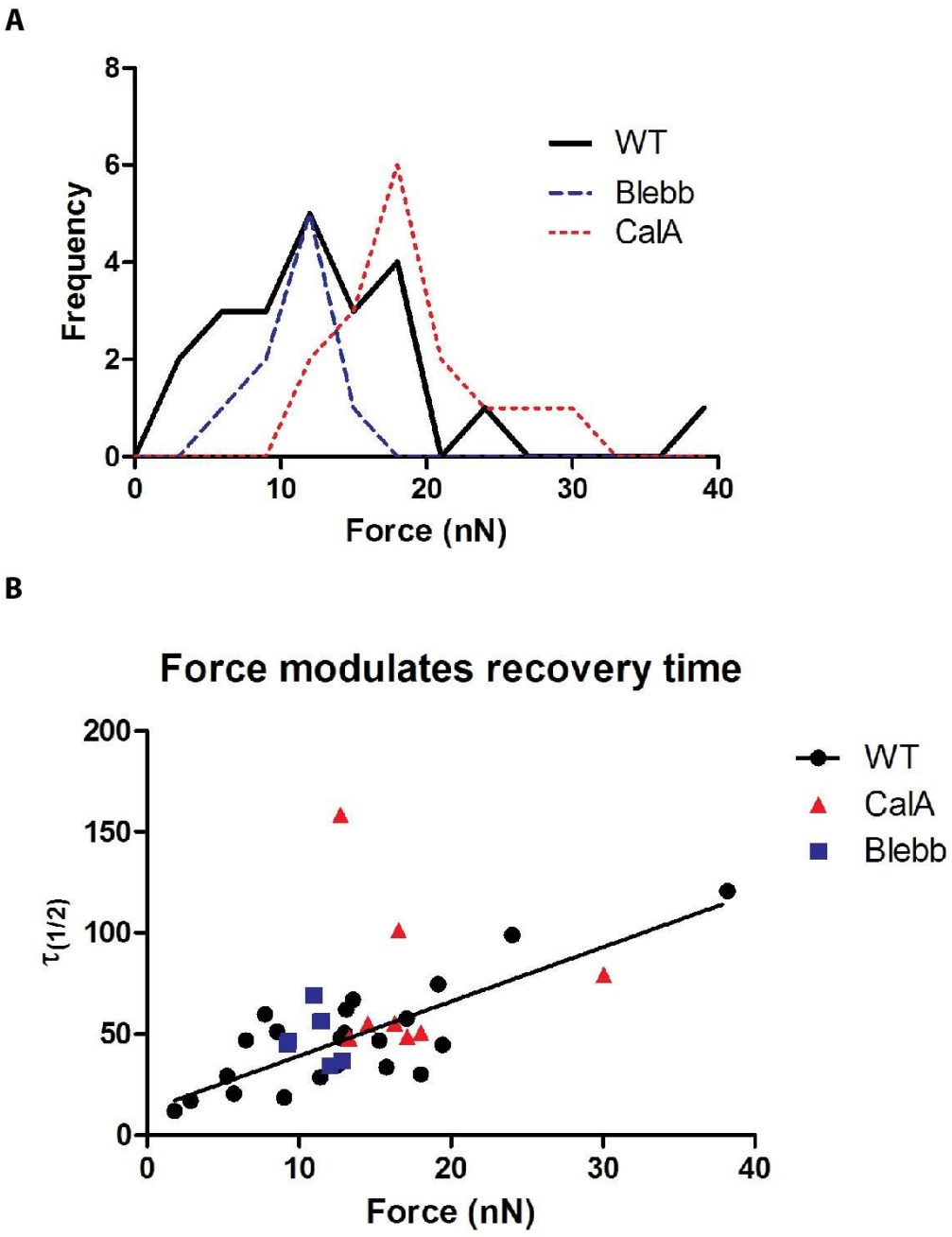

Figure 6.4. Effect of myosin II-mediated contractility modulating drugs on vinculin turnover. (A) Histogram of the number of FRAP experiments performed at specified force. Cells were treated with the myosin II inhibitor, Blebbistatin (1μM), to reduce cytoskeleton generated tension. Likewise, cells were treated with calyculin A (0.1nM) to enhance myosin II activity. (B) Vinculin WT-eGFP characteristic recovery time plotted as a function of measured FA force in the absence (black dots) or presence of myosin II inhibiting (Blebbistatin, blue squares) or enhancing (calyculin A, red triangles) drugs.

Force dependent recovery of vinculin head domain

To test the model that cytoskeleton generated tension across vinculin modulates its binding interactions within FAs, we investigated the force dependent behavior of the talin-binding vinculin head domain which lacks the actin-binding tail domain. Importantly, this mutant cannot bind the actin cytoskeleton directly and, therefore, force from the cytoskeleton cannot be transferred through the protein (Grashoff et al., 2010). We predicted that this mutant form of vinculin would exhibit force-*independent* dynamic interactions with focal adhesions.

MEF1 cells expressing VH-eGFP (Fig.5.6) were seeded onto FN-coated mPADs and allowed to adhere overnight (Fig. 6.5). Similar to WT-eGFP, VH-eGFP expressing MEF1 cells spread and developed contractile forces on mPADs. In addition, VH-eGFP demonstrated the ability to form punctuate focal adhesions that were localized and constrained to individual posts (Fig. 6.5A). Compared to VH-eGFP cells seeded on FN-coated glass substrates, cells on mPADs spread to a similar area and exhibited a similar increase in the number of focal adhesions, compared to WT. We measured the force dependent characteristic recovery time of VH-eGFP constructs and plotted the results against the previously captured WT-eGFP data (Fig. 6.5B). In contrast to WT, recovery of VH-eGFP was more dependent on the applied force across the adhesion. A linear least-squares fit had a slope of 16.7 (s/nN) compared to 2.69 (s/nN) for WT. More experiments with the VH-eGFP mutant are required to confirm this preliminary finding.

This is result is very surprising as it provides evidence to contradict the simple model that the dynamics of vinculin recruitment to focal adhesions are solely dependent upon the cytoskeleton-generated tension applied through the molecule. It also suggests

that, in addition to the auto-inhibition head-tail interaction (Cohen et al., 2005), the force applied to the focal adhesion is also an important regulator of vinculin dynamics. We show that the force applied to focal adhesions can modulate the dynamic recruitment of vinculin, independent of any direct application of cytoskeleton generated force to the molecule. A simple explanation for this result is that cytoskeleton generated force is transferred to focal adhesion causes force-induced exposure of vinculin binding sites on talin.

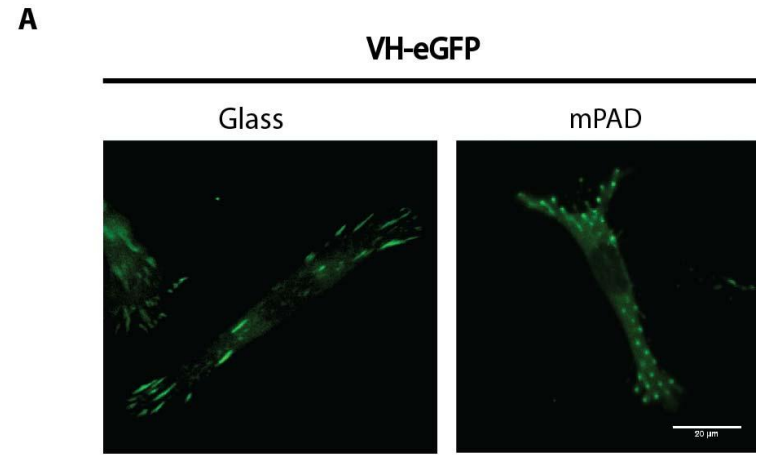

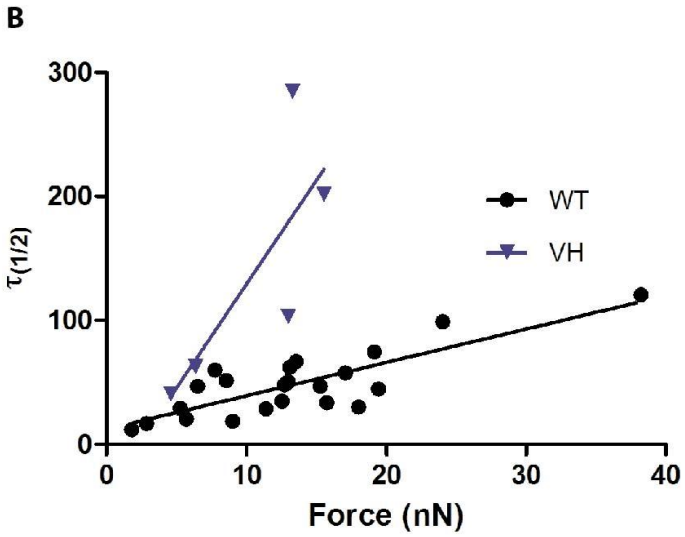

C

	Slope (s/nN)	r^2
WT	2.69 ± 0.433	0.659
VH	16.7 ± 7.73	0.610

Figure 6.5. Force dependent turnover of head and tail domain of vinculin. (A) Vinculin-null MEF1 cells expressing VH-eGFP on glass (left) and on mPAD device (right) (scale 20µm). (B) Characteristic recovery times of VH-eGFP compared to WT-eGFP. (C) Parameters of lines for linear least squares fit of WT-eGFP and VH-eGFP data.

Dynamics of vinculin-tail domain cannot be correlated to force measurements

Because the focal adhesion dynamics of the talin-binding head domain (VH-eGFP) showed a strong relationship to the applied force, we next analyzed the force

dependent dynamics of the vinculin tail (vinT-YFP). The head and tail domain of vinculin cooperate to maintain vinculin in an inactive confirmation until it becomes activated at sites of focal adhesions. In addition the tail domain contains the F-actin binding domain. We transfected YFP-conjugated tail domain (vinT-YFP) into vinculin-null MEF1 cells and seeded cells onto glass substrates (Fig. 6.6A). vinT-YFP localized to the distal tips of cell extensions and also bound to F-actin fibers, consistent with previous findings (Humphries et al., 2007). When seeded onto mPADs, vinT-YFP did not localize to discrete posts. In contrast, vinT-YFP failed to form any punctuate adhesions and, instead, exhibited diffuse staining in the cytoplasm (Fig. 6.6B). In addition, vinT-YFP did not localize (green arrow) to the distal areas of the cell, where maximum post deflection occurred (red arrow showing deflected post) (Fig. 6.6B, inset). We captured a total of 6 FRAP measurements of the vinT-YFP molecule. VinT-YFP exhibited a fast average characteristic recovery time of 20 s. These recovery times are consistent with previous reports (Humphries et al., 2007) suggesting proper vinT-YFP function.

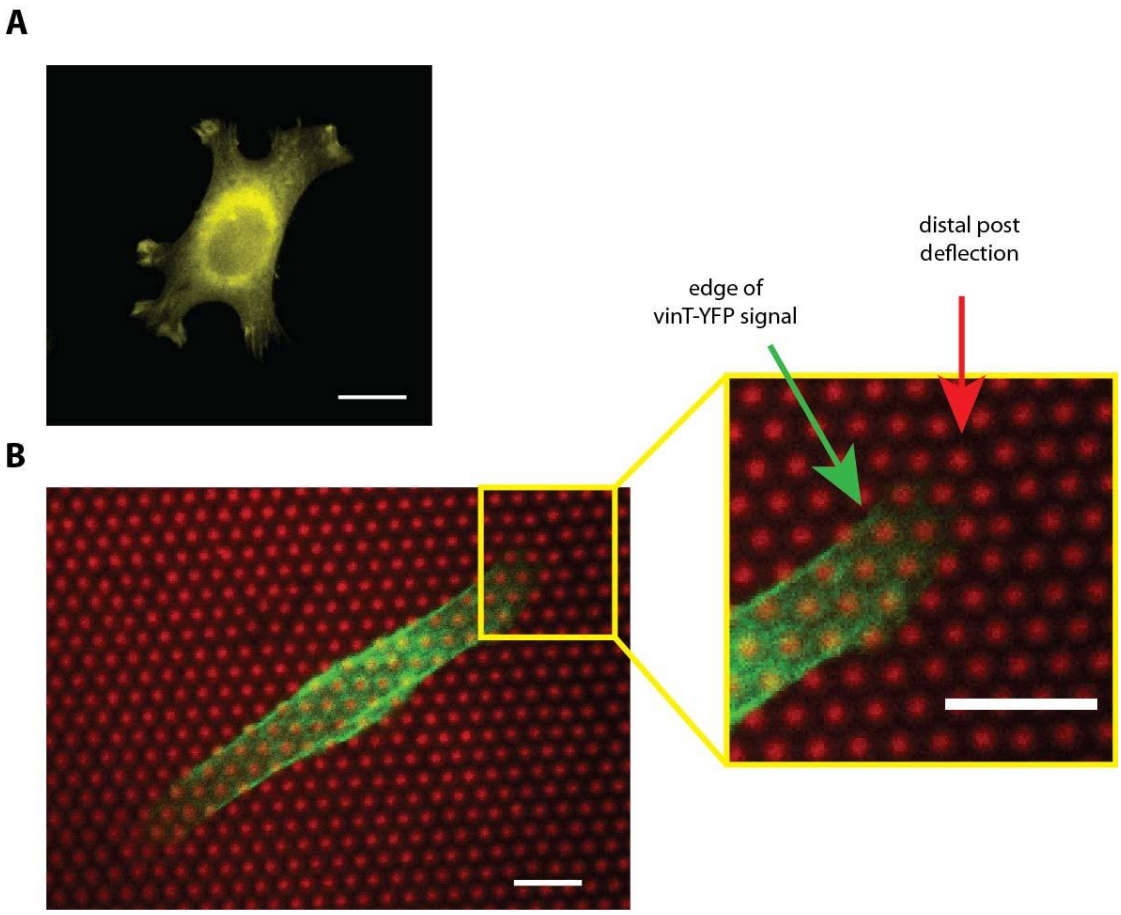

Figure 6.6. Recovery time versus force measurements cannot be made with vinculin-tail-YFP (vinT-YFP) because vinT-YFP structures span multiple posts and do not localize to deflected posts. (A) vinT-YFP construct transiently transfected into MEF1 vinculin-null cells and seeded onto FN-coated glass coverslips. Cells were fixed with 4% paraformaldehyde and mounted on glass slides followed by visualization with fluorescence microscopy (scale 10µm). vinT-YFP transfected MEF1 cells seeded onto mPAD device. In constrast to WT-eGFP and VH-eGFP vinculin molecules, the vinT-YFP does not localize to tops of mPAD pillars (scale bar 10µm). In addition, inset shows how the vinT-YFP signal attenuates (green arrowhead) approximated 4µm from distal deflected posts(red arrow head) (scale 10 µm).

Discussion

We describe a novel method for measuring force-mediated focal adhesion protein dynamics. This method utilizes micro arrayed posts to measure cell generated traction force. This approach to measuring force is advantageous because it decouples changes in substrate stiffness from changes in the microscopic material properties that could affect

ligand binding and cell response (Fu et al., 2010). In addition, the technique allows for direct measurement of the force applied to focal adhesions that co-localize with individual posts (Fu et al., 2010; Tan et al., 2003). We measured the dynamic behavior of focal adhesion associated proteins using fluorescence recovery after photobleaching. The fluorescence recovery of vinculin protein inside of the photobleached spot is dominated by the exchange dynamics between vinculin binding partners, rather than diffusion (see materials and methods). By measuring the time-dependent intensity of fluorescence recovery, we determined the characteristic recovery time of FA-associated vinculin as a function of force. The assumption that recovery is dominated by interactions with binding partners is reasonable based on our own calculations (see methods) and, in addition, recent results that used difference sizes of photobleached spots demonstrated that both vinculin and talin dynamics in focal adhesions are reaction-dominated (Wolfenson et al., 2009). We used this novel technique to test the hypothesis that the dynamics of vinculin recruitment to focal adhesions are modulated by force.

We first demonstrate that vinculin-null cells engineered to express vinculin-eGFP constructs adhere and spread on mPADs (Fig. 6.1). Importantly, vinculin-eGFP localizes to the tops of posts and form discrete, independent focal adhesions. This observed FA morphology allows us to directly measure the force applied through individual focal adhesions. In contrast, expression of the head-tail interaction vinculin mutant (T12) developed adhesions that spanned multiple posts, making it difficult to interpret how measured forces across multiple deflected forces are distributed through the focal adhesion.

We next demonstrate the feasibility of our measurement technique across of range of posts deflections (Fig. 6.2). Vinculin association and accumulation within focal adhesions can be modulated by substrate stiffness and changes in substrate strain (Balaban et al., 2001). Therefore, it is possible that at low force levels, vinculin accumulation might be beneath detectable threshold for proper execution of FRAP experiments. Time-lapse images of low-force focal adhesions e demonstrate that, indeed, our technique has the sensitivity to measure recovery times on posts transferring as low as 1 nN of force (Fig. 6.2A). The % recovery of fluorescence signal for three different forces (Fig. 6.2B) demonstrates that our system is capable of a FRAP measurements through a wide-range of forces.

We next characterized the force-dependent recruitment of vinculin to focal adhesions. Our results indicate that the dynamic recruitment of vinculin to focal adhesions is linearly correlated to applied FA force. Specifically, at low force, vinculin protein exhibits the fastest recovery time, while at high force, the recovery time is significantly slower (higher characteristic recovery time) (Fig. 6.3). To confirm the results, we used chemical inhibitors to modulate the overall traction force of the cell. Small amounts of blebbistatin (1μM) reduced the contractile state of the cell (Fig. 6.4A), but did not fully dissolve vinculin containing focal adhesions. Force versus recovery time measurements of focal adhesion exposed to blebbistatin correlated well with our non-inhibitor data (Fig. 6.4B), suggesting that force modulates vinculin dynamics within focal adhesion. Cytoskeleton tension was increased by the addition of low levels of calyculin-A (100 pM). This potent type II phophatase inhibitor blocks myosin II phosphatase, thus enhancing myosin II activity (Ishihara et al., 1989) and cell traction

forces. At low concentrations (<1nM), calyculin-A is relatively specific for myosin II phosphatase, thus minimizing the chance our results are due to off target effects that might regulate vinculin dynamics (Gupton and Waterman-Storer, 2006). Force-recovery curves for calyculin-A enhanced contractility demonstrated close alignment with our inhibitor-free data. Taken together, these data constitute the first *in-cellulo* measurements describing the relationship between applied force and the dynamics of vinculin recruitment to FAs. These results provide important, new insights into the mechanotransduction pathways that allow FAs to be force responsive.

The data also indicate that vinculin dynamics in focal adhesion are linearly related to the amount of force applied across the adhesion. In agreement with previous reports (Balaban et al., 2001; Grashoff et al., 2010), this result supports a simple model by which cytoskeleton generated tension applied across vinculin modulates its binding interactions within FAs.

To test the model that cytoskeleton generated tension across vinculin modulates its binding interactions within FAs, we investigated the force dependent behavior of the talin-binding vinculin head domain which lacks the actin-binding tail domain. Importantly, this mutant cannot bind the actin cytoskeleton and, therefore, force from the cytoskeleton cannot be transferred through the protein (Grashoff et al., 2010). We predicted that this mutant form of vinculin would exhibit force-*independent* dynamic interactions with focal adhesions. In contrast to WT, recovery of the vinculin head domain was more dependent on the applied force across the focal adhesion. A linear least-squares fit had a slope of 16.7 (s/nN) compared to 2.69 (s/nN) for WT.

This is result is very surprising as it provides evidence to contradict the simple model that the dynamics of vinculin recruitment to focal adhesions are solely dependent upon the cytoskeleton-generated tension applied through the molecule. We show that the force applied to focal adhesions can modulate the dynamic recruitment of vinculin, independent of any direct application of cytoskeleton generated force to the molecule.

A simple explanation for this result is that cytoskeleton generated forces are transferred to focal adhesions causing force-induced exposure of vinculin binding sites (VBS) on FA proteins that, in turn, modulate vinculin dynamics. Recent experimental results supporting this model demonstrated that applied tensile force to individual talin molecules exposed cryptic vinculin-binding sites which promoted binding of the vinculin head domain (del Rio et al., 2009). We therefore hypothesize that cytoskeleton generated force applied across talin exposes one or more vinculin binding sites (VBS) that are important for the force-dependent dynamics of recruitment of vinculin to FAs. Taken together, a model emerges wherein vinculin dynamics are regulated both by direct application of cytoskeleton generated force across vinculin and by force induced exposure of VBS on talin. Further experimental data are required to confirm or reject this hypothesis.

Finally, we demonstrate a technical limitation of measuring force-induced focal adhesion dynamics. Specifically, we transfected vinculin tail domain in vinculin-null cells and attempted to measure the relationship between force and tail dynamics. As can be seen from cells seeded on traction force measurement devices, vinculin tail did not localize to individual posts. Therefore, while we could measure both force and recovery time, the two could not be correlated because the tail did not localize to discrete posts

(Fig. 6.6). It is interesting to note that while the vinculin tail did localize to focal adhesions when cells are plated on glass, we did not observe the same localization on the mPADs. The stiffness difference between the two substrates could account for this observation. A possible explanation is that there is a minimum amount of force applied to a FA in order to recruit the vinculin tail. Further experiments, beyond the scope of this work, are required to test this hypothesis.

CHAPTER 7

Conclusions and Future Directions

The objective of this project was to analyze the role of vinculin in the cell adhesion strengthening process. Our central hypothesis was that vinculin modulates adhesion strength via regulating the size and/or composition of the integrin-talin-vinculin complex. The rationale for this project was that use of a novel combination of biochemical reagents and engineering techniques along with quantitative and sensitive adhesion strength measurements would provide new insights into how the structure of vinculin contributes to cell adhesion strength.

In Chapter 3 we demonstrate that focal-adhesion kinase (FAK) regulates steady-state adhesion strength by regulating vinculin localization to focal adhesions. In Chapter 4, we demonstrate that actin-myosin contractility controls cell adhesion strengthening through focal adhesion kinase and the assembly of vinculin-containing focal adhesions. Both of these results pointed to vinculin as being an important regulator of adhesive force. Indeed, previous work in our lab suggested that the assembly of vinculin-containing focal adhesions contributed 20% to the generation of cell adhesion strength.

Chapter 5 describes our efforts to further analyze the role of vinculin in the cell adhesion strengthening process. As such, we demonstrate that vinculin increases adhesion strength when expressed in vinculin-null cells. We show that the gains in adhesion strength are attributable to increases in FN-bound integrins and focal adhesion

assembly. Reduction in the strength of the head-tail interaction (T12) increased FN-bound integrins, focal adhesion assembly, and adhesion strength 25% higher than wild-type vinculin. Expression of the head domain only (VH) also increases FN-bound integrins and focal adhesion assembly, however, the adhesion strength is the same as wild-type. We hypothesized that vinculin tail linkage to the cytoskeleton allows for maximum adhesion strength by mechanically linking independent focal adhesions. Adhesion studies with co-expression of independent head and tail domains support this model and demonstrate that the physical connection between the head and tail is essential for achieving maximum adhesion strength. A logical extension of this work would involve a more detailed study of the structure-function relationship of the integrin-talin complex. Using similar approaches as were applied in Chapter 5, a detailed study of how the functional domains of talin and integrin modulate adhesion strength would provide new insight to better understand how the integrin-talin-vinculin complex works together to generate cell adhesion strength.

Chapter 6 describes the development of a novel approach for characterizing the force-dependent dynamics of focal adhesion associated proteins. Using this system, we demonstrate that the dynamics of vinculin recruitment to FAs are linearly dependent on the level of force applied to the focal adhesion. This result supports a simple model in which cytoskeleton generated tension across vinculin modulates its binding interactions within FAs. However, we also provide surprising evidence to contradict this model by showing that the force applied to focal adhesions modulates the dynamic recruitment of vinculin, independent of its interaction with the cytoskeleton. Combined, these results suggests a model by which the dynamic recruitment of vinculin to focal adhesions is, at

least in part, modulated by force applied to other focal adhesions molecules. A natural extension of this work would be to further test the hypothesis that the dynamic recruitment of vinculin to focal adhesions is modulated both by direct application of force across the vinculin molecule and by force applied to other focal adhesion molecules. An obvious candidate is the vinculin and integrin binding molecule, talin. Talin has been implicated in stretch induced exposure of vinculin binding sites (VBS). Future studies could focus on characterizing the specific role of these VBS in force-mediated dynamic recruitment of vinculin to focal adhesions.

REFERENCES

Alenghat, F.J., Fabry, B., Tsai, K.Y., Goldmann, W.H., and Ingber, D.E. (2000). Analysis of cell mechanics in single vinculin-deficient cells using a magnetic tweezer. Biochem Biophys Res Commun *277*, 93-99.

Amano, M., Chihara, K., Kimura, K., Fukata, Y., Nakamura, N., Matsuura, Y., and Kaibuchi, K. (1997). Formation of actin stress fibers and focal adhesions enhanced by Rho-kinase. Science *275*, 1308-1311.

Amano, M., Fukata, Y., and Kaibuchi, K. (2000). Regulation and functions of Rho-associated kinase. Exp Cell Res *261*, 44-51.

Arthur, W.T., and Burridge, K. (2001). RhoA inactivation by p190RhoGAP regulates cell spreading and migration by promoting membrane protrusion and polarity. Mol Biol Cell *12*, 2711-2720.

Bakolitsa, C., Cohen, D.M., Bankston, L.A., Bobkov, A.A., Cadwell, G.W., Jennings, L., Critchley, D.R., Craig, S.W., and Liddington, R.C. (2004). Structural basis for vinculin activation at sites of cell adhesion. Nature *430*, 583-586.

Balaban, N.Q., Schwarz, U.S., Riveline, D., Goichberg, P., Tzur, G., Sabanay, I., Mahalu, D., Safran, S., Bershadsky, A., Addadi, L., *et al.* (2001). Force and focal adhesion assembly: a close relationship studied using elastic micropatterned substrates. Nat Cell Biol *3*, 466-472.

Barstead, R.J., and Waterston, R.H. (1991). Vinculin is essential for muscle function in the nematode. J Cell Biol *114*, 715-724.

Belkin, A.M., and Koteliansky, V.E. (1987). Interaction of iodinated vinculin, metavinculin and alpha-actinin with cytoskeletal proteins. FEBS Lett *220*, 291-294.

Benlimame, N., He, Q., Jie, S., Xiao, D., Xu, Y.J., Loignon, M., Schlaepfer, D.D., and Alaoui-Jamali, M.A. (2005). FAK signaling is critical for ErbB-2/ErbB-3 receptor cooperation for oncogenic transformation and invasion. J Cell Biol *171*, 505-516.

Bershadsky, A.D., Ballestrem, C., Carramusa, L., Zilberman, Y., Gilquin, B., Khochbin, S., Alexandrova, A.Y., Verkhovsky, A.B., Shemesh, T., and Kozlov, M.M. (2006). Assembly and mechanosensory function of focal adhesions: experiments and models. Eur J Cell Biol *85*, 165-173.

Bois, P.R., O'Hara, B.P., Nietlispach, D., Kirkpatrick, J., and Izard, T. (2006). The vinculin binding sites of talin and alpha-actinin are sufficient to activate vinculin. J Biol Chem *281*, 7228-7236.

Borgon, R.A., Vonrhein, C., Bricogne, G., Bois, P.R., and Izard, T. (2004). Crystal structure of human vinculin. Structure *12*, 1189-1197.

Braren, R., Hu, H., Kim, Y.H., Beggs, H.E., Reichardt, L.F., and Wang, R. (2006). Endothelial FAK is essential for vascular network stability, cell survival, and lamellipodial formation. J Cell Biol *172*, 151-162.

Brindle, N.P., Holt, M.R., Davies, J.E., Price, C.J., and Critchley, D.R. (1996). The focal-adhesion vasodilator-stimulated phosphoprotein (VASP) binds to the proline-rich domain in vinculin. Biochem J *318 (Pt 3)*, 753-757.

Burridge, K., and Mangeat, P. (1984). An interaction between vinculin and talin. Nature *308*, 744-746.

Byers, B.A., Pavlath, G.K., Murphy, T.J., Karsenty, G., and Garcia, A.J. (2002). Cell-type-dependent up-regulation of in vitro mineralization after overexpression of the osteoblast-specific transcription factor Runx2/Cbfal. J Bone Miner Res *17*, 1931-1944.

Capadona, J.R., Collard, D.M., and Garcia, A.J. (2003). Fibronectin adsorption and cell adhesion to mixed monolayers of tri (ethylene glycol)-and methyl-terminated alkanthiols. Langmuir *19*, 1847-1852.

Chan, K.T., Cortesio, C.L., and Huttenlocher, A. (2009). FAK alters invadopodia and focal adhesion composition and dynamics to regulate breast cancer invasion. J Cell Biol *185*, 357-370.

Chen, B.H., Tzen, J.T., Bresnick, A.R., and Chen, H.C. (2002). Roles of Rho-associated kinase and myosin light chain kinase in morphological and migratory defects of focal adhesion kinase-null cells. J Biol Chem *277*, 33857-33863.

Chen, H., Choudhury, D.M., and Craig, S.W. (2006). Coincidence of actin filaments and talin is required to activate vinculin. J Biol Chem *281*, 40389-40398.

Chen, H., Cohen, D.M., Choudhury, D.M., Kioka, N., and Craig, S.W. (2005). Spatial distribution and functional significance of activated vinculin in living cells. J Cell Biol *169*, 459-470.

Choquet, D., Felsenfeld, D.P., and Sheetz, M.P. (1997). Extracellular matrix rigidity causes strengthening of integrin-cytoskeleton linkages. Cell *88*, 39-48.

Chrzanowska-Wodnicka, M., and Burridge, K. (1996). Rho-stimulated contractility drives the formation of stress fibers and focal adhesions. J Cell Biol *133*, 1403-1415.

Clemente, C.F., Tornatore, T.F., Theizen, T.H., Deckmann, A.C., Pereira, T.C., Lopes-Cendes, I., Souza, J.R., and Franchini, K.G. (2007). Targeting focal adhesion kinase with small interfering RNA prevents and reverses load-induced cardiac hypertrophy in mice. CircRes *101*, 1339-1348.

Cohen, D.M., Chen, H., Johnson, R.P., Choudhury, B., and Craig, S.W. (2005). Two distinct head-tail interfaces cooperate to suppress activation of vinculin by talin. J Biol Chem *280*, 17109-17117.

Cohen, D.M., Kutscher, B., Chen, H., Murphy, D.B., and Craig, S.W. (2006). A conformational switch in vinculin drives formation and dynamics of a talin-vinculin complex at focal adhesions. J Biol Chem *281*, 16006-16015.

Coll, J.L., Ben-Ze'ev, A., Ezzell, R.M., Rodriguez Fernandez, J.L., Baribault, H., Oshima, R.G., and Adamson, E.D. (1995). Targeted disruption of vinculin genes in F9 and embryonic stem cells changes cell morphology, adhesion, and locomotion. Proc Natl Acad Sci U S A *92*, 9161-9165.

Coussen, F., Choquet, D., Sheetz, M.P., and Erickson, H.P. (2002). Trimers of the fibronectin cell adhesion domain localize to actin filament bundles and undergo rearward translocation. J Cell Sci *115*, 2581-2590.

Craig, S.W., and Pardo, J.V. (1983). Gamma actin, spectrin, and intermediate filament proteins colocalize with vinculin at costameres, myofibril-to-sarcolemma attachment sites. Cell Motil *3*, 449-462.

Critchley, D.R. (2000). Focal adhesions - the cytoskeletal connection. Curr Opin Cell Biol *12*, 133-139.

Critchley, D.R. (2004). Cytoskeletal proteins talin and vinculin in integrin-mediated adhesion. Biochem Soc Trans *32*, 831-836.

Danen, E.H., and Sonnenberg, A. (2003). Integrins in regulation of tissue development and function. J Pathol *201*, 632-641.

De Arcangelis, A., and Georges-Labouesse, E. (2000). Integrin and ECM functions: roles in vertebrate development. Trends Genet *16*, 389-395.

del Rio, A., Perez-Jimenez, R., Liu, R., Roca-Cusachs, P., Fernandez, J.M., and Sheetz, M.P. (2009). Stretching single talin rod molecules activates vinculin binding. Science *323*, 638-641.

Delanoe-Ayari, H., Al Kurdi, R., Vallade, M., Gulino-Debrac, D., and Riveline, D. (2004). Membrane and acto-myosin tension promote clustering of adhesion proteins. Proc Natl Acad Sci U S A *101*, 2229-2234.

DeMali, K.A. (2004). Vinculin--a dynamic regulator of cell adhesion. Trends Biochem Sci *29*, 565-567.

DeMali, K.A., Barlow, C.A., and Burridge, K. (2002). Recruitment of the Arp2/3 complex to vinculin: coupling membrane protrusion to matrix adhesion. J Cell Biol *159*, 881-891.

Faull, R.J., Kovach, N.L., Harlan, J.M., and Ginsberg, M.H. (1993). Affinity modulation of integrin alpha 5 beta 1: regulation of the functional response by soluble fibronectin. J Cell Biol *121*, 155-162.

Forrest, A.D., Beggs, H.E., Reichardt, L.F., Dupree, J.L., Colello, R.J., and Fuss, B. (2009). Focal adhesion kinase (FAK): A regulator of CNS myelination. J Neurosci Res.

Friedland, J.C., Lee, M.H., and Boettiger, D. (2009). Mechanically activated integrin switch controls alpha5beta1 function. Science *323*, 642-644.

Fu, J., Wang, Y.K., Yang, M.T., Desai, R.A., Yu, X., Liu, Z., and Chen, C.S. (2010). Mechanical regulation of cell function with geometrically modulated elastomeric substrates. Nat Methods *7*, 733-736.

Furuta, Y., Ilic, D., Kanazawa, S., Takeda, N., Yamamoto, T., and Aizawa, S. (1995). Mesodermal defect in late phase of gastrulation by a targeted mutation of focal adhesion kinase, FAK. Oncogene *11*, 1989-1995.

Galbraith, C.G., Yamada, K.M., and Sheetz, M.P. (2002). The relationship between force and focal complex development. J Cell Biol *159*, 695-705.

Gallagher, P.J., Herring, B.P., and Stull, J.T. (1997). Myosin light chain kinases. J Muscle Res Cell Motil *18*, 1-16.

Gallant, N.D., Capadona, J.R., Frazier, A.B., Collard, D.M., and García, A.J. (2002). Micropatterned surfaces to engineer focal adhesions for analysis of cell adhesion strengthening. Langmuir *18*, 5579-5584.

Gallant, N.D., and Garcia, A.J. (2007a). Model of integrin-mediated cell adhesion strengthening. J Biomech *40*, 1301-1309.

Gallant, N.D., and Garcia, A.J. (2007b). Quantitative analyses of cell adhesion strength. Methods Mol Biol *370*, 83-96.

Gallant, N.D., Michael, K.E., and Garcia, A.J. (2005). Cell adhesion strengthening: contributions of adhesive area, integrin binding, and focal adhesion assembly. Mol Biol Cell *16*, 4329-4340.

Garcia, A.J., Ducheyne, P., and Boettiger, D. (1997). Quantification of cell adhesion using a spinning disc device and application to surface-reactive materials. Biomaterials *18*, 1091-1098.

Garcia, A.J., Huber, F., and Boettiger, D. (1998). Force required to break alpha5beta1 integrin-fibronectin bonds in intact adherent cells is sensitive to integrin activation state. Journal of Biological Chemistry *273*, 10988-10993.

García, A.J., Takagi, J., and Boettiger, D. (1998). Two-stage activation for alpha5beta1 integrin binding to surface-adsorbed fibronectin. J Biol Chem *273*, 34710-34715.

Garcia, A.J., Vega, M.D., and Boettiger, D. (1999). Modulation of cell proliferation and differentiation through substrate-dependent changes in fibronectin conformation. Mol Biol Cell *10*, 785-798.

Geiger, B., Bershadsky, A., Pankov, R., and Yamada, K.M. (2001). Transmembrane crosstalk between the extracellular matrix and the cytoskeleton. Nat Rev Mol Cell Biol *2*, 793-805.

Geiger, B., Spatz, J.P., and Bershadsky, A.D. (2009). Environmental sensing through focal adhesions. Nat Rev Mol Cell Biol *10*, 21-33.

Geiger, B., Tokuyasu, K.T., Dutton, A.H., and Singer, S.J. (1980). Vinculin, an intracellular protein localized at specialized sites where microfilament bundles terminate at cell membranes. Proc Natl Acad Sci U S A *77*, 4127-4131.

George, E.L. (1993). Defects in mesoderm, neural tube and vascular development in mouse embryos lacking fibronectin. Development, 1079-1091.

Gersbach, C.A., Phillips, J.E., and Garcia, A.J. (2007). Genetic engineering for skeletal regenerative medicine. Annu Rev Biomed Eng *9*, 87-119.

Gingras, A.R., Vogel, K.P., Steinhoff, H.J., Ziegler, W.H., Patel, B., Emsley, J., Critchley, D.R., Roberts, G.C., and Barsukov, I.L. (2006). Structural and dynamic characterization of a vinculin binding site in the talin rod. Biochemistry *45*, 1805-1817.

Goldmann, W.H., and Ingber, D.E. (2002). Intact vinculin protein is required for control of cell shape, cell mechanics, and rac-dependent lamellipodia formation. Biochem Biophys Res Commun *290*, 749-755.

Golji, J., and Mofrad, M.R. (2010). A molecular dynamics investigation of vinculin activation. Biophys J *99*, 1073-1081.

Gossen, M., Bonin, A.L., Freundlieb, S., and Bujard, H. (1994). Inducible gene expression systems for higher eukaryotic cells. Curr Opin Biotechnol *5*, 516-520.

Grashoff, C., Hoffman, B.D., Brenner, M.D., Zhou, R., Parsons, M., Yang, M.T., McLean, M.A., Sligar, S.G., Chen, C.S., Ha, T., *et al.* (2010). Measuring mechanical tension across vinculin reveals regulation of focal adhesion dynamics. Nature *466*, 263-266.

Greenwood, J.A., Pallero, M.A., Theibert, A.B., and Murphy-Ullrich, J.E. (1998). Thrombospondin signaling of focal adhesion disassembly requires activation of phosphoinositide 3-kinase. J Biol Chem *273*, 1755-1763.

Griffin, M.A., Sen, S., Sweeney, H.L., and Discher, D.E. (2004). Adhesion-contractile balance in myocyte differentiation. J Cell Sci *117*, 5855-5863.

Gupton, S.L., and Waterman-Storer, C.M. (2006). Spatiotemporal feedback between actomyosin and focal-adhesion systems optimizes rapid cell migration. Cell *125*, 1361-1374.

Hanks, S.K., Calalb, M.B., Harper, M.C., and Patel, S.K. (1992). Focal adhesion protein-tyrosine kinase phosphorylated in response to cell attachment to fibronectin. Proc Natl Acad Sci USA *89*, 8487-8491.

Hato, T., Pampori, N., and Shattil, S.J. (1998). Complementary roles for receptor clustering and conformational change in the adhesive and signaling functions of integrin alphaIIb beta3. J Cell Biol *141*, 1685-1695.

Humphries, J.D., Wang, P., Streuli, C., Geiger, B., Humphries, M.J., and Ballestrem, C. (2007). Vinculin controls focal adhesion formation by direct interactions with talin and actin. J Cell Biol *179*, 1043-1057.

Hynes, R.O. (2002). Integrins: bidirectional, allosteric signaling machines. Cell *110*, 673-687.

Hytonen, V.P., and Vogel, V. (2008). How force might activate talin's vinculin binding sites: SMD reveals a structural mechanism. PLoS Comput Biol *4*, e24.

Ilic, D., Furuta, Y., Kanazawa, S., Takeda, N., Sobue, K., Nakatsuji, N., Nomura, S., Fujimoto, J., Okada, M., and Yamamoto, T. (1995). Reduced cell motility and enhanced focal adhesion contact formation in cells from FAK-deficient mice. Nature *377*, 539-544.

Ingber, D.E. (2003). Tensegrity I. Cell structure and hierarchical systems biology. J Cell Sci *116*, 1157-1173.

Ishihara, H., Ozaki, H., Sato, K., Hori, M., Karaki, H., Watabe, S., Kato, Y., Fusetani, N., Hashimoto, K., Uemura, D., *et al.* (1989). Calcium-independent activation of contractile apparatus in smooth muscle by calyculin-A. J Pharmacol Exp Ther *250*, 388-396.

Izard, T., Evans, G., Borgon, R.A., Rush, C.L., Bricogne, G., and Bois, P.R. (2004). Vinculin activation by talin through helical bundle conversion. Nature *427*, 171-175.

Izard, T., and Vonrhein, C. (2004). Structural basis for amplifying vinculin activation by talin. J Biol Chem *279*, 27667-27678.

Izzard, C.S., and Lochner, L.R. (1976). Cell-to-substrate contacts in living fibroblasts: an interference reflexion study with an evaluation of the technique. J Cell Sci *21*, 129-159.

Izzard, C.S., and Lochner, L.R. (1980). Formation of cell-to-substrate contacts during fibroblast motility: an interference-reflexion study. J Cell Sci *42*, 81-116.

Janssen, M.E., Kim, E., Liu, H., Fujimoto, L.M., Bobkov, A., Volkmann, N., and Hanein, D. (2006). Three-dimensional structure of vinculin bound to actin filaments. Mol Cell *21*, 271-281.

Jockusch, B.M., and Isenberg, G. (1981). Interaction of alpha-actinin and vinculin with actin: opposite effects on filament network formation. Proc Natl Acad Sci U S A *78*, 3005-3009.

Johnson, R.P., and Craig, S.W. (1995). F-actin binding site masked by the intramolecular association of vinculin head and tail domains. Nature *373*, 261-264.

Kaibuchi, K., Kuroda, S., and Amano, M. (1999). Regulation of the cytoskeleton and cell adhesion by the Rho family GTPases in mammalian cells. Annu Rev Biochem *68*, 459-486.

Kanchanawong, P., Shtengel, G., Pasapera, A.M., Ramko, E.B., Davidson, M.W., Hess, H.F., and Waterman, C.M. (2010). Nanoscale architecture of integrin-based cell adhesions. Nature *468*, 580-584.

Keselowsky, B.G., and Garcia, A.J. (2005). Quantitative methods for analysis of integrin binding and focal adhesion formation on biomaterial surfaces. Biomaterials *26*, 413-418.

Kimura, K., Ito, M., Amano, M., Chihara, K., Fukata, Y., Nakafuku, M., Yamamori, B., Feng, J., Nakano, T., Okawa, K., *et al.* (1996). Regulation of myosin phosphatase by Rho and Rho-associated kinase (Rho-kinase). Science *273*, 245-248.

Kioka, N., Sakata, S., Kawauchi, T., Amachi, T., Akiyama, S.K., Okazaki, K., Yaen, C., Yamada, K.M., and Aota, S. (1999). Vinexin: a novel vinculin-binding protein with multiple SH3 domains enhances actin cytoskeletal organization. J Cell Biol *144*, 59-69.

Kong, F., Garcia, A.J., Mould, A.P., Humphries, M.J., and Zhu, C. (2009). Demonstration of catch bonds between an integrin and its ligand. J Cell Biol *185*, 1275-1284.

Koteliansky, V.E., Gneushev, G.N., Glukhova, M.A., Venyaminov, S.Y., and Muszbek, L. (1984). Identification and isolation of vinculin from platelets. FEBS Lett *165*, 26-30.

Kovács, M., Tóth, J., Hetényi, C., Málnási-Csizmadia, A., and Sellers, J.R. (2004). Mechanism of blebbistatin inhibition of myosin II. J Biol Chem *279*, 35557-35563.

Kroemker, M., Rudiger, A.H., Jockusch, B.M., and Rudiger, M. (1994). Intramolecular interactions in vinculin control alpha-actinin binding to the vinculin head. FEBS Lett *355*, 259-262.

Kumar, S., and Weaver, V.M. (2009). Mechanics, malignancy, and metastasis: the force journey of a tumor cell. Cancer Metastasis Rev *28*, 113-127.

Le Clainche, C., Dwivedi, S.P., Didry, D., and Carlier, M.F. (2010). Vinculin is a dually regulated actin filament barbed end-capping and side-binding protein. J Biol Chem *285*, 23420-23432.

Lee, S.E., Chunsrivirot, S., Kamm, R.D., and Mofrad, M.R. (2008). Molecular dynamics study of talin-vinculin binding. Biophys J *95*, 2027-2036.

Leucht, P., Kim, J.B., Currey, J.A., Brunski, J., and Helms, J.A. (2007). FAK-Mediated mechanotransduction in skeletal regeneration. PLoS ONE *2*, e390.

Lim, Y., Lim, S.T., Tomar, A., Gardel, M., Bernard-Trifilo, J.A., Chen, X.L., Uryu, S.A., Canete-Soler, R., Zhai, J., Lin, H., *et al.* (2008). PyK2 and FAK connections to p190Rho guanine nucleotide exchange factor regulate RhoA activity, focal adhesion formation, and cell motility. J Cell Biol *180*, 187-203.

Lotz, M.M., Burdsal, C.A., Erickson, H.P., and McClay, D.R. (1989). Cell adhesion to fibronectin and tenascin: quantitative measurements of initial binding and subsequent strengthening response. J Cell Biol *109*, 1795-1805.

Maheshwari, G., Brown, G., Lauffenburger, D.A., Wells, A., and Griffith, L.G. (2000). Cell adhesion and motility depend on nanoscale RGD clustering. J Cell Sci *113 (Pt 10)*, 1677-1686.

Mammoto, A., Connor, K., Mammoto, T., Yung, C., Huh, D., Aderman, C., Mostoslavsky, G., Smith, L.E., and Ingber, D. (2009). A mechanosensitive transcriptional mechanism that controls angiogenesis. Nature *457*, 1103-1108.

Mammoto, A., Huang, S., Moore, K., Oh, P., and Ingber, D.E. (2004). Role of RhoA, mDia, and ROCK in cell shape-dependent control of the Skp2-p27kip1 pathway and the G1/S transition. J Biol Chem *279*, 26323-26330.

Mandai, K., Nakanishi, H., Satoh, A., Takahashi, K., Satoh, K., Nishioka, H., Mizoguchi, A., and Takai, Y. (1999). Ponsin/SH3P12: an l-afadin- and vinculin-binding protein localized at cell-cell and cell-matrix adherens junctions. J Cell Biol *144*, 1001-1017.

McBeath, R., Pirone, D.M., Nelson, C.M., Bhadriraju, K., and Chen, C.S. (2004). Cell shape, cytoskeletal tension, and RhoA regulate stem cell lineage commitment. Dev Cell *6*, 483-495.

Menkel, A.R., Kroemker, M., Bubeck, P., Ronsiek, M., Nikolai, G., and Jockusch, B.M. (1994). Characterization of an F-actin-binding domain in the cytoskeletal protein vinculin. J Cell Biol *126*, 1231-1240.

Michael, K.E., Dumbauld, D.W., Burns, K.L., Hanks, S.K., and Garcia, A.J. (2009). Focal adhesion kinase modulates cell adhesion strengthening via integrin activation. Mol Biol Cell *20*, 2508-2519.

Mierke, C.T., Kollmannsberger, P., Zitterbart, D.P., Smith, J., Fabry, B., and Goldmann, W.H. (2008). Mechano-coupling and regulation of contractility by the vinculin tail domain. Biophys J *94*, 661-670.

Mohl, C., Kirchgessner, N., Schafer, C., Kupper, K., Born, S., Diez, G., Goldmann, W.H., Merkel, R., and Hoffmann, B. (2009). Becoming stable and strong: the interplay

between vinculin exchange dynamics and adhesion strength during adhesion site maturation. Cell Motil Cytoskeleton *66*, 350-364.

Narumiya, S., Ishizaki, T., and Uehata, M. (2000). Use and properties of ROCK-specific inhibitor Y-27632. Methods Enzymol *325*, 273-284.

Owen, J.D., Ruest, P.J., Fry, D.W., and Hanks, S.K. (1999). Induced focal adhesion kinase (FAK) expression in FAK-null cells enhances cell spreading and migration requiring both auto- and activation loop phosphorylation sites and inhibits adhesion-dependent tyrosine phosphorylation of Pyk2. Mol Cell Biol *19*, 4806-4818.

Palecek, S.P., Loftus, J.C., Ginsberg, M.H., Lauffenburger, D.A., and Horwitz, A.F. (1997). Integrin-ligand binding properties govern cell migration speed through cell-substratum adhesiveness. Nature *385*, 537-540.

Pardo, J.V., Siliciano, J.D., and Craig, S.W. (1983a). A vinculin-containing cortical lattice in skeletal muscle: transverse lattice elements ("costameres") mark sites of attachment between myofibrils and sarcolemma. Proc Natl Acad Sci U S A *80*, 1008-1012.

Pardo, J.V., Siliciano, J.D., and Craig, S.W. (1983b). Vinculin is a component of an extensive network of myofibril-sarcolemma attachment regions in cardiac muscle fibers. J Cell Biol *97*, 1081-1088.

Parizi, M., Howard, E.W., and Tomasek, J.J. (2000). Regulation of LPA-promoted myofibroblast contraction: role of Rho, myosin light chain kinase, and myosin light chain phosphatase. Exp Cell Res *254*, 210-220.

Pasapera, A.M., Schneider, I.C., Rericha, E., Schlaepfer, D.D., and Waterman, C.M. (2010). Myosin II activity regulates vinculin recruitment to focal adhesions through FAK-mediated paxillin phosphorylation. J Cell Biol *188*, 877-890.

Peng, X., Wu, X., Druso, J.E., Wei, H., Park, A.Y., Kraus, M.S., Alcaraz, A., Chen, J., Chien, S., Cerione, R.A., *et al.* (2008). Cardiac developmental defects and eccentric right ventricular hypertrophy in cardiomyocyte focal adhesion kinase (FAK) conditional knockout mice. Proc Natl Acad Sci U S A *105*, 6638-6643.

Pirone, D.M., Liu, W.F., Ruiz, S.A., Gao, L., Raghavan, S., Lemmon, C.A., Romer, L.H., and Chen, C.S. (2006). An inhibitory role for FAK in regulating proliferation: a link between limited adhesion and RhoA-ROCK signaling. J Cell Biol *174*, 277-288.

Polte, T.R., Eichler, G.S., Wang, N., and Ingber, D.E. (2004). Extracellular matrix controls myosin light chain phosphorylation and cell contractility through modulation of cell shape and cytoskeletal prestress. Am J Physiol Cell Physiol *286*, C518-528.

Polte, T.R., and Hanks, S.K. (1995). Interaction between focal adhesion kinase and Crk-associated tyrosine kinase substrate p130Cas. Proc Natl Acad Sci U S A *92*, 10678-10682.

Quach, N.L., Biressi, S., Reichardt, L.F., Keller, C., and Rando, T.A. (2009). Focal Adhesion Kinase Signaling Regulates the Expression of Caveolin 3 and beta1 Integrin, Genes Essential for Normal Myoblast Fusion. Mol Biol Cell.

Ren, X.D., Kiosses, W.B., Sieg, D.J., Otey, C.A., Schlaepfer, D.D., and Schwartz, M.A. (2000). Focal adhesion kinase suppresses Rho activity to promote focal adhesion turnover. J Cell Sci *113*, 3673-3678.

Renshaw, M.W., Price, L.S., and Schwartz, M.A. (1999). Focal adhesion kinase mediates the integrin signaling requirement for growth factor activation of MAP kinase. J Cell Biol *147*, 611-618.

Ridley, A.J., and Hall, A. (1992). The small GTP-binding protein rho regulates the assembly of focal adhesions and actin stress fibers in response to growth factors. Cell *70*, 389-399.

Ridley, A.J., Schwartz, M.A., Burridge, K., Firtel, R.A., Ginsberg, M.H., Borisy, G., Parsons, J.T., and Horwitz, A.R. (2003). Cell migration: integrating signals from front to back. Science *302*, 1704-1709.

Riveline, D., Zamir, E., Balaban, N.Q., Schwarz, U.S., Ishizaki, T., Narumiya, S., Kam, Z., Geiger, B., and Bershadsky, A.D. (2001). Focal contacts as mechanosensors: externally applied local mechanical force induces growth of focal contacts by an mDia1-dependent and ROCK-independent mechanism. J Cell Biol *153*, 1175-1186.

Samarel, A.M. (2005). Costameres, focal adhesions, and cardiomyocyte mechanotransduction. Am J Physiol Heart Circ Physiol *289*, H2291-2301.

Sastry, S.K., and Burridge, K. (2000). Focal adhesions: a nexus for intracellular signaling and cytoskeletal dynamics. Exp Cell Res *261*, 25-36.

Schaller, M.D., Borgman, C.A., Cobb, B.S., Vines, R.R., Reynolds, A.B., and Parsons, J.T. (1992). pp125FAK, a structurally distinctive protein-tyrosine kinase associated with focal adhesions. Proceedings of the National Academy of Science, USA *89*, 5192-5196.

Schaller, M.D., Hildebrand, J.D., and Parsons, J.T. (1999). Complex formation with focal adhesion kinase: A mechanism to regulate activity and subcellular localization of Src kinases. Mol Biol Cell *10*, 3489-3505.

Schober, M., Raghavan, S., Nikolova, M., Polak, L., Pasolli, H.A., Beggs, H.E., Reichardt, L.F., and Fuchs, E. (2007). Focal adhesion kinase modulates tension signaling to control actin and focal adhesion dynamics. J Cell Biol *176*, 667-680.

Serrels, B., Serrels, A., Brunton, V.G., Holt, M., McLean, G.W., Gray, C.H., Jones, G.E., and Frame, M.C. (2007). Focal adhesion kinase controls actin assembly via a FERM-mediated interaction with the Arp2/3 complex. NatCell Biol *9*, 1046-1056.

Shen, T.L., Park, A.Y., Alcaraz, A., Peng, X., Jang, I., Koni, P., Flavell, R.A., Gu, H., and Guan, J.L. (2005). Conditional knockout of focal adhesion kinase in endothelial cells reveals its role in angiogenesis and vascular development in late embryogenesis. J Cell Biol *169*, 941-952.

Shibue, T., and Weinberg, R.A. (2009). Integrin {beta}1-focal adhesion kinase signaling directs the proliferation of metastatic cancer cells disseminated in the lungs. Proc Natl Acad Sci U S A.

Sieg, D.J., Hauck, C.R., Ilic, D., Klingbeil, C.K., Schaefer, E., Damsky, C.H., and Schlaepfer, D.D. (2000). FAK integrates growth-factor and integrin signals to promote cell migration. Nat Cell Biol *2*, 249-256.

Siesser, P.M., Meenderink, L.M., Ryzhova, L., Michael, K.E., Dumbauld, D.W., García, A.J., Kaverina, I., and Hanks, S.K. (2007). A FAK/Src chimera with gain-of-function properties promotes formation of large peripheral adhesions associated with dynamic actin assembly. Cell Motil Cytoskeleton.

Siu, E.R., Wong, E.W., Mruk, D.D., Porto, C.S., and Cheng, C.Y. (2009). Focal adhesion kinase is a blood-testis barrier regulator. Proc Natl Acad Sci U S A *106*, 9298-9303.

Sniadecki, N.J., Anguelouch, A., Yang, M.T., Lamb, C.M., Liu, Z., Kirschner, S.B., Liu, Y., Reich, D.H., and Chen, C.S. (2007). Magnetic microposts as an approach to apply forces to living cells. Proc Natl Acad Sci U S A *104*, 14553-14558.

Sparrow, J.C., and Schöck, F. (2009). The initial steps of myofibril assembly: integrins pave the way. Nat Rev Mol Cell Biol *10*, 293-298.

Sprague, B.L., and McNally, J.G. (2005). FRAP analysis of binding: proper and fitting. Trends Cell Biol *15*, 84-91.

Steenbergen, C., Hill, M.L., and Jennings, R.B. (1987). Cytoskeletal damage during myocardial ischemia: changes in vinculin immunofluorescence staining during total in vitro ischemia in canine heart. Circ Res *60*, 478-486.

Stephens, L.E., Sutherland, A.E., Klimanskaya, I.V., and al., e. (1995). Deletion of beta 1 integrins in mice results in inner cell mass failure and peri-implantation lethality. Genes & Development, 1883-1895.

Straight, A.F., Cheung, A., Limouze, J., Chen, I., Westwood, N.J., Sellers, J.R., and Mitchison, T.J. (2003). Dissecting temporal and spatial control of cytokinesis with a myosin II Inhibitor. Science *299*, 1743-1747.

Subauste, M.C., Pertz, O., Adamson, E.D., Turner, C.E., Junger, S., and Hahn, K.M. (2004). Vinculin modulation of paxillin-FAK interactions regulates ERK to control survival and motility. J Cell Biol *165*, 371-381.

Tan, J.L., Tien, J., Pirone, D.M., Gray, D.S., Bhadriraju, K., and Chen, C.S. (2003). Cells lying on a bed of microneedles: an approach to isolate mechanical force. Proc Natl Acad Sci USA *100*, 1484-1489.

Tanaka, E., and Sabry, J. (1995). Making the connection: cytoskeletal rearrangements during growth cone guidance. Cell *83*, 171-176.

Tomar, A., Lim, S.T., Lim, Y., and Schlaepfer, D.D. (2009). A FAK-p120RasGAP-p190RhoGAP complex regulates polarity in migrating cells. J Cell Sci *122*, 1852-1862.

Totsukawa, G., Yamakita, Y., Yamashiro, S., Hartshorne, D.J., Sasaki, Y., and Matsumura, F. (2000). Distinct roles of ROCK (Rho-kinase) and MLCK in spatial regulation of MLC phosphorylation for assembly of stress fibers and focal adhesions in 3T3 fibroblasts. J Cell Biol *150*, 797-806.

Turner, C.E., Glenney, J.R., Jr., and Burridge, K. (1990). Paxillin: a new vinculin-binding protein present in focal adhesions. J Cell Biol *111*, 1059-1068.

Vasile, V.C., Edwards, W.D., Ommen, S.R., and Ackerman, M.J. (2006). Obstructive hypertrophic cardiomyopathy is associated with reduced expression of vinculin in the intercalated disc. Biochem Biophys Res Commun *349*, 709-715.

Vogel, V., and Sheetz, M. (2006). Local force and geometry sensing regulate cell functions. Nat Rev Mol Cell Biol *7*, 265-275.

Volberg, T., Geiger, B., Citi, S., and Bershadsky, A.D. (1994). Effect of protein kinase inhibitor H-7 on the contractility, integrity, and membrane anchorage of the microfilament system. Cell Motil Cytoskeleton *29*, 321-338.

Wang, H.B., Dembo, M., Hanks, S.K., and Wang, Y. (2001). Focal adhesion kinase is involved in mechanosensing during fibroblast migration. Proc Natl Acad Sci USA *98*, 11295-11300.

Wang, N., Butler, J.P., and Ingber, D.E. (1993). Mechanotransduction across the cell surface and through the cytoskeleton. Science *260*, 1124-1127.

Watanabe, F., Miyazaki, T., Takeuchi, T., Fukaya, M., Nomura, T., Noguchi, S., Mori, H., Sakimura, K., Watanabe, M., and Mishina, M. (2008). Effects of FAK ablation on cerebellar foliation, Bergmann glia positioning and climbing fiber territory on Purkinje cells. Eur J Neurosci *27*, 836-854.

Webb, D.J., Donais, K., Whitmore, L.A., Thomas, S.M., Turner, C.E., Parsons, J.T., and Horwitz, A.F. (2004). FAK-Src signalling through paxillin, ERK and MLCK regulates adhesion disassembly. Nat Cell Biol *6*, 154-161.

Wehrle-Haller, B., and Imhof, B.A. (2003). Integrin-dependent pathologies. The Journal of Pathology, 481-487.

Wei, W.C., Kopec, A.K., and Tang, M.J. (2009). Requirement of focal adhesion kinase in branching tubulogenesis. J Biomed Sci *16*, 5.

Wolfenson, H., Lubelski, A., Regev, T., Klafter, J., Henis, Y.I., and Geiger, B. (2009). A role for the juxtamembrane cytoplasm in the molecular dynamics of focal adhesions. PLoS ONE *4*, e4304.

Worthylake, R.A., and Burridge, K. (2003). RhoA and ROCK promote migration by limiting membrane protrusions. J Biol Chem *278*, 13578-13584.

Wozniak, M.A., and Chen, C.S. (2009). Mechanotransduction in development: a growing role for contractility. Nat Rev Mol Cell Biol *10*, 34-43.

Wozniak, M.A., Desai, R., Solski, P.A., Der, C.J., and Keely, P.J. (2003). ROCK-generated contractility regulates breast epithelial cell differentiation in response to the physical properties of a three-dimensional collagen matrix. J Cell Biol *163*, 583-595.

Xing, Z., Chen, H.C., Nowlen, J.K., Taylor, S.J., Shalloway, D., and Guan, J.L. (1994). Direct interaction of v-Src with the focal adhesion kinase mediated by the Src SH2 domain. Mol Biol Cell *5*, 413-421.

Xu, L.H., Yang, X., Bradham, C.A., Brenner, D.A., Baldwin, A.S., Jr., Craven, R.J., and Cance, W.G. (2000). The focal adhesion kinase suppresses transformation-associated, anchorage-independent apoptosis in human breast cancer cells. Involvement of death receptor-related signaling pathways. J Biol Chem *275*, 30597-30604.

Xu, W., Baribault, H., and Adamson, E.D. (1998a). Vinculin knockout results in heart and brain defects during embryonic development. Development *125*, 327-337.

Xu, W., Coll, J.L., and Adamson, E.D. (1998b). Rescue of the mutant phenotype by reexpression of full-length vinculin in null F9 cells; effects on cell locomotion by domain deleted vinculin. J Cell Sci *111 (Pt 11)*, 1535-1544.

Yanase, M., Ikeda, H., Ogata, I., Matsui, A., Noiri, E., Tomiya, T., Arai, M., Inoue, Y., Tejima, K., Nagashima, K., *et al.* (2003). Functional diversity between Rho-kinase- and MLCK-mediated cytoskeletal actions in a myofibroblast-like hepatic stellate cell line. Biochem Biophys Res Commun *305*, 223-228.

Yang, M.T., Fu, J., Wang, Y.K., Desai, R.A., and Chen, C.S. (2011). Assaying stem cell mechanobiology on microfabricated elastomeric substrates with geometrically modulated rigidity. Nat Protoc *6*, 187-213.

Yang, M.T., Sniadecki, N.J., and Chen, C.S. (2007). Geometric considerations of micro- to nanoscale elastomeric post arrays to study cellular traction forces. Adv Mater *19*, 3119-+.

Young, S.R., Gerard-O'Riley, R., Kim, J.B., and Pavalko, F.M. (2009). Focal adhesion kinase is important for fluid shear stress-induced mechanotransduction in osteoblasts. J Bone Miner Res *24*, 411-424.

Zaidel-Bar, R., Itzkovitz, S., Ma'ayan, A., Iyengar, R., and Geiger, B. (2007). Functional atlas of the integrin adhesome. Nat Cell Biol *9*, 858-867.

Zemljic-Harpf, A.E., Miller, J.C., Henderson, S.A., Wright, A.T., Manso, A.M., Elsherif, L., Dalton, N.D., Thor, A.K., Perkins, G.A., McCulloch, A.D., *et al.* (2007). Cardiac-myocyte-specific excision of the vinculin gene disrupts cellular junctions, causing sudden death or dilated cardiomyopathy. Mol Cell Biol *27*, 7522-7537.

Zemljic-Harpf, A.E., Ponrartana, S., Avalos, R.T., Jordan, M.C., Roos, K.P., Dalton, N.D., Phan, V.Q., Adamson, E.D., and Ross, R.S. (2004). Heterozygous inactivation of the vinculin gene predisposes to stress-induced cardiomyopathy. Am J Pathol *165*, 1033-1044.

Zhang, X., Jiang, G., Cai, Y., Monkley, S.J., Critchley, D.R., and Sheetz, M.P. (2008). Talin depletion reveals independence of initial cell spreading from integrin activation and traction. Nat Cell Biol *10*, 1062-1068.

Zhao, J.H., Reiske, H., and Guan, J.L. (1998). Regulation of the cell cycle by focal adhesion kinase. J Cell Biol *143*, 1997-2008.

Zhu, C., Bao, G., and Wang, N. (2000). Cell mechanics: mechanical response, cell adhesion, and molecular deformation. Annu Rev Biomed Eng *2*, 189-226.

Ziegler, W.H., Liddington, R.C., and Critchley, D.R. (2006). The structure and regulation of vinculin. Trends Cell Biol *16*, 453-460.